



Ion selectivity of the unusual K⁺ channel KtrAB

DISSERTATION

zur Erlangung des Doktorgrades
der Naturwissenschaften

vorgelegt beim Fachbereich 14
Biochemie, Chemie und Pharmazie
der Johann Wolfgang Goethe-Universität
in Frankfurt am Main

von

Vedrana Mikušević
Geboren in Zagreb, ehemalige SFR Jugoslawien
Kroatische Staatsbürgerin

Frankfurt, 2020

(D30)

“Nothing in life is to be feared, it is only to be understood. Now is the time to understand more, so that we may fear less.”

Marie Curie

Vom Fachbereich 14 Biochemie, Chemie und Pharmazie der Johann Wolfgang Goethe-Universität als Dissertation angenommen:

Dekan: Prof Dr. Clemens Glaubitz

1. Gutachter: Jun. Prof. Dr. Inga Hänel

2. Gutachter: Prof. Dr. Klaus Fendler

Datum der Disputation

I. Publications

Diskowski M, Mikusevic V, Stock C and Hänel I (2015) Functional diversity of the superfamily of K⁺ transporters to meet various requirements. *Biological Chemistry*. 396(9-10):1003-1014.

Diskowski M, Mehdipour AR, Wunnicke D, Mills DJ, Mikusevic V, Bärland N, Hoffmann J, Morgner N, Steinhoff HJ, Hummer G, Vonck J, Hänel I. (2017) Helical jackknives control the gates of the double-pore K⁺ uptake system KtrAB. *eLife*. 6. pii: e24303.

Hellwig N, Peetz O, Ahdash Z, Tascón I, Booth PJ, Mikusevic V, Diskowski M, Politis A, Hellmich Y, Hänel I, Reading E, Morgner N. (2018) Native mass spectrometry goes more native: investigation of membrane protein complexes directly from SMALPs. *Chemical Communication*. 54(97):13702-13705.

Mikusevic V, Schrecker M, Patiño-Ruiz M, Fendler K, Hänel I (2019) A channel profile report of the unusual K⁺ channel KtrB. *The Journal of General Physiology*. 151(12):1357-1368.

Tascón I, Sousa JS, Corey RA, Mills DJ, Griwatz D, Aumüller N, Mikusevic V, Stansfeld PJ, Vonck J and Hänel I (2020) Structural basis of the proton-coupled potassium transport in the KUP family. *Nature Communications*. In press.

II. Index	
I. Publications	5
II. Index	7
I. Summary	10
II. Zusammenfassung	16
III. Declaration of scientific collaborations	23
1. Introduction	24
1.1 Biological Membrane	24
1.1.1 Electrical properties of biological membranes	24
1.2 Ion transport across biological membranes	26
1.2.1 Main principles of membrane transport	27
1.2.2 Biological significance of K^+ and Na^+ distribution	28
1.3 Ion channels	29
1.3.1 K^+ channels and their architecture	30
1.3.2 Selectivity filter tailored for K^+	32
1.4 Superfamily of K^+ transporters	35
1.5 Regulator of K^+ conductance (RCK)	37
1.6 The Na^+ and ATP-dependent K^+ translocating complex KtrAB	38
1.6.1 Selectivity and translocation of K^+ by subunit KtrB	39
1.6.2 Influence of RCK protein KtrA on K^+ translocation	41
2. Aims and Objectives	43
3. Materials and Methods	44
3.1 Material	44
3.1.1 Chemicals	44
3.1.2 Buffers and solutions	45
3.1.3 Strain and Plasmids	46
3.2 Growth media	48
3.3 Molecular biology	48
3.3.1 Preparation of competent cells and transformation	48
3.3.2 Plasmid isolation	48
3.3.3 Site-directed mutagenesis	49
3.3.4 Creating the KtrB _{TVGYG} variant	49
3.3.5 Agarose gel electrophoresis	49
3.4 Whole-cell assays	50
3.4.1 Complementation assay	50
3.4.2 K^+ uptake experiments in whole-cells	50
3.5 Biochemical methods	51

3.5.1	BCA assay.....	51
3.5.2	SDS-Polyacrylamide gel electrophoresis (PAGE).....	51
3.6	Protein production and purification	52
3.6.1	Overexpression	52
3.6.2	Isolation of membranes	53
3.6.3	Protein purification from isolated membranes	53
3.6.4	Protein purification of KtrB-3C-His ₁₀ with SMALPs.....	54
3.7	Reconstitution into liposomes	54
3.7.1	Purification of <i>E. coli</i> total lipid extract.....	55
3.7.2	Preparation of different liposome mixtures.....	55
3.7.3	Preparation of Polystyrene beads	55
3.7.4	Reconstitution of KtrB into pre-formed liposomes	56
3.8	Biochemical and biophysical techniques	56
3.8.1	ITC	56
3.8.2	Determination of the liposome size	57
3.8.3	ACMA assay.....	57
3.8.4	Laser-induced liquid bead ion desorption-Mass spectrometry (LILBID-MS)	58
3.9	Electrophysiology	59
3.9.1	Theoretical Background of SSM-based electrophysiology	59
3.9.1.1	Capacitive coupling on the SSM	60
3.9.2	SSM-based electrophysiology	62
3.9.2.1	Equipment	62
3.9.2.2	Preparation of the gel bridge.....	62
3.9.2.3	Chlorination of the reference electrode	63
3.9.2.4	Preparation of the SSM setup.....	63
3.9.2.5	Preparation of lipids	63
3.9.2.6	Preparation of the sensor chip	64
3.9.2.7	Membrane parameters	64
3.9.2.8	Applying liposomes to the SSM	65
3.9.2.9	Flow protocol and signal recording	65
3.9.2.10	Run down control	66
3.10	Data evaluation of the signal decay in SSM and ACMA	67
4.	Results	68
4.1	Establishing protein purification protocols for functional assays	68
4.1.1	Large-scale purification of an improved KtrB-3C-His ₁₀ construct	69
4.1.2	Purification of KtrB-3C-His ₁₀ using styrene-maleic acid copolymer lipid particle (SMALP).....	70

4.2	Integrity of the KtrB dimer	71
4.3	Ion binding of KtrB-3C-His₁₀	72
4.3.1	Binding affinities of different cations to KtrB-3C-His ₁₀	72
4.3.2	Binding competition to the SF of KtrB	76
4.4	Establishing functional assays to address ion translocation	77
4.4.1	SSM-based electrophysiology	77
4.4.2	Establishing fluorescence-based assay for studying KtrB	79
4.4.2.1	<i>Optimization of liposome reconstitution</i>	80
4.5	Ion transport specificity of KtrB	82
4.5.1	Ion specificity of VaKtrB-His ₆ explored with SSM-based electrophysiology 82	
4.5.2	Transport kinetics of VaKtrB-His ₆ explored with SSM-based electrophysiology	84
4.5.3	Evaluating ion translocation with the fluorescence-based ACMA assay.	88
4.5.4	Competitive ion uptake through KtrB	89
4.6	Motifs responsible for ion selectivity	90
4.6.1	Converting the poorly conserved selectivity filter to -TVGYG-	90
4.6.2	Modifying the intramembrane loop of KtrB	91
4.6.2.1	Purification of intramembrane loop variant.....	91
4.6.2.2	ACMA-based fluorescence assay with KtrB _{G316S} -containing liposomes..	92
4.7	The role of Na⁺ for KtrAB	94
4.7.1	K ⁺ currents of KtrB in the presence of small cations.....	94
4.7.2	Na ⁺ dependency of KtrAB	96
4.7.3	Potential second binding site for Na ⁺	97
5.	Discussion	100
5.1	Selectivity of KtrAB is a result of ion binding and translocation	100
5.2	Size restriction by the intramembrane loop in KtrB	104
5.3	Na⁺ dependency of KtrAB	106
6.	Directories	109
6.1	List of abbreviations	109
7.	References	111
8.	Supplement	126
9.	Acknowledgments	132
10.	CV	134

I. Summary

Bacteria constantly attempt to hold up ion gradients across their membranes to maintain their resting potential for routine cell function, while coping with sudden environmental changes. Under abrupt hyperosmotic conditions, as faced when invading a host, most bacteria restore their turgor pressure by taking up potassium ions to prevent death by plasmolysis. Here, the potassium transporter AB, or KtrAB for short, is a key player. KtrAB consists of the membrane-embedded KtrB dimer, which includes two pores organized in tandem, and a cytoplasmic, octameric KtrA ring, which regulates these two pores. The KtrB subunits alone were suggested to function as rather non-selective ion channels translocating potassium and sodium ions. The KtrA subunits confer transport velocity, K^+ selectivity as well as Na^+ and nucleotide dependency to the Ktr system. The nucleotide regulation by binding to KtrA is rather well characterized. In contrast, the regulatory role of Na^+ remains elusive. Controversially discussed is how selective the ion translocation by KtrB is and how KtrA affects it. Although there are several functional and structural data available of KtrAB and its homolog TrkAH, the selectivity of the ion translocation was never thoroughly addressed. The functional characterization of whether KtrAB is a selective ion channel and how selectivity is achieved is in the focus of this thesis. Since selectivity is usually defined by the ion channels' selectivity filter contained in the pore-forming domain, a particular attention was laid on the ion-translocating subunits KtrB.

KtrB belongs to the superfamily of K^+ transporters (SKT). Each KtrB monomer consists of four covalently attached M1-P-M2 motifs, each motif is made of two transmembrane (TM or M) helices that are connected by a pore (P) helix. The four motifs, referred to as domains D1 to D4, are arranged in a pseudo-fourfold symmetry and together form the pore for potassium ion translocation. Each pore contains two structural features thought to be involved in ion selectivity and ion gating. These are the non-canonical selectivity filter and the intramembrane loop. The selectivity filter is localized at the extracellular side of the pore and mostly shaped by the backbone carbonyl groups of the loops connecting the P and M2 helices in each domain. In KtrB, each P-loop contains only one highly conserved glycine residue instead of the classical -TVGYG- signature sequence of a K^+ channel. This simple constructed selectivity filter led to the hypothesis that KtrAB would only have low ion selectivity. The intramembrane loop is formed by broken helix D3M2 and is located directly under the selectivity filter. It consists mostly of polar residues and acts as a molecular gate restricting ion fluxes. The intramembrane loop has been shown to be regulated by nucleotide binding to KtrA. Additionally, it could directly

or indirectly be affected by Na⁺ binding. Further, the loop might even be involved in ion selectivity because it presents a physical barrier inside the pore.

To address the ion selectivity of the Ktr system, first, the ion binding specificity of KtrB was investigated. Binding affinities of different cations to KtrB were determined using isothermal titration calorimetry (ITC). For this, KtrB from *Vibrio alginolyticus* was heterologously produced in and purified from *Escherichia coli*. 12 L of culture roughly yielded 4 to 8 mg of the functional KtrB dimer in detergent solution. ITC measurements were performed in two different buffers, one choline-Cl-based and one LiCl-based buffer. No differences in the affinity between Na⁺ ($K_D = 1.8$ mM), K⁺ ($K_D = 2.9$ mM), Rb⁺ ($K_D = 1.9$ mM) or Cs⁺ ($K_D = 1.6$ mM) were detected in the choline-Cl-based buffer; only Li⁺ did not bind. In contrast, ITC measurements in LiCl-based buffer revealed a significant preference for K⁺ ($K_D = 91$ μ M) over Rb⁺ ($K_D = 2.4$ mM), Cs⁺ ($K_D = 1.7$ mM) and particularly Na⁺ (for which no binding was observed). Similarly, the presence of low millimolar NaCl concentrations in the choline-Cl-based buffer led to a decreased K_D value of 260 μ M. Hence, small cations, which usually are present in the natural environment, seem to modulate the selectivity filter for a better binding of K⁺ ions providing K⁺ selectivity. In fact, the low binding affinities of the other ions could indicate that they do not even bind to the selectivity filter but to the cavity. However, ITC competition experiments showed that all four ions compete for the same or overlapping binding sites, with Rb⁺ and Cs⁺ even blocking K⁺ binding at concentrations 10-fold above their binding affinities. Importantly, at physiological NaCl concentrations of 200 mM, the apparent binding affinity for K⁺ to KtrB was still 3.5 mM. This suggested that Na⁺ can also bind to KtrB's selectivity filter but with a comparably low binding affinity providing an unexpectedly high preference for K⁺ ions.

Ion binding is required for ion translocation, yet the preferred K⁺ binding is no guarantee for its preferred translocation, as shown for other ion channels. In this work, two assays were established for the investigation of ion translocation by KtrB, an electrophysiological method based on solid-supported membranes (SSM) and an ion flux assay based on 9-amino-6-chloro-2-methoxyacridine (ACMA) fluorescence. Further, the liposome preparation and the reconstitution of KtrB were optimized, gaining homogeneous proteoliposomes with active KtrB. The cations (Li⁺, Na⁺, K⁺, Rb⁺, and Cs⁺) used for ITC measurements were also employed for SSM-based electrophysiology. Generally, SSM-based electrophysiology allows measuring pre-steady-state ion binding and steady-state ion translocation. Thus, the obtained data needed to be carefully evaluated to distinguish between both cases. Of the five tested cations, Li⁺ was the only one not resulting in

transient currents at 100 mM concentration jumps. The biggest peak current was observed for the biggest ion Cs^+ , while Rb^+ gave a smaller signal followed by K^+ and then Na^+ . The resulting order of signal intensity was: $\text{Na}^+ < \text{K}^+ < \text{Rb}^+ < \text{Cs}^+$. However, when comparing the electrical charges by integrating the transient currents, a reversed order resulted ($\text{Na}^+ > \text{K}^+ > \text{Rb}^+ > \text{Cs}^+$) suggesting that Na^+ and K^+ are better translocated than Rb^+ and particularly Cs^+ . For distinguishing between ion binding and translocation, half-maximal decay times of transient currents at different lipid-to-protein ratios (LPRs) were compared. In the case of ion transport, decay times should increase with increasing LPRs because steady-state transport rates are reached slower at low protein concentrations, while in the case of ion binding, the decay times should not be affected by the LPRs. LPRs used were 5:1, 10:1, and 50:1. With increasing LPR, the decay times at 100 mM KCl jumps increased from 15.2 via 17.5 to 44.5 ms, respectively. Similarly, albeit to a lesser extent, the decay times for Rb^+ increased with increasing LPRs (8.3, 11.7, and 15.6 ms, respectively). For the small Na^+ , decay times of ~42 ms were identified, while for the biggest cation Cs^+ , decay times of ~10 ms were determined. The decay times for both cations did not differ with changing LPRs. Hence, the determination of the decay times suggested that K^+ and, to a lesser extent, Rb^+ are translocated. For further exploring the ion translocation with SSM-based electrophysiology, Michaelis-Menten constants (K_M) were determined by performing cation concentration jumps between 1 and 100 mM for NaCl, KCl, RbCl, and CsCl. In the case of ion translocation, a rate-limiting step slower than the actual ion binding may result in increased K_M values compared to the K_D values. However, the K_M values of Cs^+ (2 mM) and Rb^+ (6 mM) were similar to their binding affinities suggesting only binding. A K_M of ~36 mM was determined for Na^+ and may demonstrate the low binding affinity for Na^+ . The K_M of K^+ (16 mM) was significantly increased compared to its K_D (91 μM) again pointing towards its translocation through KtrB. Taken together, only K^+ was identified by SSM-based electrophysiology as the ion translocated through KtrB, while Cs^+ consistently was shown to only bind. The data for Na^+ and Rb^+ was inconclusive, a final claim of whether they are translocated could not be made.

As an alternative method for measuring ion fluxes, the ACMA-based fluorescence assay was established. KtrB-containing liposomes (LPR of 100:1) loaded with either NaCl, KCl, RbCl or CsCl were diluted into a LiCl-containing buffer. Subsequently, continuous ion efflux was indirectly monitored: The addition of Carbonyl cyanide *m*-chlorophenyl hydrazone (CCCP) allowed the influx of one proton for every ion leaving the liposomes, which ultimately resulted in ACMA quenching. The ACMA assay revealed a size-dependent ion permeation profile with fast fluxes for Na^+ , followed by K^+ and very slow

fluxes for Rb⁺. Cs⁺ did not flux through KtrB. The rapid Na⁺ fluxes appeared to contradict the proposed K⁺ selectivity of KtrB. However, this assay could not be performed under mixed ion conditions allowing the evaluation of competing cation.

However, the already higher K⁺ binding affinity determined with ITC in the presence of Na⁺ could indicate the preferred translocation of K⁺ under mixed ion conditions. To look at ion translocation under competing ion concentrations, *in vivo* K⁺ uptake assays into K⁺- and Na⁺-depleted cells were performed in the presence of competing Rb⁺ and Na⁺ concentrations. The 25-fold excess of Rb⁺ outcompeted the binding of K⁺ and abolished its uptake. In contrast, a 25-fold excess of Na⁺ had no inhibitory effect on the uptake of K⁺. Consequently, KtrB also selectively translocates K⁺ over Na⁺ and thus classifies as a selective K⁺ channel.

Knowing that KtrB is selective for K⁺, the question arose which motifs are responsible for its selectivity. Of course, the selectivity filter was the first target evaluated. In previous studies, it was shown that mutating the conserved glycine residues reduced selectivity or even led to an exclusively Na⁺-translocating system. Consequently, here the selectivity filter sequences in all four domains were converted from their non-canonical sequences to the canonical -TVGYG- sequence, aiming to increase the K⁺ selectivity of KtrB further. Growth complementation assays at low K⁺ concentrations using *E. coli* strain LB2003 producing wild-type KtrB or KtrB_{TVGYG} allowed to evaluate the activity of the proteins. The assay revealed that cells producing KtrB_{TVGYG} did not grow at low K⁺ concentrations in comparison to cells producing wild-type KtrB. Thus, the symmetrical -TVGYG- motif is not compatible with the asymmetrical pore of KtrB.

Besides the selectivity filter, KtrB holds the intramembrane loop controlling K⁺ uptake as a molecular gate. This loop does not allow ion permeation in the ADP-bound KtrAB conformation, while ions can permeate in the ATP-bound conformation. In KtrB alone, the loop was shown to restrict K⁺ fluxes, while Na⁺ was not affected. It needed to be evaluated whether the loop is generally responsible for the size-dependent ion translocation and thus adds to the selectivity of KtrB. Therefore, the loop was mutated, and ion fluxes were evaluated using the ACMA-based assay. Changing glycine residue 316 of the intramembrane loop to a serine residue was previously shown to increase the uptake velocity of potassium ions into whole-cells. Consistent with this, variant KtrB_{G316S} presented 60-fold increased K⁺ fluxes in the ACMA-based assay, while the Rb⁺ fluxes were eightfold faster. The translocation of Na⁺ remained unchanged, and Cs⁺ stayed impermeable. It was concluded that only changing one single amino acid lowered the

physical barrier for fluxes of the bigger ions K^+ and Rb^+ , resulting in an increased open probability of the gate or its less efficient closing.

Because Na^+ is the most abundant extracellular cation KtrB's K^+ over Na^+ selectivity is physiologically most relevant. The ITC measurements revealed that KtrB becomes very selective for K^+ over Na^+ through the presence of Na^+ itself. Previously, it was known that the KtrAB system is absolutely dependent on Na^+ . In its absence, K^+ was not taken up, while its presence resulted in an increased K^+ uptake velocity when compared to KtrB. To further address the role of Na^+ on the KtrAB system, SSM-based electrophysiology, whole-cell K^+ uptake assays, MD simulations, and complementation assays were performed. Similar to the ITC measurements, SSM-based electrophysiology on KtrB revealed a stimulating effect of Na^+ on the K^+ currents with a half-maximal activation (AC_{50}) at 0.5 mM NaCl. The maximum signal enhancement was reached between 2.5 and 10 mM of NaCl. Additional data indicated that the enhanced K^+ currents are not a result of Na^+ symport or antiport, as previously suggested, but possibly of Na^+ binding to the cytoplasmic side of KtrB. However, both, the SSM-based electrophysiology and whole-cell K^+ uptake assays confirmed that the rate of K^+ translocation through KtrB remained unaffected by Na^+ . Instead, the number of K^+ ions binding to KtrB could be increased, as indicated by the increased peak currents. To address the secondary effect Na^+ has on the KtrAB system, whole-cell K^+ uptake experiments at different Na^+ concentrations were performed determining the respective V_{max} and K_M values. Consistent with previous measurements, it was seen that increasing the Na^+ concentration resulted in increased V_{max} values. Yet more exciting at the same time, the K_M considerably decreased more than 20-fold from 1 mM to 37 μ M approaching the K_D for K^+ binding determined by ITC. In conclusion, Na^+ does not only modulate the affinity for K^+ to KtrAB, but it also influences the kinetics of K^+ gating probably by stabilizing the open conformation of the gate and thus minimizing the rate-limiting step during translocation.

The identification of a potential Na^+ binding site in KtrB was contemplated from untargeted MD simulations on KtrB. These MD simulations revealed a site, formed by Q93 in D1M2, E149 in D2M1, and N182 in D2P_{helix}, coordinating a cation. Interestingly, this site is close to the intramembrane loop, and thus, Na^+ binding at this site could affect gating. *E. coli* LB2003 growth complementation assay at different K^+ concentrations were used to investigate the effects of mutations in the potential second binding site on KtrB and KtrAB, respectively. It was expected that cells expressing KtrB variants grow normally since KtrB's translocation activity does not depend on Na^+ . For KtrAB variants-

expressing cells, a growth deficiency was anticipated for specific mutations. And indeed, while all KtrB variants complemented the growth of LB2003, Q93L and E149K in KtrAB showed growth deficits at low K^+ concentrations. The two mutations might be the result of two different effects. Hypothetically, mutation Q93L could have impaired the coordination of the sodium ion, while E149K completely abolished Na^+ binding if this is genuinely the Na^+ binding site.

In summary, the data obtained in this thesis uncovered the unique ion binding and translocation profile of KtrAB, which is defined by the unusually designed selectivity filter together with the uncommon intramembrane loop. The presence of Na^+ stimulates both K^+ binding and translocation, resulting in the essential K^+ over Na^+ selectivity. A potential Na^+ binding site has been identified in KtrB, possibly allowing the further structural characterization of the regulatory impact of Na^+ .

II. Zusammenfassung

Bakterien müssen für eine routinemäßige Zellfunktion ständig Ionengradienten über ihren Membranen aufrechterhalten, während sie durch wechselnde Umweltbedingungen fortlaufend herausgefordert werden. Beispielsweise kommt es beim Eindringen in einen Wirt meistens zu abrupten hyperosmotischen Änderungen, welche den Turgordruck bedrohen. Die meisten Bakterien stellen ihren Turgordruck wieder her, indem sie Kaliumionen aufnehmen, um den Tod durch Plasmolyse zu verhindern. Hier spielt der Kaliumtransporter AB, kurz KtrAB, eine Schlüsselrolle. Der KtrAB-Komplex besteht aus einem in die Membran eingebetteten KtrB-Dimer, welches aus zwei parallelen Poren gebildet wird und einem cytoplasmatischen, octameren KtrA-Ring der diese beiden Poren reguliert. Es wurde bisher angenommen, dass die Kanal-ähnliche KtrB-Untereinheit unselektiv Kalium- und Natriumionen translozieren kann. Nur in Anwesenheit der KtrA-Untereinheiten wurde gezeigt, dass das nun Na⁺ und Nukleotid abhängige Ktr-System eine höhere Transportgeschwindigkeit und K⁺-Selektivität aufweist. Die Regulation durch Nukleotiden-Bindung an KtrA ist gut charakterisiert. Im Gegensatz dazu ist die regulatorische Rolle von Na⁺ nicht endgültig geklärt. Umstritten ist ebenfalls, wie selektiv die Ionentranslokation durch KtrB ist und wie KtrA diese beeinflusst. Obwohl für KtrAB und sein Homolog, TrkAH, mehrere funktionelle und strukturelle Daten erhältlich sind, wurde die Selektivität der Ionentranslokation nie intensiv untersucht. Aus diesem Grund steht die funktionelle Charakterisierung der Selektivität von KtrAB im Mittelpunkt dieser Arbeit. Da die Selektivität in der Regel durch den in KtrB enthaltenen Selektivitätsfilter definiert wird, lag ein besonderes Augenmerk auf der Ionen-translozierenden Untereinheit KtrB.

KtrB gehört zur Überfamilie der K⁺ Transporter (SKT). Jedes KtrB-Monomer besteht aus vier kovalent gebundenen M1-P-M2-Motiven, die jeweils aus zwei Transmembran- (TM- oder M-) Helices bestehen, die durch eine Poren- (P-) Helix miteinander verbunden sind. Die vier als Domänen D1 bis D4 bezeichneten Motive sind pseudovierfach symmetrisch angeordnet und bilden zusammen die Pore für die Translokation von Kalium. Jede Pore enthält zwei Strukturmerkmale, von denen angenommen wird, dass sie an der Ionenselektivität und der Steuerung der Ionentranslokation beteiligt sind. Hierbei handelt es sich um einen nicht-kanonischen Selektivitätsfilter und eine Intramembranschleife. Der Selektivitätsfilter befindet sich auf der extrazellulären Seite der Pore und wird hauptsächlich durch die Carbonylgruppen des Rückgrats der P-Schleifen geformt, die die P- und M2-Helices von jeder Domäne verbinden. In KtrB enthält jede P-Schleife nur einen hochkonservierten Glycinrest anstelle der klassischen TVGYG-Sequenz des K⁺-

Kanals. Dieser einfach aufgebaute Selektivitätsfilter führte zu der Hypothese, dass KtrAB nur eine geringe Ionenselektivität aufweist. Die Intramembranschleife wird durch die gebrochene D3M2-Helix gebildet und befindet sich direkt unter dem Selektivitätsfilter. Sie besteht hauptsächlich aus polaren Resten und wirkt als molekulares Tor, welches den Ionenfluss beschränkt. Weiterhin wurde gezeigt, dass die Intramembranschleife durch Nukleotidbindung an KtrA reguliert wird. Zusätzlich kann sie direkt oder indirekt durch Na⁺-Bindung beeinflusst werden. Ferner könnte die Intramembranschleife sogar an der Ionenselektivität beteiligt sein, da sie eine physikalische Barriere innerhalb der Pore darstellt.

Um die Ionenselektivität des Ktr-Systems zu untersuchen, wurde zunächst die Bindung von KtrB zu unterschiedlichen Ionen untersucht. Die Bindungsaffinitäten verschiedener Kationen an KtrB wurden mittels isothermer Titrationskalorimetrie (ITC) bestimmt. Hierzu wurde KtrB aus *V. alginolyticus* in *Escherichia coli* heterolog hergestellt und gereinigt. Aus 12 L Kultur wurden ungefähr 4 bis 8 mg funktionelles KtrB-Dimer mit Detergens gereinigt. ITC-Messungen wurden in zwei verschiedenen Puffern durchgeführt, einem Puffer auf Cholin-Cl-Basis und einem Puffer auf LiCl-Basis. In dem Puffer auf Cholin-Cl-Basis wurden keine Unterschiede in der Affinität zwischen Na⁺ ($K_D = 1,8 \text{ mM}$), K⁺ ($K_D = 2,9 \text{ mM}$), Rb⁺ ($K_D = 1,9 \text{ mM}$) oder Cs⁺ ($K_D = 1,6 \text{ mM}$) festgestellt; nur Li⁺ zeigte keine Bindung. Im Gegensatz dazu zeigten ITC-Messungen in LiCl-basiertem Puffer eine signifikante Präferenz für K⁺ ($K_D = 91 \text{ }\mu\text{M}$) gegenüber Rb⁺ ($K_D = 2,4 \text{ mM}$), Cs⁺ ($K_D = 1,7 \text{ mM}$) und insbesondere Na⁺ (für das keine Bindung beobachtet wurde). In ähnlicher Weise führte das Vorhandensein niedriger millimolarer NaCl-Konzentrationen im Choline-Cl-Puffer zu einem verringerten K_D -Wert von 260 μM . Es konnte angenommen werden, dass kleine Kationen den Selektivitätsfilter für eine bessere K⁺-Ionenbindung modulieren und so die K⁺-Selektivität präferiert wird. Die geringen Bindungsaffinitäten der anderen Ionen könnte darauf hinweisen, dass diese nicht einmal an den Selektivitätsfilter selbst binden, sondern irgendwo im Protein. ITC-Kompetitionsexperimente zeigten jedoch, dass alle vier Ionen um die gleichen oder überlappenden Bindungsstellen konkurrieren. Es wurde gezeigt, dass Rb⁺ und Cs⁺ die K⁺-Bindung blockierten, bei Konzentrationen 10-fach über ihren Bindungsaffinitäten. Natrium hingegen bewirkte eine Reduktion der Affinität von K⁺ zu KtrB bei physiologischen Konzentrationen von 200 mM NaCl. Die Bindungsaffinität betrug immer noch 3,5 mM, was darauf hindeutet, dass Na⁺ auch an KtrBs Selektivitätsfilter binden kann, jedoch mit einer vergleichsweise geringen Bindungsaffinität. Dementsprechend kann abgeleitet werden, dass eine unerwartet hohe Bindungsselektivität für K⁺-Ionen besteht.

Ionenbindung ist für die Ionentranslokation zwingend erforderlich, sie ist jedoch keine Garantie für Translokation, wie auch schon für andere Ionenkanäle gezeigt wurde. Für die Untersuchung der Ionentranslokation durch KtrB wurden in dieser Arbeit zwei Assays etabliert, eine elektrophysiologische Methode auf Basis Festkörper-unterstützter Membranen (*solid-supported membrane*: SSM) und ein auf 9-Amino-6-Chlor-2-Methoxyacridin (ACMA) basierender Flux-Assay. Ferner wurden die Vorbereitungen der Liposomen für die Rekonstitution von KtrB optimiert. Dies resultierte in homogene Proteoliposomen mit aktivem KtrB erhalten. Die für ITC-Messungen verwendeten Kationen (Li^+ , Na^+ , K^+ , Rb^+ und Cs^+) wurden auch für die SSM-basierten elektrophysiologischen Experimente verwendet. Im Allgemeinen ermöglicht die SSM-basierte Elektrophysiologie die Messung der *pre steady-state* und *steady-state* Signale, welche entsprechend mit der Ionenbindung und -translokation korrelieren. Eine Unterscheidung kann schwierig sein, daher mussten die erhaltenen Daten sorgfältig ausgewertet werden, um zwischen diesen beiden Fällen zu unterscheiden. Von den fünf getesteten Kationen war Li^+ das Einzige, für welches keine transienten Ströme gemessen wurden. Der höchste Peakstrom wurde für das größte Ion Cs^+ beobachtet, während für Rb^+ ein kleinerer Peakstrom gemessen wurde, gefolgt von K^+ und dann Na^+ . Die resultierende Reihenfolge der Signalintensität war: $\text{Na}^+ < \text{K}^+ < \text{Rb}^+ < \text{Cs}^+$. Die Integration der transienten Ströme ergab jedoch eine invertierte Ionenpräferenz ($\text{Na}^+ > \text{K}^+ > \text{Rb}^+ > \text{Cs}^+$), welche darauf hindeutet, dass Na^+ und K^+ besser transloziert werden als Rb^+ oder insbesondere Cs^+ . Um zwischen Ionenbindung und Translokation zu unterscheiden, wurden die halbmaximalen Abklingzeiten ($\tau_{1/2}$) der transienten Ströme bei verschiedenen Lipid-zu-Protein-Verhältnissen (*lipid-to-protein ratios*: LPRs) verglichen. Im Falle des Ionentransports sollten die Abklingzeiten mit abnehmenden LPRs zunehmen, da bei niedrigen Proteinkonzentrationen langsamere *steady-state* Signale erreicht werden. Im Falle der Ionenbindung hängt die Abklingzeiten nicht von den LPRs ab. Die verwendeten LPRs waren 5:1, 10:1 und 50:1. Mit zunehmender LPR nahmen die halbmaximalen Abklingzeiten bei konstanten 100 mM KCl-Sprüngen von 15,2 über 17,5 auf 44,5 ms zu. In ähnlicher Weise, wenn auch in geringerem Maße, wurde dasselbe für Rb^+ beobachtet. Hier entsprachen die halbmaximalen Abklingzeiten 8,3, 11,7 und 15,6 ms für die entsprechenden LPRs. Für das kleine Na^+ wurden $\tau_{1/2}$ -Werte von ~ 42 ms für alle LPRs ermittelt, während für das große Cs^+ Werte von ~ 10 ms ermittelt wurden. Die halbmaximalen Abklingzeiten der beiden Ionen schienen unabhängig von den LPRs zu sein. Die Betrachtung der Abklingzeiten legte daher nahe, dass K^+ und in geringerem Maße Rb^+ transloziert werden. Zur weiteren Untersuchung der Ionentranslokation mit SSM-basierter Elektrophysiologie wurden Michaelis-Menten-

Konstanten (K_M) bestimmt, indem Konzentrationssprünge zwischen 1 und 100 mM mit NaCl, KCl, RbCl und CsCl durchgeführt wurden. Im Falle einer Ionentranslokation führt ein langsamer, geschwindigkeitsbestimmender Schritt häufig zu erhöhten K_M -Werten im Vergleich zu K_D -Werten. Die K_M -Werte für Cs^+ (2 mM) und Rb^+ (6 mM) waren ähnlich zu den zuvor bestimmten Bindungsaffinitäten. Dies deutet darauf hin, dass diese beiden Ionen nur an KtrB binden. Ein K_M von ~ 36 mM wurde für Na^+ bestimmt und könnte auch für eine niedrige Bindungsaffinität von Na^+ zu KtrB sprechen. Der K_M von K^+ (16 mM) war im Vergleich zu seinem K_D (91 μM) signifikant erhöht, was wiederum auf seine Translokation durch KtrB hinweist. Zusammengenommen konnte nur K^+ durch SSM-basierte Elektrophysiologie als Ion identifiziert werden, welches von KtrB transloziert wird, während Cs^+ nur bindet. Die Daten für Na^+ und Rb^+ waren nicht schlüssig, um eine endgültige Aussage darüber zu treffen, ob diese beiden Ionen transloziert werden.

Als alternative Methode zur Messung von Ionenflüssen wurde ein ACMA-basierter Fluoreszenzassay für KtrB etabliert. KtrB-haltige Liposomen (LPR von 100:1), die entweder mit NaCl, KCl, RbCl oder CsCl beladen waren, wurden in einem LiCl-haltigen Puffer verdünnt. Anschließend wurde der kontinuierliche Ionenausfluss indirekt mit ACMA evaluiert. Hierbei ermöglicht die Zugabe von Carbonylcyanid-m-chlorphenylhydrazon (CCCP) das Einströmen von Protonen (H^+) im Austausch von Kationen, welche die Liposomen durch das Protein verlassen. Der H^+ -Influx führt schließlich zum Quenchen der ACMA-Fluoreszenz. Der ACMA-Assay ergab ein größenabhängiges Ionenpermeationsprofil mit schnellen Efflux für Na^+ , gefolgt von K^+ und sehr langsamem Efflux für Rb^+ . Cs^+ schien nicht durch KtrB zu fließen. Der schnelle Na^+ -Efflux widerspricht der selektiven K^+ -Translokation. In diesem Assay konnten jedoch keine Ionengemische genutzt werden, da der ACMA-Assay keine Unterscheidung zwischen den translozierten Ionenspezies erlaubt.

Indessen könnte die mit ITC bereits bestimmte höhere K^+ -Bindungsaffinität in Gegenwart von Na^+ für eine bevorzugte Translokation von K^+ gegenüber Na^+ sprechen. Um die Ionentranslokation in gemischten Kationenlösungen zu untersuchen, wurden *in vivo* K^+ -Aufnahmetests in K^+ - und Na^+ -entleerten Zellen, in Gegenwart von konkurrierenden Rb^+ - und Na^+ -Konzentrationen, durchgeführt. Der 25-fache Überschuss an Rb^+ nivellierte die K^+ -Aufnahme komplett. Im Gegensatz dazu hatte ein 25-facher Überschuss an Na^+ keine hemmende Wirkung auf die Aufnahme von K^+ . Folglich transloziert KtrB K^+ über Na^+ mit hoher Präferenz und kann somit als selektiver K^+ -Kanal klassifiziert werden.

Nachdem bewiesen wurde, dass KtrB für K^+ selektiv ist, stellte sich die Frage, welche strukturellen Motive für die Selektivität verantwortlich sind. Zunächst wurde der

Selektivitätsfilter als erstes Ziel ins Auge gefasst. In früheren Studien wurde gezeigt, dass die Mutation der konservierten Glycinreste die Selektivität verringert oder Ktr sogar zu einem ausschließlich Na⁺-translozierenden System konvertieren. Folglich wurden in dieser Studie die Sequenz des Selektivitätsfilters in allen vier Domänen von der nicht-kanonischen in die kanonische TVGYG-Sequenz mutiert. Dies sollte die K⁺-Selektivität von KtrB weiter erhöhen. Wachstumskomplementationen von *E. coli*-Stamm LB2003, welcher Wildtyp KtrB oder KtrB_{TVGYG} produziert, ermöglichte die Bewertung der K⁺-Aufnahme durch das jeweilige Protein bei niedrigen K⁺-Konzentrationen. Der Test ergab, dass Zellen, die KtrB_{TVGYG} produzierten, bei niedrigen K⁺-Konzentrationen nicht wachsen, während Zellen die Wildtyp KtrB produzieren das Wachstum von LB2003 komplementierten. Demzufolge ist das symmetrische TVGYG-Motiv nicht mit der asymmetrischen Pore von KtrB kompatibel.

KtrB enthält neben dem Selektivitätsfilter die Intramembranschleife, die die K⁺-Aufnahme als molekulares Tor reguliert. Diese Intramembranschleife erlaubt keine Ionenpermeation in der ADP-gebundenen KtrAB-Konformation, während Ionen in der ATP-gebundenen Konformation permeieren können. Frühere Studien an KtrB zeigten, dass die Intramembranschleife die K⁺-Ströme verringert, während Na⁺-Ströme unbeeinflusst blieben. Darauf aufbauend wurde hier untersucht, ob die Intramembranschleife im Allgemeinen für die größenabhängige Ionentranslokation verantwortlich ist und somit die Selektivität von KtrB erhöhen kann. Dafür wurde die Intramembranschleife mutiert und der Ionenflux mithilfe des ACMA-Assays analysiert. Zuvor wurde zude bereits gezeigt, dass der Austausch des Glycinrests 316 der Intramembranschleife in einen Serinrest die Aufnahmegeschwindigkeit von Kaliumionen in ganze Zellen erhöht. In Übereinstimmung damit zeigte die Variante KtrB_{G316S} im ACMA-Assay 60-fach erhöhten K⁺-Efflux, während der Efflux von Rb⁺ 8-fach schneller waren. Die Translokation von Na⁺ blieb unverändert, ebenso blieb KtrB für Cs⁺ unpassierbar. Folglich senkt eine einzige Aminosäure die physikalische Barriere für die Flüsse der größeren Ionen K⁺ und Rb⁺, vermutlich durch eine Erhöhung der Offenwahrscheinlichkeit der Schleife.

Physiologisch am relevantesten ist die KtrB-Selektivität für K⁺ gegenüber Na⁺, da Na⁺ das am häufigsten vorkommende extrazelluläre Kation ist. Die ITC-Messungen ergaben, dass KtrB durch die Anwesenheit von Na⁺ K⁺ selektiver bindet. Bisher war bekannt, dass die K⁺-Translokation durch das KtrAB-System von Na⁺ abhängig ist. In der Abwesenheit von Na⁺ wurde K⁺ nicht mehr aufgenommen, während das Vorhandensein zu einer, im Vergleich zu KtrB, erhöhten K⁺-Aufnahmegeschwindigkeit führte. Um die Rolle von Na⁺

auf das KtrAB-System weiter zu untersuchen, wurden SSM-basierte elektrophysiologische Messungen, die K⁺-Aufnahmeaktivität in intakten Zellen, MD-Simulationen und Komplementationstests durchgeführt. Ähnlich wie bei den ITC-Messungen ergab die SSM-Experimente mit KtrB einen simulierenden Effekt von Na⁺ auf die K⁺-Ströme mit einem AC₅₀-Wert von 0,5 mM NaCl. Die maximale Signalverstärkung wurde zwischen 2,5 und 10 mM NaCl erreicht. Zusätzliche Daten deuten darauf hin, dass die erhöhten K⁺-Ströme nicht auf Na⁺-Symport oder Antiport zurückzuführen sind, wie zuvor vorgeschlagen, sondern möglicherweise auf Na⁺-Bindung an die zytoplasmatische Seite von KtrB. Sowohl die SSM-Experimente, als auch die K⁺-Aufnahmeaktivität in intakten Zellen bestätigten jedoch, dass die Rate der K⁺-Translokation durch KtrB von Na⁺ nicht beeinflusst wurde. Stattdessen könnte die Anzahl der K⁺-Bindestellen in KtrB erhöht sein, was durch die erhöhten Peakströme nahegelegt wird. Um den sekundären Effekt von Na⁺ auf das KtrAB-System zu untersuchen, wurden K⁺-Aufnahmeaktivitäten in intakten Zellen bei verschiedenen Na⁺-Konzentrationen durchgeführt, und die jeweiligen V_{max}- und K_M-Werte wurden bestimmt. In Übereinstimmung mit früheren Messungen wurde festgestellt, dass eine Erhöhung der Na⁺-Konzentration zu erhöhten V_{max}-Werten führte. Gleichzeitig kam es zu einer 20-fachen abnahme des K_Ms von 1 mM auf 37 μM. Dieser K_M ist vergleichbar mit dem durch ITC ermittelten K_D für K⁺. Zusammenfassend moduliert Na⁺ nicht nur die Affinität für K⁺ zu KtrAB, sondern beeinflusst auch die Kinetik der K⁺-Aufnahme, wahrscheinlich durch Stabilisierung der offenen Konformation der Intramembranschleife und minimiert somit den geschwindigkeitsbestimmenden Schritt der K⁺-Translokation.

Der Hinweis auf eine potenzielle Na⁺-Bindungsstelle in KtrB wurde aus ungezielten MD-Simulationen von KtrB in Betracht gezogen. Diese MD-Simulationen ergaben eine potenzielle Kationenbindestelle, welche von Q93 in D1M2, E149 in D2M1 und N182 in D2P-Helix gebildet wurde. Interessanterweise befindet sich diese Stelle in der Nähe der Intramembranschleife, und daher könnte die Na⁺-Bindung an dieser Stelle die Regulation der K⁺-Translokation beeinflussen. Wachstumskomplementationen mit *E. coli* LB2003 bei verschiedenen K⁺-Konzentrationen wurden verwendet, um die Auswirkungen von Mutationen an der potenziellen Bindungsstelle auf KtrB und KtrAB zu untersuchen. Es wurde erwartet, dass Zellen, die KtrB-Varianten exprimieren, typischerweise wachsen, da die Translokationsaktivität von KtrB nicht von Na⁺ abhängt. Für Zellen, welche KtrAB-Varianten exprimieren, wurde ein Wachstumsdefizit für spezifische Mutanten erwartet. Während alle KtrB-Varianten das Wachstum von LB2003 ermöglichten, zeigten Q93L und E149K in KtrAB Wachstumsdefizite bei niedrigen K⁺-Konzentrationen. Insofern, dass es sich tatsächlich um die Na⁺-Bindungsstelle handelt, könnte die Mutation Q93L

die Koordination des Natriumions beeinträchtigt haben, während E149K vermutlich die Na⁺-Bindung vollständig aufgehoben hat.

Zusammenfassend deckten die in dieser Arbeit erhaltenen Daten das einzigartige Ionenbindungs- und Translokationsprofil von KtrAB auf, das durch den außergewöhnlich gestalteten Selektivitätsfilter zusammen mit der ungewöhnlichen Intramembranschleife definiert wird. Die Präsenz von Na⁺ stimuliert sowohl die K⁺-Bindung als auch die Translokation, was zu der essenziellen K⁺-Über-Na⁺-Selektivität führt. In KtrB wurde eine potenzielle Na⁺-Bindungsstelle identifiziert, die möglicherweise eine weitere strukturelle Charakterisierung der regulatorischen Auswirkungen von Na⁺ ermöglicht.

III. Declaration of scientific collaborations

Except where stated otherwise by reference or acknowledgment, the work presented was generated by myself under the supervision of my advisors during my doctoral study. All contributions from colleagues are explicitly referenced in the thesis. The figures listed below were obtained in the context of collaborative research:

Figure 17 LILBID spectra of KtrB in SMALPs. Adapted from Hellwig *et al.* 2018. LILBID-MS spectra of KtrB/SMALP complex using a soft mode (low laser power, 10 mJ) and harsh mode (high laser power, 18 mJ) were compared. The soft laser mode yielded different charged states of the protein/SMALP-complex (indicated with 5-, 4-, 3-, 2- and 1-), while the harsh mode revealed different charged states of only the monomeric protein (indicated with 3-, 2- and 1- in orange). Sample preparation was performed by Vedrana Mikusevic, Institute of Biochemistry, Goethe-University Frankfurt. LILBID-MS analysis was performed by Dr. Oliver Peetz and Dr. Nils Hellwig, Institute of Physical and Theoretical Chemistry, Goethe-University Frankfurt.

Figure 39 MD simulations revealed a second cation binding site within the membrane plane. (a) MD simulations on the influence of cations on the intramembrane loop (red) revealed a second binding site for cations within the membrane plane. It is located at the height of the intramembrane loop and (b-c) mainly formed by residues Q93, E149 and N182. MD simulations were performed by Dr. Ahmad Reza Mehdipour, Department of Theoretical Biophysics, Max Planck Institute of Biophysics in Frankfurt.

Figure 43 Comparison of the simulated closed and open state of KtrB's intramembrane loop. MD simulations on the flexibility of the intramembrane loop show a closed (purple, left) or open (red, center) state in comparison with the loop positions in the x-ray structure (right, modeled on pdb: 4J7C) in a 1 μ s simulation. The intramembrane loop impedes on the hydration of the cavity below the selectivity filter. MD simulations were performed by Dr. Ahmad Reza Mehdipour, Department of Theoretical Biophysics, Max Planck Institute of Biophysics in Frankfurt.

Whenever a figure, table or text is identical to a previous publication, it is stated explicitly in the thesis that copyright permission and/or co-author agreement has been obtained.

1. Introduction

1.1 Biological Membrane

Biological membranes are composed of lipids, membrane proteins, and carbohydrates, which form a very efficient barrier, separating the cell's interior from the outside. Their semi-permeable nature allows the flow of some substrates into cells while excluding others. For the balance of nutrients, ions and other substrates, biological membranes harbor different types of integral and peripheral membrane proteins. These are incorporated in the lipid bilayer composed of hundreds of different lipids (Alberts, B., Wilson, J. H. and Hunt, 2008). The lipid to protein ration (LPR) of a membrane can vary between one and four depending on the cell type or organism. The LPR in bacterial membranes varies from two to three in most cases. Some proteins and lipids are occasionally covalently bound to carbohydrates (Guidotti, 1972).

1.1.1 Electrical properties of biological membranes

Under physiological conditions, membranes are nearly impermeable for ions without the aid of specific proteins. Active transport of charged substrates and the regulated opening of ion channels are the reasons why cells can keep gradients across the membrane and establish a membrane potential. This potential is composed of an electrical gradient due to the separation of charges and a chemical gradient established by unevenly distributed ion species. Only if both the electrical and the chemical gradient are dissipated, the diffusion equilibrium is reached, and the electrochemical gradient is zero. To describe the diffusion of a specific ion and its presiding equilibrium potential the Nernst-Equation (Nernst, 1889) is used:

$$E_m = E_1 - E_2 = \frac{RT}{zF} \ln \left(\frac{[c]_2}{[c]_1} \right)$$

Here R is the universal gas constant ($R = 8.314 \text{ J}/(\text{mol}\cdot\text{K})$), T is the absolute temperature in Kelvin [K], z is the charge of the specific ion and F is the Faraday constant ($F = 96485.35 \text{ C}/\text{mol}$). $[c]_i$ and $[c]_o$ represent the internal and external ion concentrations, respectively. A negative inside equilibrium potential of for example -120 mV is equivalent to the same voltage. Different ion species can, therefore, be presented as:

$$E_{[K^+]} = \frac{RT}{F} \ln \left(\frac{[K^+]_a}{[K^+]_i} \right)$$

$$E_{[Na^+]} = \frac{RT}{F} \ln \left(\frac{[Na^+]_a}{[Na^+]_i} \right)$$

$$E_{[Cl^-]} = \frac{RT}{F} \ln \left(\frac{[Cl^-]_i}{[Cl^-]_a} \right)$$

The total membrane potential is made up of the sum of the different equilibrium potentials of each ion species multiplied by their respective permeability. Because membranes are usually permeable for more than just one ion species, another model to describe the membrane potential needs to be adduced. The Goldman-Hodgkin-Katz equation (Goldman, 1943; Hodgkin and Katz, 1948) is the best approximation since it includes the permeability coefficients P for the different ions:

$$V_m = \frac{RT}{F} \ln \left(\frac{\sum P_K c_o^K + \sum P_A c_i^A}{\sum P_K c_i^K + \sum P_A c_o^A} \right)$$

To better understand the membrane impermeability, it can be considered as part of an electric circuit. The hydrophobic core of the lipid bilayer serves as a resistor with high electric resistance ($R = U/I$ [Ω]; here U is the voltage [V] and I is the current [A]) or low electric conductance ($g = 1/R$ [S]) separating two electrolyte solutions from each other. Additionally, biological membranes show behavior of a plate capacitor with a respective capacitance of $C = \epsilon \epsilon_0 A/d$ [F]. The hydrophobic core of the membrane molds a dielectric layer, while the electrolyte solutions on both sides of the bilayer can be considered capacitor plates. Consequently, the surface area on one side of the capacitor plate (A), the dielectric constant of the hydrocarbon core of the membrane (ϵ), and the permittivity constant (ϵ_0) are directly proportional to the capacitance C , while the space distance between the plates (d , given by the membrane) is inversely proportional. Therefore, the lipid bilayer serves as a selective barrier for all big hydrophilic and/or charged molecules, similar to nonpolar solvents (Bretschneider and de Weille, 2006). This selectivity is achieved by a low relative permittivity ϵ_r of the hydrocarbon core of the membrane (~ 2), compared to the relative permittivity of the surrounding water (~ 80) as a polar solvent. The required energy for moving an ion into a low-dielectric reaction field is very high and is described by the Born energy (Neumcke and Lauger, 1969). An extremely high Born energy implies a very low permeability and can be overcome by

locally lowering the energy barrier. This is accomplished by membrane integral proteins such as channels or transporters, which mediate the selective transport of substrates.

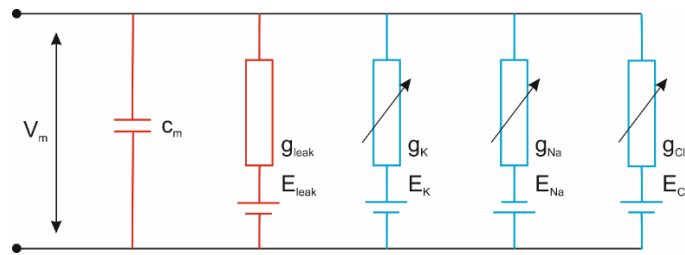


Figure 1 Representation of the equivalent electric circuit model. The membrane may be considered a parallel circuit of an ohmic resistor and a capacitor (RC element). Capacitor and resistor of the membrane and leak current are shown in red, while the capacitor and resistor of K^+ , Na^+ and Cl^- channels are shown in blue. V_m indicates the membrane potential, g the conductance and E the equilibrium potential of the ion species.

As both the membrane resistance (R_m) and the membrane capacitance (C_m) occur over the cell membrane, they are electrically parallel. Consequently, a membrane can be regarded as RC element in a parallel circuit. Channels and transporters change the electric properties of the membrane, which can be described by extending the RC element by other in parallel-connected RC elements (Figure 1) (Hodgkin and Huxley, 1952a). Ion channels are viewed as a series connection of voltage sources and resistors. Applying an electrochemical gradient across the membrane increases its resistance. Channel opening, in turn, reduces the resistance, and the translocation is in linear correlation with the transmembrane potential. The difference in ion distribution across the bilayer defines the membrane potential (Bretschneider and de Weille, 2006). Ion pumps and channels generate this difference.

1.2 Ion transport across biological membranes

Some molecules can just diffuse in and out of the cell, while others need appropriate structures to get across the membrane. A lot of molecules even need an energetic push to get in or out of the cells. Small nonpolar molecules can usually diffuse across the membrane, while charged substrates like ions need assistance. Ions, since they are either positively or negatively charged, tend to prefer hydrophilic environments such as water as a solvent despite their small size. Ion transport across the membrane does not happen spontaneously, because the inner core of the bilayer is very hydrophobic. This results in a low dielectric field with a high Born energy making it unfavorable for ions to be placed inside (Parsegian, 1969). Therefore, ions rely on membrane-integral proteins

to provide a hydrophilic environment for their passage in an otherwise hydrophobic membrane.

1.2.1 Main principles of membrane transport

There are two vital principles of moving molecules across cell membranes, passive fluxes and active transport (Figure 2). Both allow the movement of substrates across the otherwise impermeable lipid bilayer by lowering the high energy barrier. Passive transport, namely facilitated diffusion, does not require energy, while active transport does (Voet and Voet, 2011).

Active transport or the “uphill” movement of substrates can be further separated into primary or secondary active transport. Transporters that use a primary energy source such as light or ATP hydrolysis to move a substrate against its electrochemical gradient are called primary active transporters. Secondary active transporters move more than one substrate across the membrane. They usually facilitate the uphill movement of one substrate by the downhill movement of another in a symport or antiport fashion.

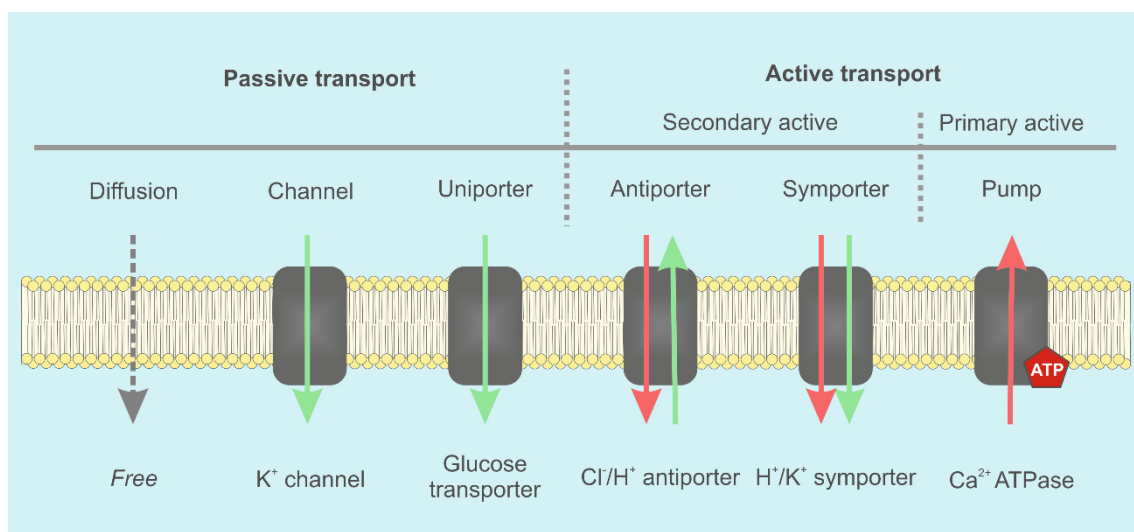


Figure 2 Overview of the different transporter classes. For each transporter class a typical example is shown. Transport processes along the electrochemical gradient are marked with green arrows, those against the electrochemical gradient with red arrows and simple diffusion is indicated by a grey arrow.

Facilitated passive transport allows molecules to diffuse over the membrane along their electrochemical gradient in the so-called “downhill” movement. Uniporters structurally resemble secondary active transporters, but instead of coupling a second substrate for active transport, they facilitate the movement of the substrate along its electrochemical

gradient. The translocation rate resembles that of a secondary active transporter (Wolfersberger, 1994). Channels or uniporters allow passive transport of a particular ion species across membranes through selective pores by lowering the energy barrier of the membrane for facilitated diffusion. The transport rates of channels are usually much faster (greater than 10^6 s^{-1}) than those of transporters ($1\text{-}1000 \text{ s}^{-1}$) (Ashcroft, Gadsby and Miller, 2009). This discrimination is, however, not always reliable since there are low-conducting channels and there can be transporter with high-turnover (Gadsby, 2009). Directionality and speed of transport depend on the ion species and the regulation of the open vs. closed state of the channel. One of the most famous channel examples is the bacterial K^+ channel KcsA from *Streptomyces lividans* (Doyle *et al.*, 1998).

1.2.2 Biological significance of K^+ and Na^+ distribution

Generally, all cellular organisms rely on a defined distribution of substrates across their bilayer for survival. Two cations that are of significant importance to cell function are potassium and sodium from the first group of elements. Concentrations of those two cations are usually kept at different levels between the inside and outside of cells. In almost all cells, K^+ is the central intracellular cation, while Na^+ is predominantly kept on the extracellular side. Their positive charges make these two ions impermeable to the membrane, and they can only cross the bilayer with the help of specific proteins. The partitioning and tightly regulated passage of K^+ and Na^+ is fundamental for normal cell function. Sodium, as the most abundant extracellular cation, is usually present in 10-fold excess on the outside compared to the inside (Purves *et al.*, 2001), while K^+ ions are accumulated ~ 100 -fold inside the cells resulting in high millimolar concentrations (Meury and Kepes, 1981). Low internal Na^+ and high K^+ concentrations in mammals are mostly maintained by active pumps like the Na^+/K^+ ATPase (Kaplan, 2002). Many other organisms have different systems to uphold this ion distribution; particularly secondary active Na^+/H^+ exchangers (Padan and Schuldiner, 1993; Dibrova *et al.*, 2015) together with K^+ channels (Ryan *et al.*, 2010) and members of the superfamily of K^+ transporter (SKT) (Rubio, Gassmann and Schroeder, 1995; Nanatani *et al.*, 2015) keep the K^+/Na^+ homeostasis in balance. Here, the highly abundant Na^+/H^+ exchangers play a crucial role in pH and Na^+ homeostasis (Dibrova *et al.*, 2015), but dependent on the organism or location, they fulfill different duties. In mammals, NHE exchangers are specialized in extruding protons by using a Na^+ gradient regulating the cellular pH (Donowitz, Ming Tse and Fuster, 2013), while in bacteria the H^+ gradient is used to remove intracellular Na^+ via NhaA and NhaB (Pinner *et al.*, 1993; Taglicht, Padan and Schuldiner, 1993).

Additionally, some specialized proton motive force-independent primary active Na^+ pumps like the Na^+ -translocating oxaloacetate decarboxylase or the Na^+ -translocating NADH:ubiquinone oxidoreductase export Na^+ ions (Dimroth, 1980; Tokuda and Unemoto, 1982). To accumulated K^+ , most prokaryotic and simple eukaryotic organisms use specific systems, which are absent in mammals. These systems are members of the superfamily of K^+ transporters, Trk, Ktr, Kdp, and HKT (Durell *et al.*, 1999; Levin and Zhou, 2014; Diskowski *et al.*, 2015) and members of the secondary active transporters Kup family (Grabov, 2007).

Na^+ and K^+ together are essential for maintaining the electrolyte balance. The resting membrane potential of eukaryotic cells is generally maintained by upholding K^+/Na^+ homeostasis, which is mostly dominated by the high permeability of K^+ (Hodgkin and Horowicz, 1959). Keeping the internal Na^+ concentrations low is further required for Na^+ to facilitate the uphill transport of different substrates into the cells via secondary active transport. In neurons, the Na^+ influx generates an action potential upon signal perception. In contrast, the efflux of K^+ is essential for the hyperpolarization to end the action potential (Purves *et al.*, 2001). Further, K^+ serves the regulation of the cell volume (Meury, Robin and Monnier-Champeix, 1985; Tivey, Simmons and Aiton, 1985), has a vital role in the preservation of the pH homeostasis (Adler and Fraley, 1977; Ochrombel *et al.*, 2011) and is required for the activation of several enzymes (Evans and Sorger, 1966; Suelter, 1970), including the ribosomes (Rozov *et al.*, 2019). Particularly prokaryotes, plants and yeasts rely on high internal K^+ concentrations because they are often facing drastically changing environmental conditions. While the resting membrane potential in bacteria is mostly established by the H^+ gradient resulting from the respiratory chain (Mitchell, 1961; Saraste, 1999), particularly the regulation of the cytoplasmic pH (Bakker and Mangerich, 1983; Kroll and Booth, 1983; Booth, 1985; Ochrombel *et al.*, 2011), and maintaining of the turgor pressure (Schultz, Epstein and Solomon, 1963; Hastings and Gutknecht, 1978) by the uptake and release of K^+ are essential. Recent studies also suggested that K^+ fluxes are crucial for electrical signaling within bacterial communities (Liu *et al.*, 2017; Stratford *et al.*, 2019).

1.3 Ion channels

While active transporters bind their substrate and present it to the other side by an alternating access mechanism, channels form pores in the membrane. These pores are usually selective for a certain ion species and often can be gated allowing the opening

and closing of the pore. Because ion channels do not undergo large conformational changes, they usually provide fast ion fluxes between 10^6 to $\sim 10^9$ molecules per second (Ashcroft, Gadsby and Miller, 2009).

1.3.1 K^+ channels and their architecture

Almost 70 years ago, Hodgkin and Huxley proposed that the ionic conductance across excitable membranes correlates to changes in both Na^+ and K^+ permeability (Hodgkin and Huxley, 1952a, 1952c, 1952b, 1952d) which was attributed to ion channel function (Hodgkin and Keynes, 1955). A few years later, the first K^+ channel gene was cloned, which revealed the amino acid sequence for the Shaker K^+ channel from *Drosophila melanogaster* (Kamb, Tanouye and Tseng-Crank, 1988; Pongs *et al.*, 1988; Tempel, Jan and Jan, 1988). This research has spurred many functional and later also structural studies on K^+ channels. Soon most K^+ channels were predicted to be tetramers (MacKinnon, 1991) and the -TVGYG- motif (Figure 3 a-c), known as the signature sequence, was identified to be responsible for the K^+ selectivity (Heginbotham, Abramson and MacKinnon, 1992; Heginbotham *et al.*, 1994). All these data were confirmed by the publication of the first x-ray structure of the bacterial K^+ channel KcsA from *Streptomyces lividans*, for which the Nobel Prize in Chemistry was awarded to Roderick MacKinnon in 2003 (Doyle *et al.*, 1998; Zhou *et al.*, 2001).

Up until today, most transmembrane domains of K^+ channels share a common architecture. The pore-forming motifs are defined by two transmembrane (TM or M) helices linked by a pore (P)-helix (Figure 3). Four of these TM1-P-TM2 motifs form a channel by organizing around a fourfold or pseudo-fourfold symmetry axis, which provides the ion permeation pathway. Despite this typical architecture, three groups of ion channels are known, the 2TM/P, the 4TM/2P and the 6TM/P K^+ channels (Figure 3 d) (Kubo *et al.*, 1993; Lesage *et al.*, 1996). In 2TM/P channels, each subunit consists of two TM helices flanking a P-helix (M1-P-M2). Subunits of this group make up the homotetrameric inward-rectifying K^+ channels (Kir), of which currently seven subfamilies (Kir1- Kir7) are known (Hibino *et al.*, 2010). 4TM/2P channels are homodimers formed by two subunits with each two P-regions and four TM-helices, hence two covalently linked M1-P-M2 motifs. Channels exhibiting this type of structure are known as “leak” K^+ channels (Goldstein *et al.*, 1998). Subunits of 6TM/P channels also contain of only one M1-P-M2 motif, also referred to as S5-P-S6. However, N-terminally, the 6TM/P proteins have four (S1-S4) additional TM helices attached. A homotetramer forms a channel.

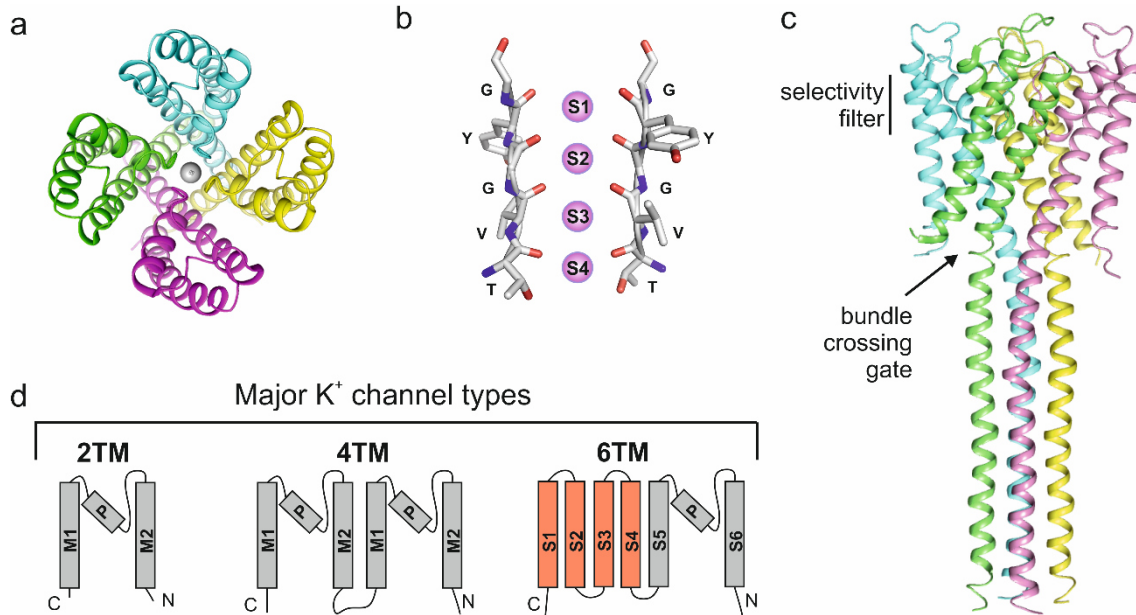


Figure 3 Topology of the three main K⁺ channel types and general features illustrated on KcsA. (a) Top view of the structure of the tetrameric KcsA from *Streptomyces lividans* (pdb:3EFF), subunits colored in yellow, pink, green, and blue, respectively. (b) Selectivity filter of KcsA showing the -TVGYG- signature sequence with K⁺ binding sites, S1 to S4, shown as purple spheres. (c) Side view of full-length of KcsA with the selectivity filter as indicated close to the extracellular side. Further, the bundle crossing gate restricts the ion permeation at the intracellular side. (d) Topology model of 2TM/P, 4TM/2P, and 6TM/P channel subunits. Non-pore-forming transmembrane helices are shown in red.

Functionally, many 6TM/P channels form voltage-gated K⁺ channels (Kv) (Kim and Nimigeon, 2016). All three groups of K⁺ channels can have either C- or N-terminally fused domains or auxiliary subunits, controlling the ion fluxes (Coetzee *et al.*, 1999; Biggin, Roosild and Choe, 2000). P channel subunits. Non-pore-forming transmembrane helices are shown in red. Within the described classes of K⁺ channels generally two main features are important for controlling ion permeation. One is the above mentioned K⁺ selectivity filter motif with the -TVGYG- signature (Heginbotham, Abramson and MacKinnon, 1992; Heginbotham *et al.*, 1994), and the other is a mostly intracellularly located channel gate (Doyle *et al.*, 1998; Liu, Sompornpisut and Perozo, 2001; MacKinnon, 2003). Both features create a physical barrier for the ions (Liu, Jurman and Yellen, 1996; Liu *et al.*, 1997; del Camino and Yellen, 2001). The physical barrier created by the intracellular gate is of hydrophobic character (Uysal *et al.*, 2009), mostly formed by hydrophobic parts of helices M2 (S6) generating a constriction known as the bundle crossing gate (Labro and Snyders, 2012; Kim and Nimigeon, 2016) (Figure 3 a). Details about the restrictions by the selectivity filter (Figure 3 d) will be discussed in the next section (1.3.2).

1.3.2 Selectivity filter tailored for K⁺

The general concept of channel selectivity is that one specific ion is selected for and can permeate at fast rates, while all other ions are excluded. K⁺ channels have a specific feature that helps them to select for the “right” kind of ion, K⁺. This feature is provided by the -TVGYG- amino acid sequence, which is conserved in almost all K⁺ channels (Heginbotham, Abramson and MacKinnon, 1992; Heginbotham *et al.*, 1994). The backbone carbonyl oxygens of the -TVGYG- residues shape the narrowest part of a K⁺ channel pore. Very early studies already proposed a multi-stage mechanism for K⁺ translocation (Hille, 1973) without structural evidence. This hypothesis was further strengthened by barium (Ba²⁺) block experiments on BK K⁺ channels (Neyton and Miller, 1988a, 1988b), proposing at least four binding sites in a selectivity filter (SF). The first ion channel structure was that of the K⁺ channel KcsA from *Streptomyces lividans* (Doyle *et al.*, 1998; Zhou *et al.*, 2001). It revealed precisely four consecutive binding sites (S1-S4) coordinating K⁺ ions stripped of water molecules (Figure 4) as predicted beforehand (Hille, 1973; Neyton and Miller, 1988b, 1988a). It was further suggested that the arrangement of carbonyl groups is perfectly fitted for K⁺ ions, but not for the 0.38 Å smaller Na⁺ (Doyle *et al.*, 1998; Hille, Armstrong and MacKinnon, 1999; Zhou *et al.*, 2001). Hence, the selectivity filter would ideally coordinate K⁺, while the carbonyl groups would be too far apart to coordinate the smaller Na⁺ (Bezannilla and Armstrong, 1972). This model was termed the “snug-fit” model. Even though the “snug-fit” model is common textbook knowledge, it does not account for the inherent flexibility of the protein since it assumes a rigid selectivity filter. In contrast, computational approaches suggested that selectivity mainly originates from the intrinsic flexibility of the distinct binding sites in the selectivity filter (Noskov, Bernéche and Roux, 2004; Noskov and Roux, 2006).

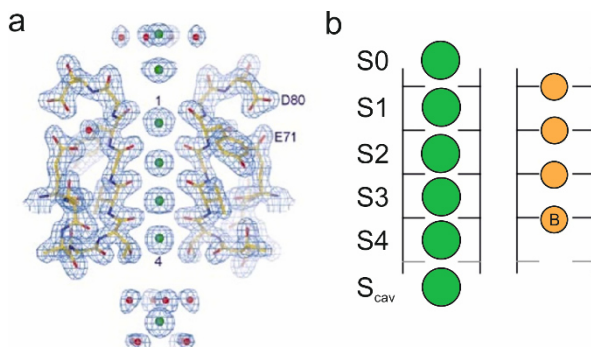


Figure 4 K⁺ channel selectivity filter binding. (a) Electron density from the high-resolution structure of the K⁺ channel KcsA. K⁺ ions (green) and water molecules (red) are shown along the permeation pathway in the center. Adapted from Zhou *et al.*, 2001. (b) Illustration of hypothetical K⁺ (green) and Na⁺ (orange) positions in the selectivity filter. Adapted from Nimigean and Allen, 2011.

This flexibility could also explain why K⁺ channels are not entirely flawless. Some K⁺ channels were shown to also conduct Na⁺, although at considerably lower rates. For KcsA, a binding site for Na⁺ or Li⁺ was identified in the selectivity filter between S3 and

S4 binding the smaller ion in the carbonyl oxygen plane (Thompson *et al.*, 2009). This B-site was shown to constrain the binding and conductance of K⁺ (Shrivastava *et al.*, 2002; Thomas, Jayatilaka and Corry, 2007). Na⁺ coordination in the narrow SF is believed to be challenging due to the high energy required to de-solvate the smaller, borderline kosmotropic cation (Collins, 1995). The physicochemical properties of the channel-ion interaction have greatly been debated over the last decades, trying to explain selectivity. Several experiments on K⁺ channels all come to the same conclusion that K⁺ ions are preferred over Na⁺ ions at equilibrium. X-ray crystallography showed that small amounts of K⁺ can outcompete Na⁺ within the selectivity filter (Morais-Cabral, Zhou and MacKinnon, 2001; Zhou *et al.*, 2001; Zhou and MacKinnon, 2003; Thompson *et al.*, 2009). K⁺ preference at equilibrium was also shown by atomistic molecular dynamic (MD) simulations and free energy calculations (Åqvist and Luzhkov, 2000; Noskov and Roux, 2006; Varma and Rempe, 2007; Egwolf and Roux, 2010; Kim and Allen, 2011). Electrophysiology experiments using a Ba²⁺ block still showed preferred K⁺ binding (Neyton and Miller, 1988a; Piasta, Theobald and Miller, 2011) to the selectivity filter at equilibrium and so did isothermal calorimetry experiments (ITC) experiments using mixed ion conditions (Lockless, Zhou and MacKinnon, 2007; Liu, Bian and Lockless, 2012; Liu and Lockless, 2013) and many more (Baukrowitz and Yellen, 1996; Bhate *et al.*, 2010; Imai *et al.*, 2010). However, equilibrium binding to the selectivity filter cannot be the only determinant of selective ion translocation.

Previous studies showed that reducing the number of binding sites to 3 or 2 also reduces the K⁺ over Na⁺ selectivity (Zhou and MacKinnon, 2004; Derebe *et al.*, 2011). The non-selective channels NaK (Alam and Jiang, 2009b, 2009a), with two instead of four binding sites (Figure 5), was shown to thermodynamically prefer K⁺ over Na⁺ in its selectivity filter (Liu and Lockless, 2013), while still presenting non-selective conductance (Liu and Lockless, 2013; Sauer *et al.*, 2013). This indicated that the number of consecutive binding sites could be crucial. Replacing the SF of NaK with one of eukaryotic cyclic nucleotide-gated (CNG) channels gained an additional binding site (S2), leading to a slightly increased K⁺ preference (Derebe *et al.*, 2011; Sauer *et al.*, 2013; Kopec *et al.*, 2018). In contrast, channels having four consecutive binding sites always showed a high selectivity for K⁺ over Na⁺. Hence, all four ion binding sites (S1-S4) provided by the TVGYG scaffold are required for selective ion translocation. Recent structural and MD studies are in agreement with this premise and showed that direct contacts of ions sitting in neighboring SF sites initiate fast K⁺ conductance (Köpfer *et al.*, 2014; Kopec *et al.*, 2018) and account for the conductance near diffusion limit. This multi-ion mechanism assuming a Coulomb knock-on was already proposed more than half a century ago by

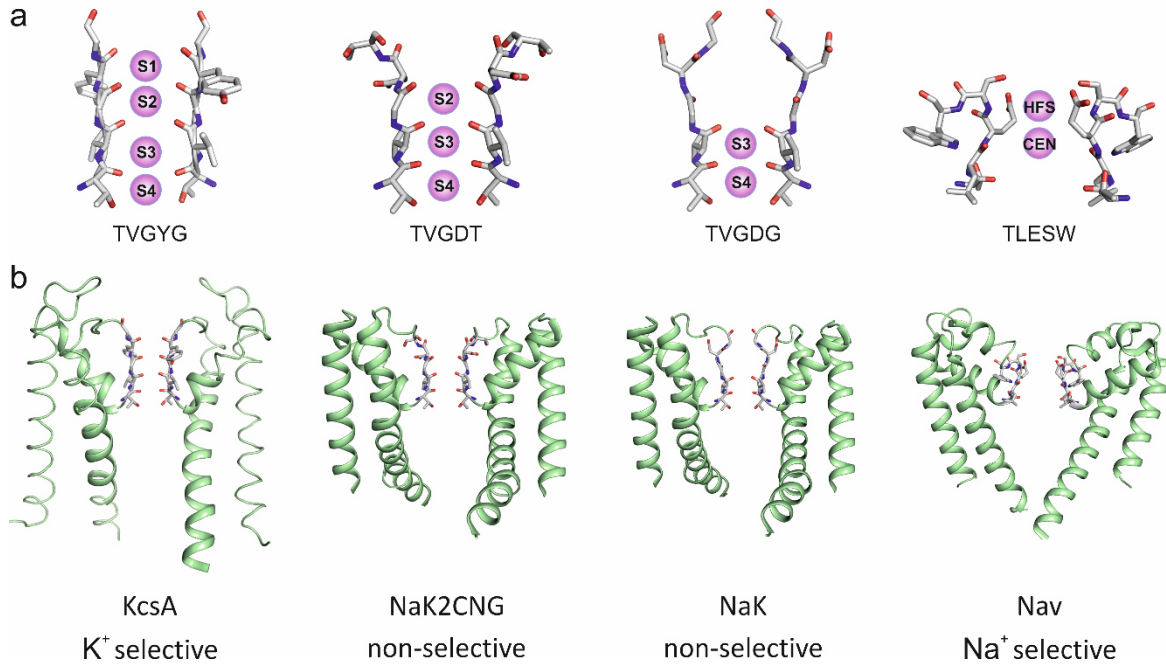


Figure 5 Structures of K⁺ selective, non-selective and Na⁺ selective channels. Comparison of the selectivity filter structures and the overall structures of KcsA (pdb:3EFF), NaK2CNG (pdb:3K0D), NaK (pdb:3E8F) and Nav (pdb:4F4L). (a) Selectivity filters of high to low K⁺ over Na⁺ selective channels from left to right, respectively. Relevant cation binding sites are indicated by purple spheres. (b) Comparison of the overall structures (green) of KcsA, NaK2CNG, NaK and Nav from left to right.

Hodgkin and Keynes (Hodgkin and Keynes, 1955).

Yet, there is also a drawback in explaining selectivity solely based on the number of binding sites in a row, since the whole selectivity filter region needs to be considered. It was shown that by keeping the SF sequence and mutating residues close by the filter, selectivity, conductance, and C-type inactivation were influenced (Starkus *et al.*, 1997; Cordero-Morales *et al.*, 2006, 2011; McCoy and Nimigeon, 2012). Further, there is a family of K⁺ channel-like proteins with imperfect selectivity filters, namely the superfamily of K⁺ transporters (SKT, described in section 1.4). Some of the SKT members were shown to be somewhat selective, despite their SFs being formed by nonidentical sequences compared to the canonical selectivity filters. Structures of three of these members, TrkH (Cao *et al.*, 2011, 2013), KtrB (Vieira-Pires, Szollosi and Morais-Cabral, 2013; Diskowski *et al.*, 2017) and KdpA (Huang, Pedersen and Stokes, 2017; Stock *et al.*, 2018) reveal SFs with only one binding site. While TrkH was shown to be non-selective (Cao *et al.*, 2011, 2013), KdpA and KtrB were proposed to be very selective (Tholema *et al.*, 1999; Durell, Bakker and Guy, 2000; Van der Laan, Gaßel and Altendorf, 2002). Consequently, the SKT family challenges the described criteria for selectivity since its members appear to have less than four binding sites, and some potential binding sites seem to be less ideal in terms of the coordination distances of K⁺ while still being selective for them.

1.4 Superfamily of K⁺ transporters

The superfamily of K⁺ transporters is a group of K⁺ channel-like proteins present in all kingdoms of life excluding animals. Members of this superfamily are the eukaryotic Trk1/2 from fungi, HKT1/2 from plants and the prokaryotic KtrB/D, KdpA and TrkG/H (Figure 6). The eukaryotic members are single-subunit systems, while the prokaryotic members organize with additional proteins into multi-subunit systems. With or without the additional subunits, SKT members function as channels, primary or secondary active transporters, while structurally resembling ion channels. All SKT members presumably evolved from ancestral, simple 2TM-K⁺ channels, like the homotetrameric KcsA from *S. lividans*, by gene duplication and fusion (Durell *et al.*, 1999; Durell, Bakker and Guy, 2000; Hänel *et al.*, 2011). The resulting four covalently linked M1-P-M2 motifs are organized into four domains (D1-D4) around a central axis forming the ion permeation pathway. The different domains of each protein vary in length and amino acid sequence. KdpA and TrkH/G have two additional transmembrane helices (Durell *et al.*, 1999; Durell, Bakker and Guy, 2000). These additional helices are flanking the core domains D1 to D4 and are attached to the N-terminal end of D1, respectively. The selectivity filter sequences, which are found in the loops between the P-helices and the M2 helices, are poorly conserved compared to the canonical K⁺ selectivity filters (Diskowski *et al.*, 2015). Most SKT members have only one conserved glycine residue per P-loop. All prokaryotic members of the SKT family, KtrB/D, KdpA and TrkH/G, have additionally a conserved intramembrane loop formed by broken helix D3M2 located below the selectivity filter, which constricts the pore and participates in ion gating (Durell *et al.*, 1999). This loop is mostly comprised of small polar residues flanked by glycines, except in KdpA where it is composed of non-polar residues. This suggests a different function of the loop for KdpA (Stock *et al.*, 2018) in comparison to its gating function in KtrB/D and TrkH/G (Diskowski *et al.*, 2015). All SKT members contain a conserved arginine residue located in D4M2. It was shown to be essential for activity (Becker *et al.*, 2007; Kato *et al.*, 2007; Cao *et al.*, 2011) and suggested to be involved in gating of KtrB (Diskowski *et al.*, 2017). Of the SKT members, the eukaryotic members Trk1/2 and HKT1/2 are not known to form complexes with further regulatory subunits. Despite their channel-like structures they were proposed to function as K⁺/Na⁺ symporters (Rubio, Gassmann and Schroeder, 1995; Rubio *et al.*, 1999) but further details about active transport are missing. KdpA assembles with three additional subunits to a primary active multi-subunit complex, which actively pumps K⁺ upon ATP hydrolysis (Altendorf and Epstein, 1994; Altendorf *et al.*, 1998; Bramkamp, Gassel and Altendorf, 2004). The complex is composed of KdpA, the P-type ATPase KdpB, regulatory subunit KdpF and the stabilizing subunit KdpC. The channel-like KdpA and KdpB together provide an ion permeation pathway (Huang, Pedersen and Stokes, 2017; Stock *et al.*, 2018). The other SKT multi-subunit members KtrB/D and TrkH/G form homodimers and assemble

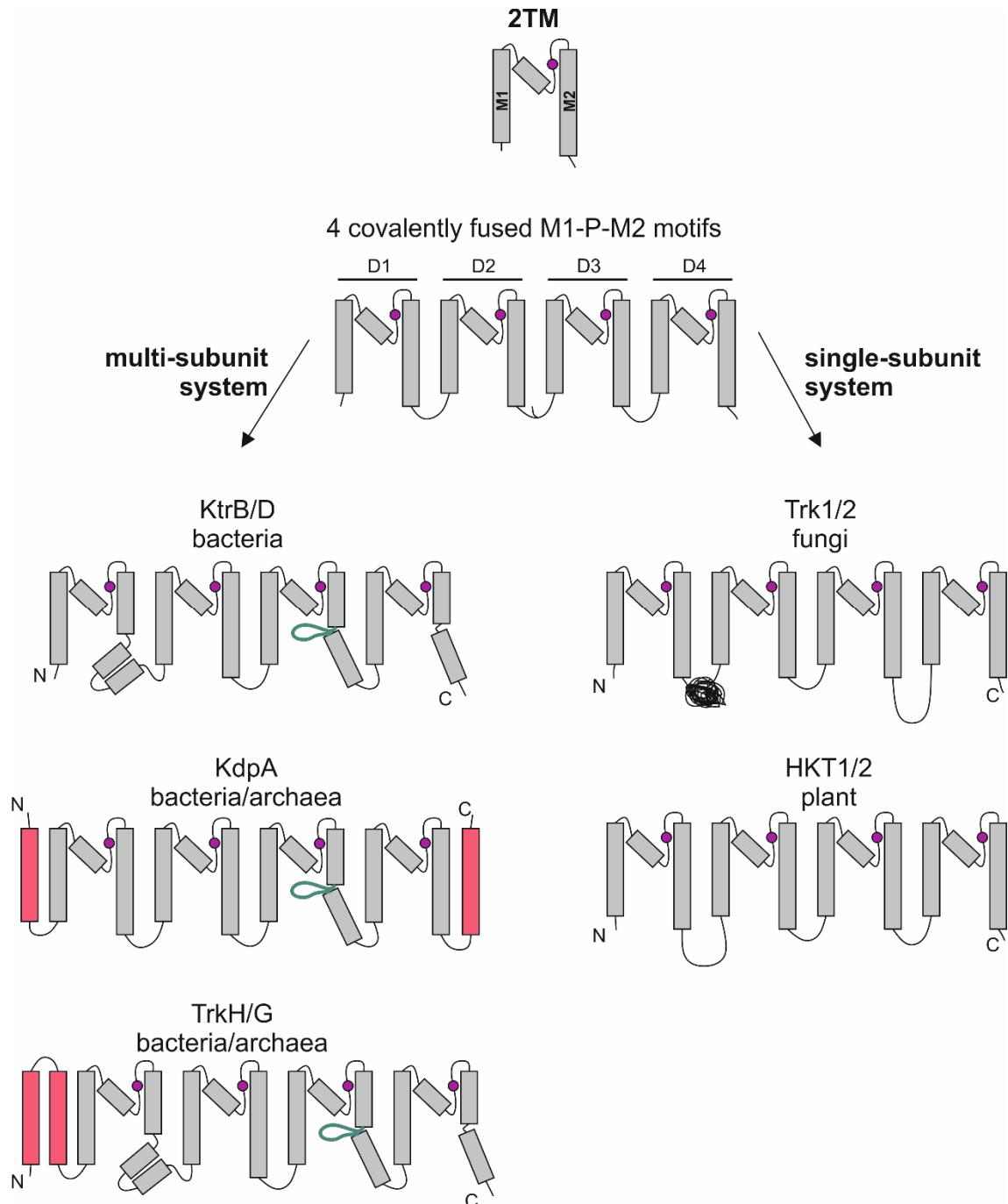


Figure 6 Superfamily of K⁺ transporters (SKT). Members of the SKT likely evolved from ancestral 2TM-type channels by gene duplication and fusion. SKT proteins are formed by four domains (D1-D4), each of which consists of a membrane helix (M1) connected via a pore helix (P) to the second transmembrane helix (M2). Thus, SKT proteins are monomers formed by four M1-P-M2 motifs (in grey). The location of the selectivity filter within the P-loop is shown in purple. The intramembrane loop which might form the gate of prokaryotic members is shown in teal. Additional transmembrane helices are shown in light pink. Bacterial KtrB/D, KdpA and TrkH/G proteins form multimeric complexes with associated cytoplasmic subunits and/or membrane-bound subunits, whereas fungal Trk1/2 and plant HKT1/2 systems are single-subunit systems. Figure adapted from Diskowski *et al.* 2015.

with their regulatory proteins KtrA/C and TrkA, respectively, which all belong to the regulator of K⁺ conductance (RCK) family (Cao *et al.*, 2013; Vieira-Pires, Szollosi and Morais-Cabral,

2013). Consequently, complexes KtrAB, KtrCD, TrkAH and TrkAG likely all function as gated ion channels.

1.5 Regulator of K⁺ conductance (RCK)

The regulator of K⁺ conductance (RCK) family modulates the function of many eukaryotic and prokaryotic K⁺ channels. They are also termed KTNs (K⁺ transport, nucleotide-binding), although not all of them are nucleotide regulated (Jiang, Lee, Chen, Cadene, Brian T. Chait, *et al.*, 2002; Hite *et al.*, 2015). Each RCK domain consists of a conserved N-lobe and a less conserved C-lobe, which are connected by a hinge region. The N-lobe contains the highly conserved Rossmann-fold and those RCK proteins binding nucleotides show a characteristic GxGxxG...D/E motif (Bellamacina, 1996; Jiang *et al.*, 2001). Most RCK proteins are covalently fused as single or tandem domains to the channel they regulate. Others are associated with their respective K⁺ channels as soluble cytoplasmic subunits, which again are made of single or tandem proteins (Schrecker, Wunnicke and Hänelt, 2019). Despite this difference in association, RCK domains/proteins always form dimers, which organize into an “octameric” ring made of four dimers. This ring is then termed the gating ring (Figure 7). The ring-like structure is formed through interactions of the N-lobes, generating a dimer-to-dimer interface.

RCKs are regulated by a large variety of ligands such as the cations Na⁺ (Hite *et al.*, 2015), Ca²⁺ (Jiang, Lee, Chen, Cadene, Brian T. Chait, *et al.*, 2002), Mg²⁺ and Zn²⁺ (Hou *et al.*, 2010) or nucleotides like ATP (Kröning *et al.*, 2007) and ADP (Kong *et al.*, 2012), NAD/NADH (Roosild *et al.*, 2002) and c-di-AMP (Corrigan and Gründling, 2013). Upon ligand binding, the gating ring undergoes a conformational change. When gating a single pore, the ring expands, in contrast, it appears to change between a two-fold and four-fold symmetric conformation when gating two parallel pores. The ligand-induced conformational change is then transferred from the ring to the K⁺ channel by promoting structural movements in the channel domains/subunits in three possible ways or combinations thereof: First, in channels with fused RCK versions, the linker connecting the RCK domains pull open the C-terminus of the respective channel-forming subunit for gating (Jiang, Lee, Chen, Cadene, Brian T. Chait, *et al.*, 2002; Kong *et al.*, 2012; Hite, Tao and MacKinnon, 2017). Second, the interface between the RCK and the channel, both in the fused and associated versions, triggers conformational changes in the pore regions (Cao *et al.*, 2013; Vieira-Pires, Szollosi and Morais-Cabral, 2013; Diskowski *et al.*, 2017). Third, conformational changes in the RCK domains are transferred to the channel via interaction with voltage(like)-sensing domains (Hite, Tao and MacKinnon, 2017; Tao, Hite and MacKinnon, 2017). A detailed, comparative analysis of channel regulation

by RCK domains/proteins can be found in a recent review (Schrecker, Wunnicke and Hänel, 2019).

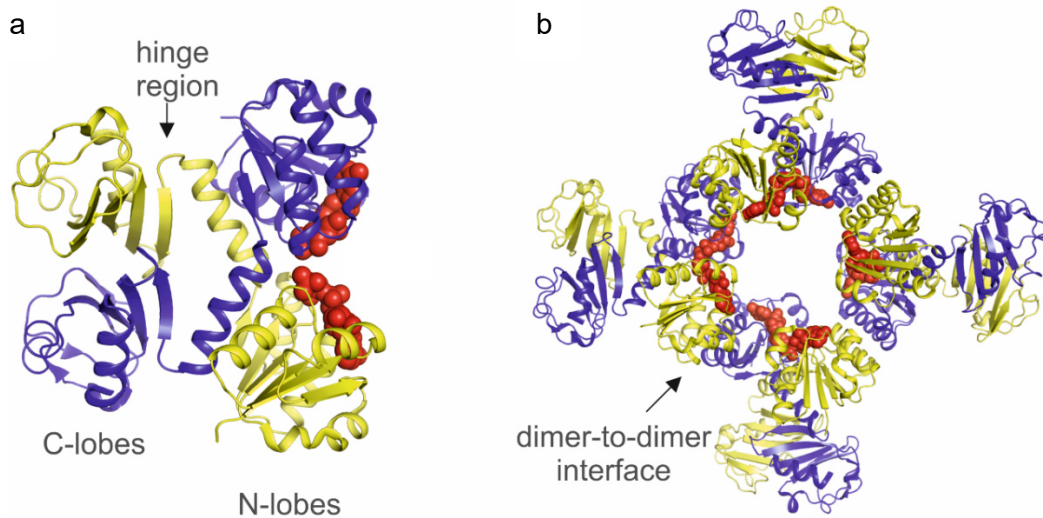


Figure 7 The RCK gating ring of KtrA. (a) Shown are the KtrA dimer (blue and yellow), as the smallest unit of the RCK gating ring, and (b) the respective top view of the octameric gating ring made up of four KtrA dimers (PDB: 4J90). Each dimer has a N- and C-lobe, which crossover via the hinge region. Nucleotides (red) are positioned next to the Rossmann fold. The dimer-to-dimer interface is formed by the N-lobes.

1.6 The Na⁺ and ATP-dependent K⁺ translocating complex KtrAB

In 1998, Nakamura and colleagues first mentioned a new type of K⁺ uptake system from the Gram-negative marine bacterium *Vibrio alginolyticus*. They named it KtrAB since the new K⁺ uptake system showed sequence homology to the K⁺ transport system KtrII from *Enterococcus hirae*. KtrAB consists of the membrane-embedded KtrB, which belongs to the superfamily of K⁺ transporters, and the cytoplasmic KtrA, which is a member of the RCK protein family. KtrB alone was shown to translocate K⁺ and Na⁺ ions. The presence of KtrA confers Na⁺ and ATP dependency, increased transport velocity and K⁺ selectivity to the system (Tholema *et al.*, 1999; Kröning *et al.*, 2007). The architecture of the complex is exceptional when compared to the classical 2-TM K⁺ channel because KtrB assembles into a dimer with two separate pores for K⁺ translocation. The dimer is regulated by a gating ring made of eight soluble KtrA subunits. Thus, unlike most other RCK-gated potassium channels, KtrAB is functioning without a covalently linked RCK domain. The first 3.5 Å crystal structure of KtrAB from *Bacillus subtilis* was published in 2013 by Vieira-Pires *et al.*, revealing the complex in an ATP-bound state (Vieira-Pires, Szollosi and Morais-Cabral, 2013) (Figure 8 a). A few years later, the structural models of the ADP-bound KtrAB complex from *V. alginolyticus* and *B. subtilis* were published (Szollosi *et al.*, 2016; Diskowski *et al.*, 2017) (Figure 8 b), permitting the proposal of gating

mechanisms. The structures revealed essential features, like the selectivity filter, the intramembrane loop and the interaction helix transferring conformational changes from the cytoplasmic ring to the ion translocating subunit. The following sections will outline the findings of the last 21 years since KtrAB's first discovery.

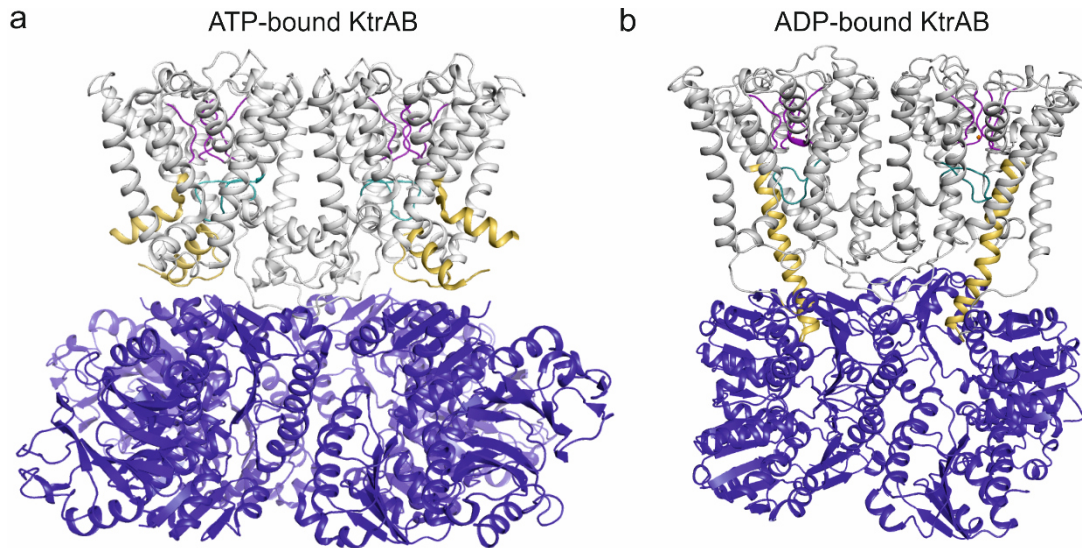


Figure 8. Structural models of KtrAB in the open and closed states. Side views of KtrAB in the (a) ATP-bound (pdb: 4J7C) and (b) ADP-bound conformation (Diskowski *et al.*, 2017) are shown. (a+b) Ion translocating subunit KtrB is shown in light grey with the selectivity filter in purple, the intramembrane loop in teal and interaction helices D1M2b in yellow. The N- and C-lobes of the octameric ring of KtrA are shown in blue. The C-lobes in (b) are missing in the ADP-bound model, they were not resolved.

1.6.1 Selectivity and translocation of K^+ by subunit KtrB

KtrB has, as a member of the SKT proteins, four covalently linked M1-P-M2 domains organized in a pseudo-4-fold symmetry axis forming the ion permeation pathway. The membrane-embedded KtrB assembles to a dimer with two separate pores for ions to traverse. The dimer is formed by interacting C-termini that reach into the neighboring protomers. Each protomer has a selectivity filter close to the extracellular side and an intramembrane loop in the center of the permeation pathway (Figure 9). These two features could, in principle, provide the requirements for selective ion translocation. However, KtrB's selectivity filter has only one instead of four binding sites; accordingly, it only spans ~ 3.1 instead of ~ 12 Å (Vieira-Pires, Szollosi and Morais-Cabral, 2013). The poorly conserved selectivity filter is formed by only one highly conserved glycine residue of each P-loop equivalent to the middle glycine of the -TVGYG- sequence. The glycines are located at positions 70, 185, 290, and 402 in *Vibrio alginolyticus*, forming a binding site equivalent to S3 in, for example, KcsA. Similar to canonical selectivity filters, the coordination of K^+ in KtrB is provided by the backbone carbonyl oxygens. Additional binding sites have not been found. It was shown by mutagenesis studies, that the

glycine residues of each P-loop determine the affinity and selectivity of the KtrAB system (Tholema *et al.*, 2005). The K⁺ uptake system can be transformed into a Na⁺ uptake system by replacing only one glycine with a serine. How such a simple selectivity filter provides selective K⁺ passage was unknown and poses the central question addressed in this thesis.

Beside the selectivity filter for initial, likely selective ion binding, another process is needed to control the flux of K⁺. In KtrB, the intracellular cavity below the selectivity filter is directly obstructed by the intramembrane loop (Figure 9 b and d). Some 2TM/P K⁺ channels have added to the selectivity filter a bundle crossing gate on the intracellular side, creating a constriction for ions (Figure 3). Such a gate is formed by helix M2 in, for example, KcsA (Perozo, Marien Cortes and Cuello, 1998; Liu, Sompornpisut and Perozo, 2001; Blunck *et al.*, 2006) and was shown to be crucial for efficient ion translocation in K⁺ channels (Liu *et al.*, 1997; Jiang, Lee, Chen, Cadene, Brian T Chait, *et al.*, 2002). This usually hydrophobic part of the helical bundle crossing creates a steric hindrance for K⁺ ions (del Camino and Yellen, 2001; Kitaguchi, Sukhareva and Swartz, 2004). In KtrB, helix M2 is always broken and pointing away from the center of the pore. Instead, ion permeation through KtrB is controlled by a bulky, non-helical segment in the middle of broken helix D3M2, which constricts the permeation pathway inside the membrane plane. This segment known as the intramembrane loop (Hänelt, Löchte, *et al.*, 2010; Vieira-Pires, Szollosi and Morais-Cabral, 2013) consists of mostly hydrophilic residues. It contains several polar residues, mostly serines and threonines, and is flanked with several glycines. Site-directed mutagenesis within the intramembrane loop to more polar residues in KtrB alone led to increased uptake velocities (V_{\max}) of K⁺ translocation (Hänelt, Löchte, *et al.*, 2010). Deleting the entire intramembrane loop had no effect on the K_M value compared to wild-type KtrB, but it led to 10-fold faster K⁺ uptake in KtrB, with a V_{\max} of 350 nmol * min⁻¹ * mg⁻¹ dry weight compared to 35 nmol * min⁻¹ * mg⁻¹ dry weight (Hänelt, Löchte, *et al.*, 2010). The loop was shown to be influenced by three additional elements, one of which is a conserved arginine residue in D4M2 and the other two are the conformational changes of helices D4M2 and D1M2 (Figure 9 a-c). The arginine residue is also conserved in the homologues TrkH, for which it was speculated to stabilize the intramembrane loop through electrostatic interactions (Cao *et al.*, 2011). The function of this residue is still controversial, since changing it to alanine in TrkH from *Vibrio parahaemolyticus* led to increased K⁺ uptake (Cao *et al.*, 2011), while in Ktr from *Synechocystis sp.* the same mutation decreased K⁺ uptake (Kato *et al.*, 2007). Conformational changes of the helices D4M2 and D1M2 are a consequence of conformational changes in the gating ring, which are thought to stabilize the open or closed state of the channel by interacting with the intramembrane loop.

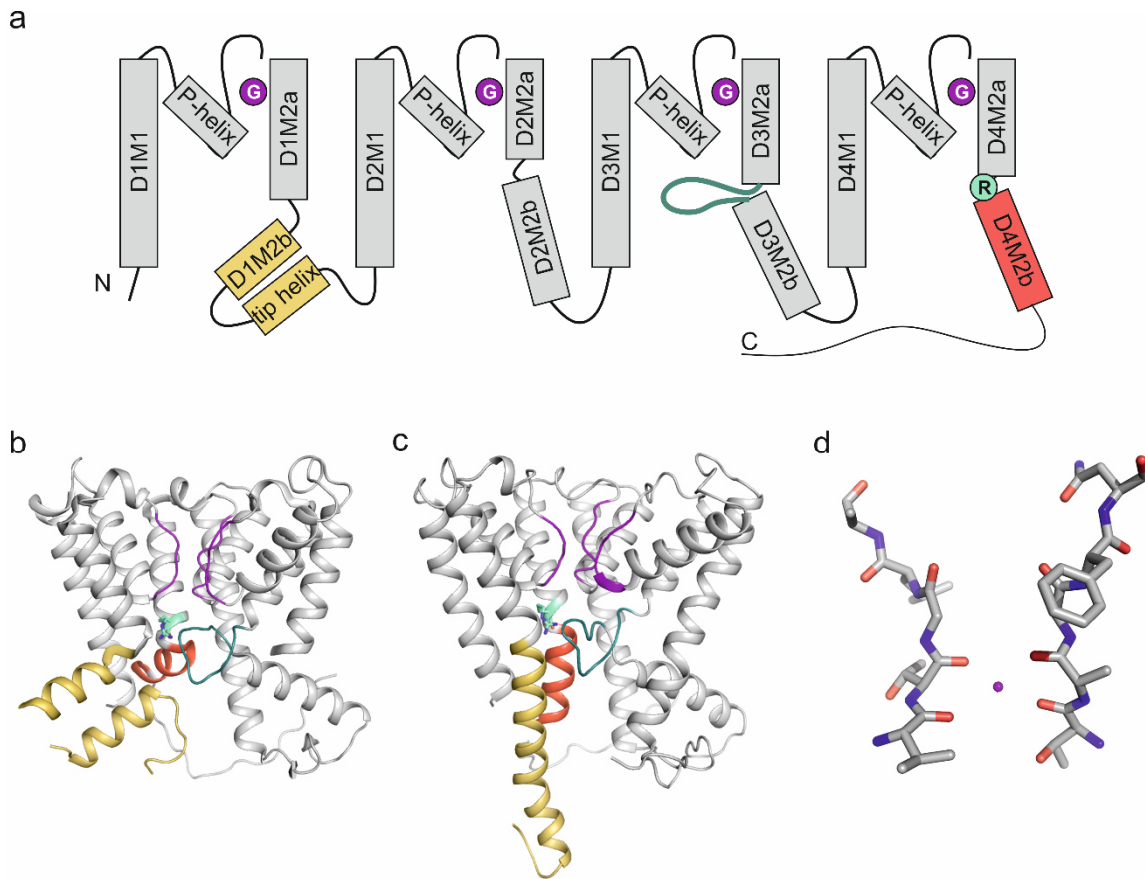


Figure 9 Topology of KtrB. (a) A KtrB monomer is formed by four domains (D1-D4), each of which consists of a membrane helix (M1), connected via a pore helix (P) to the second transmembrane helix (M2). Adapted from Diskowski *et al.*, 2017. KtrB structures (b+c) of the open (pdb: 4J7C) and closed (Diskowski *et al.*, 2017) conformation are shown, respectively. D2 was removed for clarity. (a-c) Helix D1M2b (yellow) forms the contact to the gating ring KtrA and undergoes a conformational change together with D4M2b (red). (a+d) The selectivity filter is formed by the backbone carbonyl oxygens of the four glycine residues sitting in the P loops. (a-c) Below the selectivity filter the intramembrane loop (green) and a conserved arginine (cyan) are located.

1.6.2 Influence of RCK protein KtrA on K⁺ translocation

KtrA is a RCK protein, which assembles into an octameric gating ring and is regulated by the binding of nucleotides to the -GxGxxG...D/E- motif in each subunit (Bellamacina, 1996; Albright *et al.*, 2006). This motif is responsible for the binding of ATP and ADP with micromolar affinities, which induce conformational changes in the KtrA gating ring (Albright *et al.*, 2006; Kröning *et al.*, 2007; Diskowski *et al.*, 2017). Further, the nucleotide-induced activation was shown to depend on divalent cation binding to the γ -phosphates of ATP of the intra-dimer interface (Teixeira-Duarte, Fonseca and Morais-Cabral, 2019). Functional assays revealed that ATP initiates K⁺ uptake, while ADP reduces the uptake of K⁺ through KtrAB (Kröning *et al.*, 2007; Vieira-Pires, Szollosi and Morais-Cabral, 2013; Szollosi *et al.*, 2016). The conformational change of the gating ring upon nucleotide binding is then conveyed to the intramembrane loop through helices D1M2 and D4M2 of KtrB (Diskowski *et al.*, 2017). The

KtrA gating ring adopts a square-shaped conformation in the presence of ATP (Albright *et al.*, 2006; Vieira-Pires, Szollosi and Morais-Cabral, 2013), which correlates to the open channel. In this state, helix D1M2b forms a helical hairpin and together with D4M2b both helices point away from the central cavity (Vieira-Pires, Szollosi and Morais-Cabral, 2013), allowing the loop to move freely. The binding of ADP stabilizes the gating ring in its oval-shaped conformation leading to channel inactivation (Albright *et al.*, 2006; Diskowski *et al.*, 2017). The helical hairpin of D1M2b is completely reversed into an extended helix protruding into the gating ring. Extended helices D1M2b and D4M2b move toward the central cavity reducing the water accessibility to the cytoplasmic side as shown by MD simulations (Diskowski *et al.*, 2017). This locks the intramembrane loop in the closed conformation, thereby blocking ion translocation.

However, despite the knowledge about nucleotide-induced conformational changes of KtrA, it has to be mentioned that the physiological relevance of ATP and ADP binding is still unclear. The binding affinities for ATP and ADP are with 2.6 and 1.6 μM , respectively, very similar; thus, the constant intracellular excess of ATP should always trigger channel activation (Diskowski *et al.*, 2017). This controversy could be solved by the recently shown regulation of KtrAB by the C-lobe binding of c-di-AMP. For KtrAB from Gram-positive bacteria channel closure upon c-di-AMP has been shown and its binding site has been identified (Corrigan *et al.*, 2013; Kim *et al.*, 2015). This binding site is, however, not conserved in KtrA from Gram-negative bacteria (Schrecker, Wunnicke and Hänelt, 2019). It thus remains to be seen, whether cyclic nucleotides like c-di-AMP can also bind to KtrA of *V. alginolyticus* and influence channel activity.

Another open question is the influence of Na^+ on KtrA-controlled K^+ translocation through KtrB. Previous studies revealed that Na^+ is absolutely required for K^+ uptake through KtrAB, while the translocation through KtrB alone is Na^+ independent. However, it remained unclear how Na^+ modulates KtrAB. It was suggested that KtrAB could, in fact, function as a K^+/Na^+ symporter (Tholema *et al.*, 1999). Alternatively, Na^+ could have a modulatory role on KtrA regulating channel gating in KtrB.

2. Aims and Objectives

Bacteria are continually facing changes in external osmolarity. Salt concentrations can easily vary from low millimolar to molar concentrations and affect bacterial growth (Sherman, Holm and Albus, 1922). KtrAB is supposed to be the critical player in bacteria upon hyperosmotic shock (Berry *et al.*, 2003; Holtmann *et al.*, 2003; Gries *et al.*, 2013; Nanatani *et al.*, 2015). It is thought to selectively take up potassium ions to counteract the efflux of water (Nanatani *et al.*, 2015). However, the major extracellular cation is Na⁺, and thus KtrAB has to provide a high K⁺ over Na⁺ selectivity to fulfill this function.

Unfortunately, present data are contradictory. While KtrAB engages in the selective accumulation of potassium inside bacteria upon hyperosmotic conditions (Holtmann *et al.*, 2003), KtrB was shown to take up both, K⁺ and Na⁺ (Tholema *et al.*, 2005; Hänelt, Löchte, *et al.*, 2010). In the presence of KtrA, the system becomes selective for the uptake of potassium, while at the same time it also acquired a Na⁺-dependency (Tholema *et al.*, 1999). However, the molecular basis for this selectivity has not been addressed yet. Instead, the homologous TrkAH, with a similar selectivity filter and overall architecture to KtrAB (Levin and Zhou, 2014) was shown to be non-selective for the uptake of K⁺ over Na⁺, which was suggested to be based on the poor selectivity filter with only one conserved glycine residue per P-loop (Cao *et al.*, 2013).

This thesis aims to elucidate the selectivity of the KtrAB system and to uncover the structural motifs responsible for a potential ion selectivity. A particular focus lies on studying subunit KtrB since it contains the selectivity filter and the intramembrane loop, which likely determine ion selectivity. After establishing a purification protocol for KtrB, ITC measurements will be performed to determine the selectivity of ion binding. Subsequently, SSM-based electrophysiology measurements and ACMA-based flux assays will be established to assess the selectivity of ion translocation and to evaluate structural motifs involved in ion selectivity. Finally, the functional role of Na⁺, both on selective ion binding and translocation of K⁺ through the KtrAB system, will be addressed.

3. Materials and Methods

3.1 Material

3.1.1 Chemicals

All basic substances used were supplied by Carl Roth GmbH & Co. KG, VWR International GmbH or Merck KGaA (Sigma Aldrich Chemie GmbH). Chemicals of specific purity are listed in Table 1.

Table 1 Overview of specific substances used in this work

Names (abbreviations)	Purity/Concentration	Source
1,2-Diphytanoyl-sn-glycerol-3-Phosphatidylcholine (DPhyPC)	20 mg/ml in chloroform	Avanti Polar Lipids, Inc.
2-(N-morpholino) ethanesulfonic acid (MES)	≥99%	Sigma Aldrich
4-(2-hydroxyethyl)-1-piperazine-ethanesulfonic acid (HEPES)	≥99.5%	Sigma Aldrich
Caesium chloride (CsCl)	≥99.99%	Carl Roth GmbH & Co. KG
Chloroform	≥99%	VWR AnalaR NORMAPUR
Choline chloride	≥99%	Sigma Aldrich
Dimethylsulfoxid (DMSO)	≥99.5 %	Carl Roth GmbH & Co. KG
Dipotassium phosphate (K₂HPO₄)	≥99%	Carl Roth GmbH & Co. KG
DNase I	salt-free, freeze-dried powder	AppliChem PanReac
Lithium chloride (LiCl)	≥99%	Sigma Aldrich
Magnesium chloride (MgCl₂)	≥99%	Sigma Aldrich
Monopotassium phosphate (KH₂PO₄)	≥99%	Carl Roth GmbH & Co. KG
Monosodium phosphate (NaH₂PO₄)	≥99%	Carl Roth GmbH & Co. KG
Natural <i>E. coli</i> lipids (total extract)	PE 57.5%; PG 15.1%; CA 9.8%; unknown 17.6%	Avanti Polar Lipids, Inc.
Octadecanthiol	98%	Sigma Aldrich
Potassium chloride (KCl)	≥99.5%	Carl Roth GmbH & Co. KG
Rubidium chloride (RbCl)	≥99%	Carl Roth GmbH & Co. KG
Tris-hydroxymethyl-aminomethan (Tris)	≥99%	Sigma Aldrich

3.1.2 Buffers and solutions

Buffers and solutions used in this work are summarized in Table 2.

Table 2 Overview of all standard buffers and solutions.

Buffers/solutions	Composition
10 x Running buffer	250 mM Tris; 1.9 M glycine; 1% SDS
4 x SDS-PAGE loading dye	0.5 Tris; 8% SDS (w/v); 40 % glycerol; Bromphenol blue 0.08%; β -Mercaptoethanol (10%)
9-Amino-6-chloro-2-methoxyacridine (ACMA)	400 μ M in DMSO
ACMA inside buffer	150 mM NaCl, KCl, RbCl or CsCl; 20 mM HEPES-ethanolamine pH 7.35
ACMA outside buffer	150 mM LiCl; 20 mM HEPES-ethanolamine pH 7.35
Activating (A) solution	SSM ground buffer + 100 mM x chloride salt
ÄKTA buffer	200 mM NaCl; 20 mM Tris-HCl pH 8, 0.04% DDM
Basic ITC buffer	200 mM Choline chloride or LiCl, 20 mM Tris-HCl pH 7.5
Carbonyl cyanide m-chlorophenyl hydrazone (CCCP)	400 μ M in DMSO
Coomassie staining buffer	10% acetic acid; 40% ethanol; 50% ddH ₂ O; 0.25% Coomassie Brilliant Blue R250
Destaining (Coomassie) buffer	10% ethanol; 35% acetic acid; ddH ₂ O
LILBID-MS buffer	20 mM NaCl, 20 mM Tris-HCl pH 8
Non-activating (NA) buffer	SSM ground buffer + 100 mM x chloride salt
Potassium phosphate buffer (KP_i buffer)	61.5 mM K ₂ HPO ₄ ; 38.5 mM KH ₂ PO ₄ ; pH 7
Resolving buffer for SDS-PAGE	1.5 M Tris-HCl pH 8.8; 0.4% SDS
Sodium ionophore IV (Nal)	1 mM in DMSO
Solubilization buffer (buffer S)	420 mM NaCl; 180 mM KCl; 50 mM Tris-HCl pH 8
SSM ground buffer	200 mM choline chloride; 5 mM MgCl ₂ ; 50 mM Tris, 50 mM MES and 50 mM HEPES pH 7.5
Stacking buffer for SDS-PAGE	0.5 M Tris-HCl pH 6.8; 0.4% SDS
Valinomycin (Val)	8 μ M in DMSO
Washing buffer (buffer W)	140 mM NaCl; 60 mM KCl; 20 mM Tris-HCl pH 8

3.1.3 Strain and Plasmids

E. coli strain LB2003 (Stumpe and Bakker, 1997) was used for K⁺ uptake and cell growth complementation experiments as well as protein over production. It lacks all three major K⁺ uptake systems of *E. coli* (F⁻ *thi metE rpsL gal rha kup1 ΔkdpABC5 ΔtrkA*).

Table 3 manifests all the plasmids used in this thesis.

Table 3 Overview of the plasmids used during this work

Plasmids	Resistance	Properties	Reference
pBAD18	amp ^R	cloning vector with BAD-promoter	Guzman <i>et al.</i> , 1995
pEL903	amp ^R	pBAD18-derivate, coding for KtrB-His ₆ from <i>V. alginolyticus</i>	Tholema <i>et al.</i> , 2005
piH301	amp ^R	pBAD18-derivate, coding for KtrAB-His ₆ from <i>V. alginolyticus</i>	Hänelt <i>et al.</i> , 2010
pEL903_{G316S}	amp ^R	pEL903-derivate, with residue 316 (glycine) mutated to serine	Hänelt <i>et al.</i> , 2010
pBKtrBC3H	amp ^R	pBAD24-derivate created by FX cloning, coding for KtrB-3C-His ₁₀ from <i>V. alginolyticus</i>	Provided by Schrecker
pEL903_{D1sf}	amp ^R	pEL903-derivate, -VTGLG- sequence in P _{D1} -loop was exchanged for -TVGYG-	This work
pEL903_{D1D2sf}	amp ^R	pEL903 _{D1} -derivate, -NAGFA- sequence in P _{D2} -loop was exchanged for -TVGYG-	This work
pEL903_{D1D2D3sf}	amp ^R	pEL903 _{D1D2} -derivate, -TAGFN- sequence in P _{D3} -loop was exchanged for -TVGYG-	This work
pEL903_{TVGYG}	amp ^R	pEL903 _{D1D2D3} -derivate, -TVGLT- sequence in P _{D4} -loop was exchanged for -TVGYG-	This work
pEL903_{Q93L}	amp ^R	pEL903-derivate, with residue 93 (glutamine) mutated to leucine	This work
pEL903_{Q99E}	amp ^R	pEL903-derivate, with residue 99 (glutamine) mutated to glutamate	This work
pEL903_{E149L}	amp ^R	pEL903-derivate, with residue 149 (glutamate) mutated to leucine	This work
pEL903_{Q93L/E149L}	amp ^R	pEL903-derivate, with residues 93 and 149 (glutamine and glutamate) mutated to leucine, respectively	This work
piH301_{Q93L}	amp ^R	piH301-derivate, with residue 93 (glutamine) mutated to leucine	This work

pIH301_{Q99E}	amp ^R	pIH301-derivate, with residue 99 (glutamine) mutated to glutamate	This work
pIH301_{E149L}	amp ^R	pIH301-derivate, with residue 149 (glutamate) mutated to leucine	This work
pIH301_{Q93L/E149L}	amp ^R	pIH301-derivate, with residues 93 and 149 (glutamine and glutamate) mutated to leucine, respectively	This work
pEL903_{Δ214-23}	amp ^R	pEL903-derivate, with residue 314 to 323 (intra-membrane loop) deleted	Hänelt <i>et al.</i> , 2010
pKT84	amp ^R	pHG165 containing VaKtrAB	Nakamura <i>et al.</i> , 1998

Plasmids were used for the expression of KtrB, KtrAB and their mutants. The genes are underlying the control of an araBAD-promoter as given by the original expression vector.

Table 4 lists all primers used for site-directed mutagenesis in this thesis

Table 4 Overview of the primers used during this work. Primer names, 5' to 3' sequences, melting temperatures (T_m in °C) and annealing temperatures (T_a in °C) are given.

Primers	Sequence (5' to 3')	T _m (°C)	T _a (°C)
KtrB_Q93L_for	GCTTGATGCTGATCGGCGGCTT	61	59
KtrB_Q93L_rev	AAGCCGCCGATCAGCATCAAGC	60	
KtrB_E149L_for	CTGGTGGCATTGGCGATTG	59	57
KtrB_E149L_rev	CAATCGCCAATGCCACCAG	59	
KtrB_E149K_for	CTGGTGGCAAAGGCGATTG	52	51
KtrB_E149K_rev	CAATCGCCTTTGCCACCAG	54	
KtrB_E182L_for	CTATTTGGCTTTCTCAATGCTGGCTTCG	58	60
KtrB_E182L_rev	CGAAGCCAGCATTGAGGAAAGCCGAAATAG	57	
KtrB_P_{D1}sf_for	GGGTACGGTGTGGTCGATACCGGC	76	72
KtrB_P_{D1}sf_rev	AACCGTACTAATGGCTGAAGTCGCG	71	
KtrB_P_{D2}sf_for	CTACGGTCTCTTTTCTGACAGCATG	67	68
KtrB_P_{D2}sf_rev	CCAACAGTGTTGAAAGCCGAAATAGAATG	68	
KtrB_P_{D3}sf_for	TACGGCAGTGTTGATTTAACGCAGTTCACGC	66	69
KtrB_P_{D3}sf_rev	ACCCACTGTCCGCGCACTGGCTGA	70	
KtrB_P_{D4}sf_for	GTATGGTGCAGGTTTGACGGCAGAG	72	72
KtrB_P_{D4}sf_rev	CCAACCGTTGCAAAGCAGAAATCGTTTC	71	

3.2 Growth media

Plasmid-containing LB2003 cells were either grown in KML medium or phosphate-buffered K⁺ (Potassium) minimal media based on Epstein & Kim 1971 (Epstein and Kim, 1971) depending on the application. K0 to K10 media were prepared, containing 46 mM Na₂HPO₄, 23 mM NaH₂PO₄, 1 mM Na-Citrate, 7.6 mM (NH₄)₂SO₄ and 0 to 10 mM KCl, respectively. Pre-cultures for growth in minimal medium were grown in K30 media consisting of 34 mM Na₂HPO₄, 17 mM NaH₂PO₄, 12 mM K₂HPO₄, 6 mM KH₂PO₄, 1 mM Na-Citrate and 7.6 mM (NH₄)₂SO₄. K115 medium used in growth complementation experiments, contained 46 mM K₂HPO₄, 23 mM KH₂PO₄, 1 mM Na-Citrate and 7.6 mM (NH₄)₂SO₄. All minimal media were supplemented with 6 μM Fe(II)SO₄, 0.4 mM MgSO₄, 1 μg/ml thiamine, 20 μg/ml methionine and 0.2% glycerol (v/v) as a carbon source. For site-directed mutagenesis and some other applications, plasmid-containing LB2003 cells were grown in KML medium containing 1% KCl, 0.5% yeast extract, and 1 % tryptone. For solid media, 1.5% (w/v) agar was added to either K⁺ minimal media or KML medium. All media were supplemented with 100 μg/ml of ampicillin as a selection marker, and for induction of gene expression, 0.02% L-arabinose was used.

3.3 Molecular biology

3.3.1 Preparation of competent cells and transformation

The production and transformation of competent *E. coli* LB2003 cells was achieved based on the CaCl₂ solution method according to Sambrook *et al.* (1989). Competent cells were either immediately used or mixed with sterile glycerol (20%) and stored at -80°C after flash freezing. For transformation, an aliquot of 250 μl competent cells was thawed on ice, 100 - 200 ng DNA was added to the cells and incubated for 30 minutes on ice. A heat shock for 1 min at 42 °C was performed, followed by an additional incubation on ice for 10 minutes. Subsequently, 1 ml KML medium was added, and the culture was incubated for 1 h at 37 °C under vigorous shaking. An aliquot of 100 μl was plated onto KML-agar (1.5 % (w/v) agar from Formedium™) with ampicillin and incubated overnight at 37 °C.

3.3.2 Plasmid isolation

Isolation of plasmids from 5 ml over-night cultures grown in KML medium was performed using the NucleoSpin® Plasmid Easy Pure-kit (Macherey-Nagel GmbH & Co. KG). DNA was eluted with 50 μl sterile pre-warmed H₂O as an alternative of the given elution buffer. Plasmid

concentrations were determined with the spectrometer NanoDrop® ND-1000 (PEQLAB Biotechnologie GmbH). DNA concentration was computed using the Lambert-Beer-law ($A_{260nm} = \epsilon c d$; here A is the absorption, ϵ is the extinction coefficient in $\left[\frac{ml}{\mu g \cdot cm}\right]$ (0.02 ml/($\mu g \cdot cm$) for DNA), c is the concentration in [$\mu g/ml$], and d is the optical path length [cm]) at an absorbance of 260 nm. Isolated plasmids were either used again for transformation, stored at -20°C or send for sequencing.

3.3.3 Site-directed mutagenesis

Plasmids coding for KtrB or KtrAB were used for the introduction of site-specific mutations with primers listed in Table 4, using a Thermocycler peqSTAR 2X (PEQLAB). Polymerase chain reaction was performed in the presence of Phusion high-Fidelity DNA Polymerase (Thermo Fisher Scientific Inc.) and included the following steps: initial denaturation at 98°C for 2 min, followed by 25 cycles of denaturation, annealing, and elongation. Denaturation was performed for 30 s at 95°C, primer annealing for 30 s with primer-specific temperatures (Table 4) and the elongation step for 3 ½ to 4 min at 72°C. After completion of the last cycle, a final elongation step was performed for 5 min at 72°C. The PCR product was stored at 4°C. The quality of the PCR reaction was confirmed via agarose gel electrophoresis. All PCR products were incubated for 1 h at 37°C with DpnI (Thermo Fisher Scientific Inc.) restriction enzyme to remove the methylated DNA. Finally, the PCR product was used for cell transformation.

3.3.4 Creating the KtrB_{TVGYG} variant

For generating a KtrB variant with all four selectivity filter sequences mutated to -TVGYG- the Q5® Site-Directed Mutagenesis Kit (New England BioLabs) was used. The substitution required a 4-step protocol using pEL903, encoding for *ktrB-his₆*, as the initial vector. In domains 1 to 4 of KtrB the sequences -VTGLG- (D1), -NAGFA- (D2), -TAGFN- (D3), and -TVGLT- (D4) were consecutively replaced for -TVGYG- using the primers designed by NEBaseChanger™ tool listed in Table 4.

3.3.5 Agarose gel electrophoresis

PCR products were evaluated using a 0.8% agarose gel made with TAE buffer (40 mM Tris pH 8, 1 mM EDTA). Samples were mixed with Gel Loading Dye Purple (6x) from New England

BioLabs and the GeneRuler 1kb DNA Ladder (Thermo Fisher Scientific Inc.) was used to compare the size of the sample. DNA separation was performed by applying the power supply peqPOWER 250V (PEQLAB) at 60-120 V depending on the gel size. Agarose gels were subsequently stained for 30 min in 1% ethidium bromide and looked at under UV light.

3.4 Whole-cell assays

3.4.1 Complementation assay

To determine the functionality of wild type KtrB, KtrAB and their variants in whole-cells, growth complementation assays under K⁺ limitation were performed. For this assay, *E. coli* LB2003 was transformed with different plasmids. This strain can only grow below 10 mM KCl in the medium if functional potassium transporters are expressed. Pre-cultures of plasmid-containing *E. coli* LB2003 were grown in 5 ml of K30 minimal medium [30 mM KCl] without induction while shaking overnight at 37°C. For the complementation assay, K⁺ minimal media of the following KCl concentration were prepared: 0.5, 1, 3, 5, 7 10, 30 and 115 mM. The composition of all media is described in section 3.2. Growth was followed hourly during the day by determination of the optical density at 600 nm (OD₆₀₀) after inoculation. A final measurement after 24 h was performed.

3.4.2 K⁺ uptake experiments in whole-cells

KtrB-mediated K⁺ uptake was determined according to a modified protocol from Bakker and Mangerich (1981). For this purpose, *E. coli* strain LB2003 was transformed with pKT84, coding for tag-less VaKtrAB. Cells were grown in 500 ml K3 minimal medium and harvested in the late exponential phase (OD₆₀₀ between 0.6 and 0.8). Cells were washed twice with 120 mM Tris-HCl buffer pH 8.0 and diluted to an OD₆₀₀ of 30, meaning 10 mg dry weight (dw) of cells per ml. Hence, an OD₆₀₀ of 1 corresponds to 0.3 mg dw of cells per ml (Bakker and Mangerich, 1981). Subsequently, cells were depleted from Na⁺ and K⁺ through treatment with 1 mM EDTA for 7 min at 37 °C and continuous shaking, since EDTA is known to permeabilize membranes of Gram-negative bacteria (Leive, 1968). To completely remove Na⁺, K⁺ and residual EDTA, cells were washed three times with 200 mM HEPES-triethanolamine pH 7.5. Finally, the OD₆₀₀ was adjusted to 3 with 200 mM HEPES-triethanolamine, corresponding to 1 mg dw cells/ml. Cells were energized with 0.2 % glycerol and incubated for 10 min shaking at room temperature (RT). Potassium uptake was initiated by the addition of different KCl

concentrations (0.5, 1, 2 or 5 mM) in the absence or presence of either LiCl, NaCl or RbCl of different concentrations. Samples of 1 ml were taken at different time points, transferred onto 200 μ l of silicone oil (1.04 g/cm³, Serva; Heidelberg) in a 1.5 ml reaction tube and centrifuged for 2 min at 4,100 g and RT to stop K⁺ uptake. Cells were separated from the buffer through the silicone oil. Buffer and silicone oil were removed, and the pellet was dissolved in 1 ml of 5% trichloroacetic acid (TCA). For cell disruption, the suspension was first frozen at -20 °C and then cooked for 10 min at 90 °C. Subsequently, 7 ml of 5.7 mM CsCl was added to each sample and the K⁺ concentration was determined by flame photometry. The Michaelis-Menten constants (K_M) and maximum rate velocities (V_{max}) were calculated by Lineweaver-Burk (Lineweaver and Burk, 1934) estimated through the initial uptake velocities.

$$\frac{1}{v_0} = \frac{K_M}{V_{max}} \cdot \frac{1}{[S]} + \frac{1}{V_{max}}$$

The two variables v_0 and [S] represent the turnover velocity and the substrate concentration, respectively.

3.5 Biochemical methods

3.5.1 BCA assay

The determination of total protein concentrations was accomplished using Pierce™ BCA Protein Assay Kit from Thermo Scientific. The method developed by Smith *et al.* (1985) is based on the colorimetric detection of protein. Under alkaline conditions, proteins tend to reduce Cu²⁺ to Cu⁺. Bicinchoninic acid (BCA) forms a purple complex with Cu⁺ ions, which exhibits a strong absorbance at 562 nm (Smith *et al.*, 1985). The working range of the BCA reagent reaches from 20 to 2000 μ g/ml, where the absorbance at 562 nm is in linear correlation with the protein concentration. A protein standard within that range was prepared. The assay was carried out in a 96-well plate using 25 μ l of standards or samples and 200 μ l of working reagent. For detection, a microplate reader from MTX Lab Systems was used.

3.5.2 SDS-Polyacrylamide gel electrophoresis (PAGE)

To follow the protein purification, samples of different steps were taken and submitted to an SDS-PAGE according to Laemmli (1970). Samples were prepared with SDS-PAGE loading dye [100 mM Tris-HCl pH 6.8, 2% (w/v) SDS, 2.5% (v/v) β -mercaptoethanol, 0.02% (w/v) bromophenol blue (Roth GmbH), 10% (v/v) glycerol] before loading them on a 12.5%

acrylamide gel for separation. As a standard, 3 μ l of the pre-stained RulerTM protein ladder (Thermo Fisher Scientific Inc.) were loaded together with the samples. Of each protein sample, 10 μ l was loaded to a gel system composed of a separating and a stacking gel (Table 5 and Table 6). Protein separation was achieved in a cell system PerfectBlueTM (PEQLAB) using Laemmli buffer (25 mM Tris-HCl pH 8.8, 192 mM glycerol, 0.1% (w/v) SDS) at 140 V. Proteins were visualized by staining the gels with Coomassie Blue staining buffer [10% (v/v) acetic acid, 40% (v/v) ethanol, 50% (v/v) H₂O, 0.25% (w/v) Coomassie Brilliant Blue R250 (Roth GmbH)]. For destaining was a buffer containing 10% ethanol; 35% acetic acid; ddH₂O was used.

Table 5 Separating gel

Compounds	Amount (ml)
Rotiphorese® Gel 30 (37.5 : 1) Acrylamide (Carl Roth GmbH + Co. KG)	8.00
1.5 M Tris-HCl pH 8.8, 0.4% (v/v) SDS	8.00
H ₂ O	5.40
TEMED (Carl Roth GmbH + Co. KG)	0.06
10% Ammonium persulfate (APS) (Carl Roth GmbH + Co. KG)	0.12

Table 6 Stacking gel

Compounds	Amount (ml)
Rotiphorese® Gel 30 (37.5 : 1) Acrylamide (Carl Roth GmbH + Co. KG)	1.30
0.5 M Tris-HCl pH 6.8, 0.4% (v/v) SDS	2.20
H ₂ O	5.40
TEMED (Carl Roth GmbH + Co. KG)	0.03
10% Ammonium persulfate (APS) (Carl Roth GmbH + Co. KG)	0.09

3.6 Protein production and purification

3.6.1 Overexpression

For protein purification, all *ktrB* variants were expressed in *E. coli* strain LB2003. This strain lacks all three endogenous genes encoding for potassium uptake. Cell growth under potassium limitation ensured the functionality of the produced protein (Stumpe and Bakker, 1997). LB2003 cells containing plasmids pEL903 and pEL903_{G316S}, encoding for KtrB-His₆ and KtrB_{G316S}-His₆, were grown in 12 l K3 minimal medium supplemented with 0.2% glycerol (v/v) and induced with 0.02% L-arabinose (v/v) from the start. Cells were harvested after reaching the late-exponential growth phase. Cells containing plasmid pBKtrBC3H generated by FX-cloning (Geertsma and Dutzler, 2011), encoding for KtrB-3C-His₁₀, were grown in KML

medium. 0.02% L-arabinose for gene expression was added at an OD₆₀₀ of ~1.7. Cells were harvested by centrifugation at 5,500 g and 4°C 1 ½ h after induction.

3.6.2 Isolation of membranes

After harvesting, cells resuspended in buffer S [420 mM NaCl, 180 mM KCl and 50 mM Tris-HCl pH 8 at 4°C] were supplemented with 100 µM of the serine protease inhibitor PMSF, 300 µM benzamidine, 1 mM EDTA, and a spatula of DNase I. Cells were subsequently lysed using the cell homogenizer 'Pressure cell' (Stansted Fluid Power Ltd) at 1 bar. A successful cell disruption was confirmed by measuring a 1/3 drop in OD₆₀₀ of lysed compared to unlysed cells. Cell debris and unlysed cells were separated from cytoplasm and membranes via low-speed centrifugation at 25,000 g and 4°C, for 15 min. The membrane pellet was obtained by using high-speed centrifugation overnight at 100,000 g and 4°C. The membrane pellet was homogenized and resuspended in buffer S with protease inhibitors to a protein concentration of 10 mg/ml, as determined by bicinchoninic acid-assay using a kit (Thermo Fisher).

3.6.3 Protein purification from isolated membranes

Membranes with a protein concentration set to 10 mg/ml were solubilized by using 1% β-D-dodecylmaltoside (DDM), incubated for 1 h under gentle agitation at 4°C. Unsolubilized proteins, together with some lipids, were removed upon centrifugation at 200,000 g for 20 min. For the binding of the His-tagged protein, immobilized metal-ion chromatography (IMAC) (Sulkowski, 1989) was performed using nickel-nitrilotriacetic acid-agarose (Ni²⁺-NTA). The supernatant was incubated with buffer S pre-equilibrated Ni²⁺-NTA resin (1 ml column volume per 6 L cell culture) for 1 h at 4°C in the presence of 10 mM imidazole. The Ni²⁺-NTA resin was transferred to a gravity flow column, the flow-through was collected and the beads were washed with 100-fold column volumes of buffer W [140 mM NaCl, 60 mM KCl and 20 mM Tris-HCl pH 8] with 0.04% DDM and 50 mM imidazole. Protein was eluted from the resin in six steps of half column volume with buffer W containing 0.04% DDM and 500 mM imidazole. Elution fraction E2 to E5 were combined and concentrated to ~500 µl with a 50 MWCO Centriprep (Merck Millipore Ltd) for size-exclusion chromatography. The concentrated protein samples were filtered through 2 mL Ultrafree®-CL filtration units with low-binding Durapore® PVDF membrane (Merck Millipore Ltd). For the final purification step, size-exclusion chromatography was performed using a Superdex Increase 200 10/300 GL column (GE Healthcare) equilibrated to either buffer W containing 0.04% DDM or the ITC buffers [200 mM

choline-Cl or 200 mM LiCl, 0.04% DDM and 20 mM Tris-HCl pH 7]. The flow rate was set to 0.4 ml/min and fractions of 0.5 ml (7-20 ml) were collected. The purity of the protein as well as contaminations with DNA were determined by following the absorbance at 280 and 260 nm, respectively. During the purification, samples were taken of all the steps. Coomassie staining of the gels after SDS-PAGE was used to determine the purity of the protein sample (section 3.5.2). The final protein concentration of the collected samples was determined using a NanoDrop 1000 Spectrophotometer (PaqLab) under consideration of the MW and extinction coefficients determined using the ExPASy ProtParam tool.

3.6.4 Protein purification of KtrB-3C-His₁₀ with SMALPs

As an alternative purification strategy, KtrB-3C-His₁₀ was purified using styrene-maleic acid (SMA) copolymers while avoiding the use of detergents. The membrane pellets, containing KtrB-3C-His₁₀, were weighed and suspended to 50 mg/ml (w/v) in buffer S. Solubilization was reached by the addition of 2.5% of the SMA polymer Xiran® SL 30010 P20 (Polyscope Polymers) over day. Unsolubilized proteins were removed by centrifugation at 200,000 g for 30 min. The supernatant was incubated with a pre-equilibrated Ni²⁺-NTA resin overnight in the presence of 10 mM imidazole. Subsequently, the Ni²⁺-NTA was washed with 50 column volumes of buffer W [140 mM NaCl, 60 mM KCl, 20 mM Tris-HCl, pH 8] containing 50 mM imidazole. VaKtrB-3C-His₁₀ was eluted with buffer W containing 500 mM imidazole. Elution fraction E2 to E5 were combined and loaded onto a Superose 6 Increase 10/300 GL column (GE Healthcare) equilibrated to LILBID-MS buffer [20 mM NaCl, 20 mM Tris-HCl, pH 8].

3.7 Reconstitution into liposomes

Liposomes and vesicles are the most widely used membrane models for investigation of membrane proteins. They spontaneously form multilamellar vesicles in aqueous solutions and the size can vary from 0.1 to several μm (Lasic, 1988). Unilamellar vesicles are generated by extrusion according to Hope *et al.* (1985). Liposomes can be used for a variety of applications, like for example SSM-based electrophysiology.

3.7.1 Purification of *E. coli* total lipid extract

For the purification of lipids, 1 g of natural *E. coli* total lipid extract dissolved in chloroform (25 mg/ml, Avanti Polar Lipids) was dried in a rotary evaporator. The flask was gas-flushed with N₂ and the lipids were dissolved in 5 ml of chloroform. The chloroform-lipid solution was slowly titrated to 150 ml of ice-cold acetone under vigorous stirring to precipitate the lipids. After flushing the flask with N₂, it was closed and kept in the dark at 4 °C while stirring overnight. A subsequent centrifugation step at 3,000 g for 10 minutes was used to pellet the lipids and remove the acetone. The pellet was thoroughly dried in a stream of N₂ and afterwards dissolved in 150 ml diethyl ether, stirred for ½ h at room temperature. A second centrifugation step at 3,000 g for 10 minutes followed. The supernatant, now containing the polar lipids, was dried completely in a rotary evaporator at room temperature. The yield of purification was determined by weighing the purified lipids. Lipids were dissolved in chloroform to a concentration of 100 mg/ml and stored at -20 °C.

3.7.2 Preparation of different liposome mixtures

To form liposomes from purified polar lipids, a desired amount of lipid was dried in a rotary evaporator. After drying, the lipid film was washed with 1.5 ml of 96% ethanol to eliminate any residual chloroform and the solvents were again removed in a rotary evaporator at 30 °C. Finally, the lipid film was hydrated with 50 mM potassium phosphate buffer (KPi), pH 7 to an end concentration of 10 mg/ml to achieve the formation of liposomes (Bangham, Standish and Watkins, 1965). The flask was flooded with N₂ and lipids were homogenized using an ultrasonic bath. 1 ml aliquots were allocated to cryo-tubes and frozen with liquid N₂ and stored at -80°C until use.

3.7.3 Preparation of Polystyrene beads

Polystyrene beads (BioBeads) were purchased from Bio-Rad. Activation of the BioBead surface was achieved by washing 3x with methanol. BioBeads were thoroughly washed with water to remove residual methanol. The prepared polystyrene beads were stored in water at 7 °C until use.

3.7.4 Reconstitution of KtrB into pre-formed liposomes

For protein reconstitution, prepared liposomes were thawed and washed with either SSM buffer [300 mM choline-Cl, 50 mM Tris, 50 mM MES, 50 mM HEPES, 5 mM MgCl₂ pH 7.5] or ACMA buffers [150 mM NaCl, KCl, RbCl or CsCl with 20 mM HEPES pH 7.35]. Thawed liposomes were collected by ultracentrifugation at 300,000 g for 30 min (15°C) and resuspended in the respective buffers. Liposomes were three times flash-frozen and slowly thawed before subsequent extrusion. To obtain unilamellar liposomes, 21 extrusion steps through a 400 nm-filter were performed. The extruder was pre-equilibrated with the respective buffer. Subsequently, liposomes were diluted to 4 mg/ml and titrated with 10% Triton-X-100 following the absorption at 540 nm (Geertsma *et al.*, 2008). Titration was completed reaching the point slightly after the detergent saturation limit.

Purified protein was reconstituted into *E. coli* polar lipid liposomes according to an established protocol (Hänelt, Löchte, *et al.*, 2010). Proteoliposomes with lipid to protein ratios (LPR) of 5:1, 10:1 and 50:1 were generated for SSM-based electrophysiology and liposomes with an LPR of 100:1 (w/w) for ACMA-based flux assays. The corresponding amount of protein (or buffer for control liposomes) was added to the Triton-X-100-destabilized liposomes following a series of polystyrene bead (Bio-Beads®, Bio-Rad) additions according to an adjusted protocol (Hänelt, Löchte, *et al.*, 2010). The protein-detergent-lipid mix was incubated for 30 min at room temperature under gentle agitation. To remove the detergent 60 mg/ml of wet weight polystyrene beads were added in each of the initial five reconstitution steps. Due to uneven distribution of protein in the liposomes, this was changed to 40 mg/ml with two additional steps to achieve a better protein distribution through slow reconstitution. Following the new protocol, 40 mg/ml polystyrene beads were added after 30 and 15 min at room temperature and 15 min, 30 min, 1 h, overnight and another 1 h at 4°C. The last addition is finalized with an addition of 80 mg/ml instead of 40 mg/ml to ensure the complete removal of detergent. The proteoliposomes were washed two times with their respective buffers. They were either immediately used for the ACMA assay or aliquoted and flash-frozen for SSM-based electrophysiology.

3.8 Biochemical and biophysical techniques

3.8.1 ITC

Purified KtrB was concentrated to 40-70 µM in either choline-Cl- or LiCl-ITC buffer pH 7. The salt concentrations of all used buffers were always kept at 200 mM. The Li-ITC buffer contained

200 mM LiCl and 20 mM Tris-HCl pH 7 at 24 °C and the choline-ITC buffer was composed of 200 mM Choline chloride and 20 mM Tris-HCL pH 7 at 24 °C. Protein and titration buffers were made out of the two buffers by supplementing the 200 mM with either NaCl, KCl, RbCl, or CsCl. ITC measurements were performed at 24°C with a MicroCal iTC200 System (GE) to evaluate binding affinities. A volume of 2 or 1.5 µL was used for each injection, with the exception of the first injection, which was adjusted to 0.2 µL. Measurements involved 19-26 injections with 3 min intervals in-between each injection and a reference power of 11.0 µcal/s. MicroCal ITC-ORIGIN Analysis Software was used to analyze all titrations. The heat of dilution acquired from ligand to buffer injections was subtracted before data fitting.

3.8.2 Determination of the liposome size

The liposome size was determined using the NanoSight LM10 from Malvern. This technique uses both light scattering and Brownian motion to attain the size distribution of particles in liquid solutions. The hydrodynamic radius of the tracked particles is calculated using the Stokes-Einstein equation:

$$D = \frac{kT}{6\pi\eta r}$$

The Stokes-Einstein relationship describes the diffusion of a molecule in a Newtonian fluid. It establishes a relationship between the size and density of the (considered spherical) particles and their rate of descent. D corresponds to the diffusion coefficient, k to the Boltzmann constant [1.380649×10^{-23} J/K], T is the absolute temperature, η is the dynamic viscosity of the solvent and r is the particle radius. The dynamic viscosity (η) is dependent on the used solvent and was determined with 1 µl of 100 nm Traceable Particle Size Standard (Polysciences, Inc.) diluted in 1 ml of liposome buffer. The viscosity factor (Centipoise [cP]; $1 Pa \cdot s = 1000 cP$) determined was used for all subsequent liposome measurements. All liposome samples were diluted 10^{-5} fold from 10 mg/ml for evaluation of their size.

3.8.3 ACMA assay

To monitor KtrB-mediated cation fluxes, an indirect approach was used measuring vesicular acidification with the membrane permeable pH-sensitive dye 9-amino-6-chloro-2-methoxyacridine (ACMA). At a physiological pH ACMA is in an equilibrium between a neutral

and mono-cationic state (Figure 10). ACMA has a pK_a of 8.6 with a 20:1 ratio between its mono-cationic and neutral state, respectively (Marty *et al.*, 1986).

ACMA-based ion flux assays were performed at room temperature at the Fluorolog® 3 (Horiba Scientific) fluorescence spectrometer. For this assay, 10 μ l of liposomes in the indicated ACMA inside buffer (10 mg/ml, LPR 100:1) were added to 190 μ l of ACMA outside buffer [150 mM LiCl, 20 mM HEPES-ethanolamine at pH 7.3] pre-mixed with 2 μ M of ACMA [400 μ M in DMSO]. Fluorescence was monitored at an excitation wavelength of 410 nm and an emission wavelength of 500 nm (2 nm band widths). After addition of 1 μ M H^+ ionophore carbonyl cyanide-*m*-chlorophenylhydrazone (CCCP [400 μ M in EtOH]) cation efflux was initiated by allowing the influx of H^+ which dissipates any established membrane potential. ACMA quenching by H^+ indirectly informed about which ion species were translocated and how fast by KtrB or variant KtrB_{G316S} (Su *et al.*, 2016). Finally, the maximally possible ACMA quenching was determined by the addition of either 20 nM valinomycin (Val, 8 μ M in DMSO) for vesicles containing KCl, RbCl, or CsCl or 5 μ M sodium ionophore IV (Selectophore™ by Sigma-Aldrich [1 mM in DMSO]) for vesicles containing NaCl. Fluorescence traces were normalized to the initial signals before CCCP addition. Evaluation of fluorescence changes and decay rates was done with OriginPro 2017 (section 3.10).

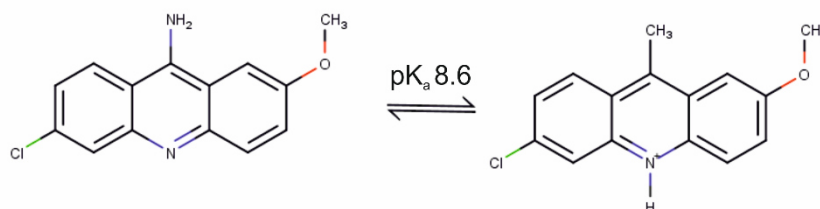


Figure 10 ACMA-dye. Structures of 9-amino-6-chloro-2-methoxyacridine under physiological conditions is present in the neutral (left) and monocationic (right) states ($pK_a = 8.6$).

3.8.4 Laser-induced liquid bead ion desorption-Mass spectrometry (LILBID-MS)

Measurements and data evaluation were performed by Dr. Oliver Peetz and Dr. Nils Hellwig (Institute of Physical and Theoretical Chemistry, Goethe-University Frankfurt). Native mass spectrometry was performed to determine the mass and integrity of the non-covalently linked KtrB-dimer in SMALPs. The main peak fraction of KtrB-SMALPs in LILBID buffer [20 mM NaCl and 20 mM Tris-HCl pH 8.0] was concentrated to 50 μ l after SEC. The native oligomeric state

was analyzed using a few μl of KtrB-containing SMALPs. Analysis was performed using a homebuilt reflectron time-of-flight (TOF) setup (Morgner *et al.*, 2007).

3.9 Electrophysiology

Nowadays, molecular mechanisms are studied with vast amounts of biophysical techniques for structural, computational and functional determinations. Electrophysiological techniques are the benchmark and perhaps the most comprehensive techniques among those. The advantage lies in their high sensitivity and fast time resolution without the need for modifications like labeling. There is a variety of different techniques to answer questions about electrogenic steps of a transport and to determine kinetic parameters such as affinities and rate constants. There are several electrophysiological techniques studying membrane proteins in living cells or native membranes like for example patch clamp, voltage and current clamp, or techniques using membrane mimetic systems like planar bilayer lipid membranes (BLM) or solid-supported membranes (SSM).

3.9.1 Theoretical Background of SSM-based electrophysiology

Solid-supported membrane (SSM)-based electrophysiology is an *in vitro* technique to study electrogenic transporter with slow uptake rates as well as fast channels (Bazzone *et al.*, 2017). SSM-based electrophysiology was proven to be a successful technique for studying electrogenic transporters (Garcia-Celma *et al.*, 2008, 2010; Wacker *et al.*, 2014; Bazzone *et al.*, 2016), ion exchangers (Patiño-Ruiz *et al.*, 2017; Patiño-Ruiz, Fendler and Călinescu, 2019), ion channels (Schulz *et al.*, 2009) and also ATPases (Pintschovius, Seifert and Fendler, 1997; Pintschovius, Fendler and Bamberg, 1999; Bartolomtnei *et al.*, 2009) from various organisms. This method has been invented approximately 30 years ago in the Lab of Klaus Fendler and has only recently gained more popularity. The foundation of the SSM consists of a self-assembling monolayer (SAM) C₁₈-mercaptan on a gold sensor (Love *et al.*, 2005). For this, vesicle or membrane fragments are adsorbed to a solid-supported membrane, made-up of phosphatidylcholine layer on top of a self-assembled monolayer (SAM) of C₁₈-mercaptan on a gold sensor. The simple adsorption of membrane vesicle is required to obtain signals due to the capacitive coupling of the SSM with the vesicles (Schulz *et al.*, 2009). The great advantage of the SSM in comparison to BLM is the high mechanical stability (Seifert, Fendler and Bamberg, 1993). For SSM-based electrophysiology measurements, the translocation of charged substrates into vesicles can be easily initiated by rapid concentration jumps. Most electrophysiological techniques, like BLM, are also restricted to fast gating channels, since

measuring transport as a macroscopic current requires high transport rates. In SSM-based electrophysiology many adsorbed vesicles amplify the signal on the supported membrane by measuring an ensemble of proteins (Grewer *et al.*, 2013; Bazzone, Barthmes and Fendler, 2017). Due to the robustness of the SSM-based electrophysiology, measurements can be carried out over the course of several hours without the loss of signal (Seifert, Fendler and Bamberg, 1993; Garcia-Celma, Szydelko and Dutzler, 2013).

3.9.1.1 Capacitive coupling on the SSM

The detection of currents via SSM-based electrophysiology is based on the capacitive coupling of protein-mediated transport processes through vesicles or membrane fragments adsorbed to the supported membrane (Seifert, Fendler and Bamberg, 1993; Pintschovius, Seifert and Fendler, 1997; Schulz, Garcia-Celma and Fendler, 2008; Bazzone *et al.*, 2013) as illustrated in Figure 11. This system can be described as an equivalent circuit similar to a BLM setup (Fahr, Lauger and Bamberg, 1981; Fendler *et al.*, 1993). The electrical properties of this capacitively coupled system are characterized by the capacitance (C) and conductance (G) of the membrane vesicles (C_p) and (G_p) and those of the solid-supported membrane (C_m) and (G_m), which can be expressed through the system time constant (τ_0) (Seifert, Fendler and Bamberg, 1993; Schulz, Garcia-Celma and Fendler, 2008):

$$\tau_0 = \frac{C_m + C_p}{G_m + G_p}$$

However, the conductance of the SSM (G_M) can be disregarded since it would be 0. The conductance G_L of the membrane vesicles illustrates their leakiness. Active transport of charged substrates into the vesicles results in pump or stationary current $I_p(t)$. Charging of the vesicle membrane will naturally also charge the SSM, because both membranes form a capacitively coupled system. The charging of the SSM will initiate a current movement in the measuring circuit allowing the detection of the capacitive current $I(t)$, which is always transient (Schulz, Garcia-Celma and Fendler, 2008). This transient current will decay with the time constant τ , which is smaller than the system time constant τ_0 . This process, however, depends on the stationary current (Bamberg *et al.*, 1979). The amplitude of the transient current $I(t)$ correlates with the stationary current $I_p(t)$, which is influenced by the $C_m/(C_m \cdot C_p)$ factor (Fahr, Lauger and Bamberg, 1981):

$$I(t) = \frac{C_m}{C_m + C_p} I_p \exp\left(-\frac{t}{\tau}\right)$$

The intensity and time resolution of the measured transient current depends on the charges translocated into the vesicle attached to the SSM. The greater the initial transport activity, the quicker the membrane potential increases, which leads to a fast drop in transient currents. Accordingly, no stationary transport can be observed on the SSM. Peak current and decay time are the significant parameters derived from the transient current (Schulz, Garcia-Celma and Fendler, 2008; Bazzone *et al.*, 2013). A critical obstacle associated with SSM electrophysiology is the difficulty to distinguish between steady-state and pre-steady-state reactions, since both can induce transient currents on the SSM (Bazzone, 2017).

Steady-state signals derive from stationary transport rates and their decay times are inversely proportional to the peak current (Schulz, Garcia-Celma and Fendler, 2008). The more protein is in the vesicles the bigger the peak current. Big peak currents account for fast charging of the membrane capacitor and a subsequent inhibition of transport leading to fast decay of the transient current. By reducing the lipid-to-protein ratio one could distinguish between pre-steady-state and steady-state signals, since increasing the LPR would slow the decay time of the steady-state signals as previously shown (Zuber *et al.*, 2005; Bazzone *et al.*, 2017).

For a pre steady-state signal, the decay time correlates with the rate of the reaction and is usually not determined by charging of the membrane capacitor. The decay time is therefore independent of the transporter density for pre steady-state signals, varying the LPR does not affect the decay time but only varies the peak current intensity. Usually, pre-steady state signals are much faster than steady state signals. However, in some cases pre-steady-state reactions can also be very slow and a critical evaluation of the data is necessary (Bazzone, 2017).

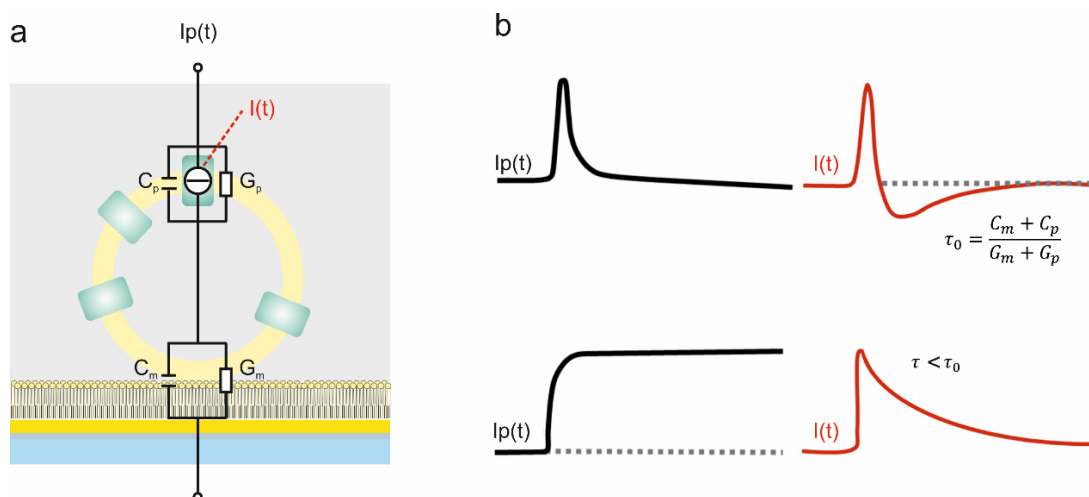


Figure 11 Representation of the capacitively coupled SSM and the proteoliposome. The electrical properties of the system can be described with an equivalent circuit, which is characterized by the conductance (G_m and G_p) and the capacitances (C_m and C_p) of the liposomal barrier and the contact region between liposomes and SSM. The transport protein is considered as a current source and generates a pump current $I_p(t)$ inducing the measured current $I(t)$ via capacitive coupling. Adapted from Schulz *et al.* 2008.

3.9.2 SSM-based electrophysiology

3.9.2.1 Equipment

Table 7 shows all equipment used for SSM-based electrophysiology measurements within the scope of this work.

Table 7 Overview of SSM equipment used in this work

Object	Typ/Specification	Manufacturer
2-way valve	NR225T011	NResearch, West Caldwell, USA
4-way valve	NR225T031	NResearch, West Caldwell, USA
Amplifier	427	Keithley
Extruder	Liposofast Basic	Avestin
Faraday cage		MPI biophysics
Manometer	GDH 14 AN	Greisinger electronics
O-ring	Silicon	Seal Science, Inc.
Oscilloscope	TDS 1002	Tektronik
Power Supply	PS-302A	Voltcraft ®
Power Supply	FPS 4A	Voltcraft ®
Reference electrode (AgCl)		MPI for biophysics
Sensor chip/gold electrode		Fraunhofer Institute for Surface Engineering and Thin Films
Solution containers	Polypropylen, 100 ml	Kartell
Sonifier	SONOREX	Bandelin
SSM cuvette		MPI for biophysics
Tubes	Internal diameter: 1.6 mm	SAINT-GOBAIN Permormance Plastics, TYGON ® Tubing
Valve control		MPI for biophysics
Voltage reference		MPI for biophysics
VYCLIC-three-way valve		VYGON

3.9.2.2 Preparation of the gel bridge

The gel bridge, which separates the reference electrode from the primary fluid pathway and prevents the mixing of electrode buffer with the SSM buffer, also serves as an electrical connection between the reference electrode and the fluid pathway. Therefore, a 2% agarose gel containing 100 mM KPi and 100 mM KCl, pH 7 was prepared. Approximately 40 µl of the

gel was filled into the cavity of the gel bridge. The gel bridge was stored at 4 °C in 100 mM KPi buffer, pH 7 until usage.

3.9.2.3 Chlorination of the reference electrode

Silver chloride electrodes were used as reference electrodes during the experiment. Due to abrasions, the chloride layer required regular regeneration. Therefore, the old chloride layer was removed by using sandpaper. Electrolysis was performed to regenerate the silver chloride layer of the reference electrode, using a power supplier, an ohmic resistor, an ampere-meter, a platinum electrode and the silver electrode connected. The electrodes were placed in a 1 M HCl solution. After applying voltage, the ohmic resistor was down-regulated to generate a current of $I = 0.5$ mA, measured by the ampere-meter. The chlorination was completed after approximately 20 min or shortly after the silver electrode exhibited a dark grey coloration due to the formation of silver chloride.

3.9.2.4 Preparation of the SSM setup

The SSM setup was filled with a mixture of 20% ethanol in water when not in use. Prior to installation of the SSM cuvette containing the sensor, the setup was washed with ddH₂O and equilibrated with 100 mM KPi (pH 7) at about 0.6 bar. This ensured that the system is free of air bubbles, before the sensor was installed.

3.9.2.5 Preparation of lipids

The lipid solution was needed to form the SSM together with the mercaptan monolayer on top of the gold electrode. It consisted of 1,2-Diphytanoyl-sn-glycerol-3-Phosphatidylcholine in chloroform (DPhyPC, 20 mg/ml) and octadecylamine in chloroform (5 mg/ml) mixed in 60:1 ratio, respectively. The mixture was dried with a rotary evaporator under fumigation with N₂ to remove the chloroform entirely. Subsequently, an appropriate amount of n-decan was added to the lipid film to obtain a concentration of 15 mg/ml. The lipid solution was transferred to a glass vial, flooded with N₂ and stored at -20 °C until usage (Bazzone *et al.*, 2013).

3.9.2.6 Preparation of the sensor chip

The sensor-chip with the diameter of 9 x 22 mm is made from borofloat-glass and has a 10 nm thick adherent chromium layer (Figure 12). On top of that is a 100 nm thick gold layer, which has an active area of a circle with the diameter of 1 mm, where the SSM is assembled (Schulz, Garcia-Celma and Fendler, 2008). The sensor chips were stored in a 10 mM octadecanethiol solution in ethanol for formation of a mercaptane monolayer. The mercaptane layer

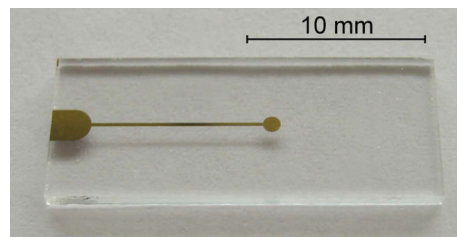


Figure 12. Sensor chip with gold electrode. The gold tip has an active area with a diameter of 1 mm where the SSM is formed. Figure from Schulz *et al.* (2008)

served as the basis for SSM formation. New gold electrodes were incubated overnight in the solution before first time usage. Already used gold electrodes required an incubation period of one hour to form the octadecanethiol layer. After washing the sensor with ethanol and drying under N₂ flow, a monolayer of hydrophobic carbon chains covered the surface (Bazzone *et al.*, 2013). To the active area of the sensor-chip 2 µl of the previously prepared lipid solution (section 3.9.2.5) was added. The lipid solution was needed for the formation of the solid-supported membrane (SSM). The sensor was quickly set up in the cuvette and after mounting, the cuvette was perfused with 100 mM KPi, pH 7 to assemble the SSM.

3.9.2.7 Membrane parameters

Before starting the experiment, the correct formation of the SSM needed to be confirmed by measuring the capacitance and conductance of the sensor chip. For measuring the conductance, a direct voltage (DC) of $U = 100$ mV was applied, which immediately led to a fast drop of current followed by a slow ongoing decay. The drop of current is the result from charging the membrane capacitor with the voltage of 100 mV. The fully charged membrane capacitor generates a constant current, which is described by the ohmic law below, and can be read out after $t = 1$ s. The optimal range for the conductance, was found to be 0.1 to 0.2 nS (Bazzone *et al.*, 2013). The higher the conductance the more damaged is the membrane. A leaky membrane allows unregulated ion flow resulting in big artefacts and bigger signal to noise ratios.

$$G = 1/R = I/U$$

In this thesis a conductance of 0.1 to 0.3 nS was within the acceptable range.

The capacitance was measured by applying a triangular voltage (AC) of $U = \pm 50$ mV. The result of an AC voltage is a square current. The reversion of the voltage source leads to a charge reversal of the membrane capacitor. The measured currents are constant as they are proportional to voltage difference.

$$C = Q/U = It/U$$

The optimal range for the capacitance of the SSM is 1.5 to 3.5 nF (Bazzone *et al.*, 2013). A high capacitance is the result of an incorrectly formed SSM, meaning the membrane does not cover the whole gold surface.

3.9.2.8 Applying liposomes to the SSM

Before applying the liposomes, the setup was equilibrated to the non-activating (NA)-solution, composed of the SSM ground buffer [50 mM Tris, 50 mM MES, 50 mM HEPES, 5 mM MgCl₂, 200 mM choline chloride, pH 7.5] with additionally 100 mM choline chloride. One aliquot of 20 μ l proteoliposome was slowly thawed on ice. The proteoliposomes or control liposomes with a lipid concentration of 10 mg/ml and an LPR of either 5:1, 10:1 or 50:1 were diluted to 2-5 mg/ml and sonicated using an ultrasonic bath (Sonorex RK 52 H, Bandelin). The sample was sonicated up to six times for 10 s with 10 s intervals on ice until the suspension appeared clear. After sonification, 32 μ l of the suspension were applied to the SSM through the outlet. Therefore, the outlet connector and gel bridge together with the reference electrode were removed (Figure 13). This was followed by an incubation period of 1 to 2 h to allow the adsorption of the liposomes to the SSM.

3.9.2.9 Flow protocol and signal recording

A simple solution exchange flow protocol was used in the present work. After the flow of the non-activating (NA) solution, the solution was changed to the activating (A) solution containing the substrate-initiated uptake, which resulted in a transient current. Subsequently, the flow of NA solution was started again to restore the initial conditions (Schulz, Garcia-Celma and Fendler, 2008). Solution flow was controlled by applying a pressure of 0.6 bar to the solution containers and automated switching of the valves. Since all solutions need to be as iso-osmotic as possible to avoid electrical artefacts on the SSM, the same SSM ground buffer was used for all the solutions during preparations. The NA and A activating solutions contained additional 100 mM of different combinations of chloride salts. These salts were LiCl, NaCl, KCl, RbCl,

CsCl and choline-Cl, respectively. All used combinations are listed in Supplement Table 12. The detected signals were recorded by the SURF²R software and exported as ASCII files to OriginPro 2017 for evaluation.

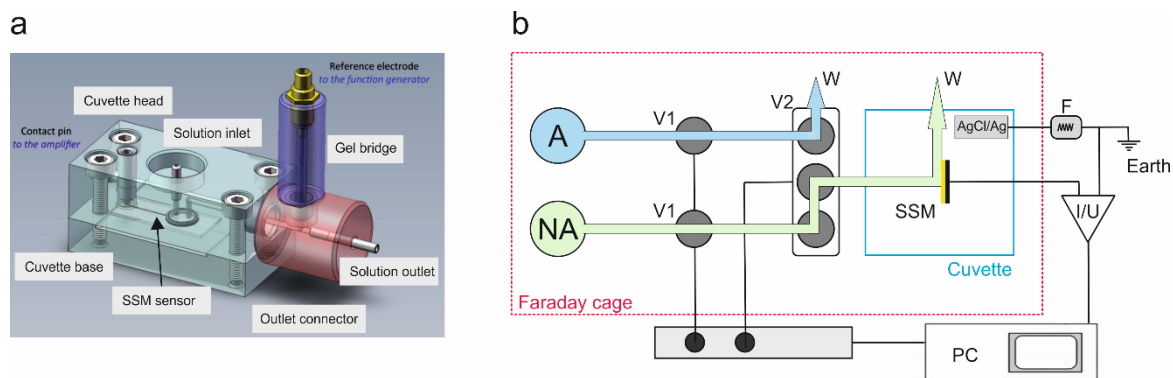


Figure 13 Schematic diagram of the SSM cuvette and single solution exchange protocols. (a) The SSM cuvette. The SSM sensor chip is inserted between the base and the head of the cuvette. Reference electrode and gel bridge are connected to the main fluid pathway. The contact pin is connected with the amplifier and the reference electrode with the function generator. Figure adapted from Bazzone *et al.* (2013). (b) System set-up for simple solution exchange with activating (A) and non-activating (NA) solution shown in blue and green, respectively. The dotted red line represents the faraday cage. An Ag/AgCl electrode serves as a reference electrode for detecting currents (I/U). The electrical properties of the SSM are determined with the function generator (F). Signal recording and valve control (V1 and V2) is accomplished by a computer (PC). All solutions are directed to the waste (W) after passing through the cuvette. Figure adapted from Schulz *et al.* (2008).

3.9.2.10 Run down control

The time-dependent stability of the SSM-based electrophysiology setup needed to be monitored during a series of measurements. Therefore, the current for the same activating-solution was measured at the beginning and end of each series and the peak currents were compared. A run-down of 15% was considered to be within the acceptable range. A linear run-down was presumed and mathematically corrected using the formula for the correction factor:

$$F = \frac{I_i}{I_i - (I_i - I_f) \frac{t}{t_f}}$$

With I_i corresponding to the initial current and I_f to the final current at the end of each series of measurements. t describes the relative time of every individual measurement and t_f the duration of the whole series of measurements. The measured currents were multiplied with the respective correction factor F .

3.10 Data evaluation of the signal decay in SSM and ACMA

General data analysis was realized using OriginPro2017. The data resulting from SSM-based electrophysiology and AMCA assays were fitted by one-phase exponential functions to obtain the respective time constants:

$$f(t) = A \exp\left(-\frac{t}{\tau}\right)$$

The half-maximal signal decay time $\tau_{1/2}$ was used as a parameter to evaluate the decay of the transient currents and was determined as follows: $\tau_{1/2} = \tau \ln(2)$. For the ACMA evaluation the rates of the fluorescence decay were determined according to $k = 1/\tau$.

4. Results

4.1 Establishing protein purification protocols for functional assays

Biochemical and biophysical characterization of KtrB always requires adequate amounts of pure and stable protein. For this purpose, *ktrB-his₆* was expressed under the control of an arabinose promoter in *E. coli* strain LB2003 transformed with pEL903. Cells were grown in K3 minimal medium (Epstein and Kim, 1971) to ensure the functionality of the produced KtrB. Since LB2003 is deficient in all major endogenous K⁺ uptake systems cell growth under K⁺ limitation is only possible upon production of functional K⁺ uptake systems such as KtrB. The growth curve of LB2003pEL903 induced from the start with 0.02% L-arabinose is shown in Supplement Figure 45. Protein was extracted via Ni²⁺-NTA affinity chromatography after cell rupture, isolation and solubilization of membranes with DDM. To further improved the purity of the extracted protein size-exclusion chromatography was performed on a Superdex 200 Increase 10/300 GL column (Figure 14 b). The purity of the protein was analyzed by SDS-PAGE showing two major fragments at apparent molecular weights of ~37 and ~70 kDa as well as higher oligomeric states (Figure 14 a and c). These are mainly corresponding to KtrB-His₆ monomers and dimers, respectively (Mikusevic, 2014). The monodisperse size-exclusion chromatography profile indicates a high homogeneity of the purified protein. A purification using this protocol resulted in ~3 mg protein from 12 L of cell culture. KtrB-His₆ purified following this protocol was further used for reconstitution into liposomes and subsequent SSM-based electrophysiology.

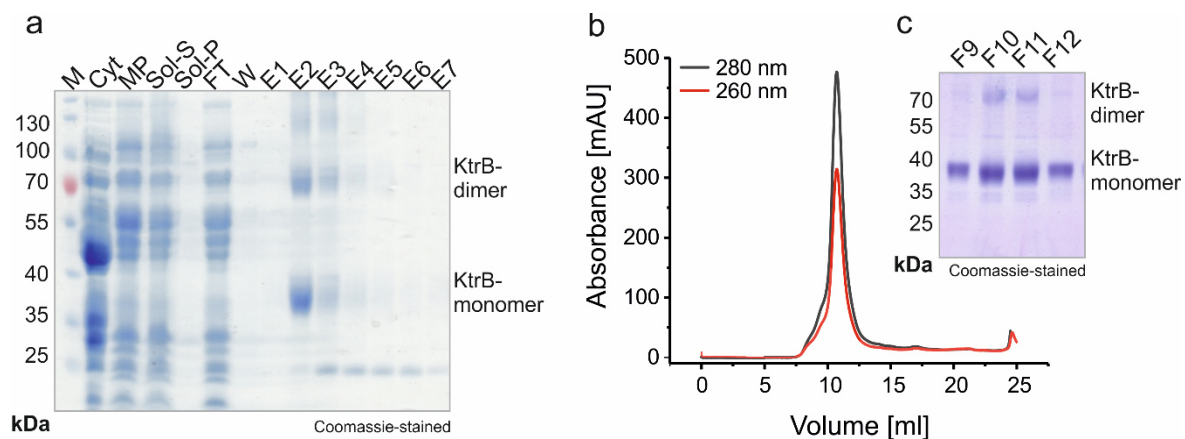


Figure 14 Purification profile of KtrB-His₆ from *E. coli* strain LB2003. (a) 10 μ l protein samples from each purification step were introduced to a 12% SDS-PAGE. The following samples were analyzed: cytoplasm (Cyt) and membrane pellet (MP) after membrane preparation, supernatant after solubilization (Sol-S), pellet after solubilization (Sol-P), flow through (FT) and the wash step (W) after binding to the Ni²⁺-NTA resin and elution fractions (E1-E7) from the Ni²⁺-NTA resin, each eluted with 1/2x column volume. The predicted molecular mass for KtrB-His₆ is 50.5 kDa, but the protein migrates at ~37 kDa. (b) Size exclusion chromatography was performed using a Superdex 200 Increase 10/300 GL column in SSM ground buffer, supplemented with 0.04% DDM. Absorbance was followed at 280 and 60 nm. The main peak centered at an elution volume of 10.8 ml. (c) Elution fractions F6 to F12 of KtrB-His₆ after size exclusion chromatography are shown in the 12% SDS-PAGE. Samples of 10 μ l were loaded.

4.1.1 Large-scale purification of an improved KtrB-3C-His₁₀ construct

The first purification strategy had the advantage that the functionality of the overexpressed protein was guaranteed by growing the cells under K⁺ limitation. However, the yields were rather low, limiting the experimental turnover. For this purpose, a new expression plasmid was used, which provided more protein but required a late induction since protein production inhibited cell growth. LB2003 cells transformed with plasmid pBKtrB-C3H were grown in KML medium (Supplement Figure 46) and the expression was induced at an OD₆₀₀ of 1.6-1.8 with 0.02% L-arabinose. 1 ½ h after induction the cells were harvested for optimal protein yields. Membranes were prepared and solubilized with DDM, before the protein was extracted by Ni²⁺-NTA affinity chromatography. Fractions containing KtrB-3C-His₁₀ were pooled, concentrated and loaded onto a Superdex 200 Increase 10/300 GL column. The purity of the protein was further improved with size-exclusion chromatography (SEC) as shown by SDS-PAGE (Figure 15 a). Additionally, a buffer exchange from buffer W to LiCl- or choline-Cl-based ITC buffers was realized with the SEC run. The elution profile shows a peak centered around an elution volume of 10.8 ml correlating to the KtrB-dimer (Figure 15 b). An average purification from 12 L medium, with the new established protocol, almost tripled the yielded from ~3 mg to ~8 mg of pure protein. Concentrations between 40- 70 µM of detergent-purified KtrB-3C-His₁₀ were used for ITC experiments or reconstitution into liposomes.

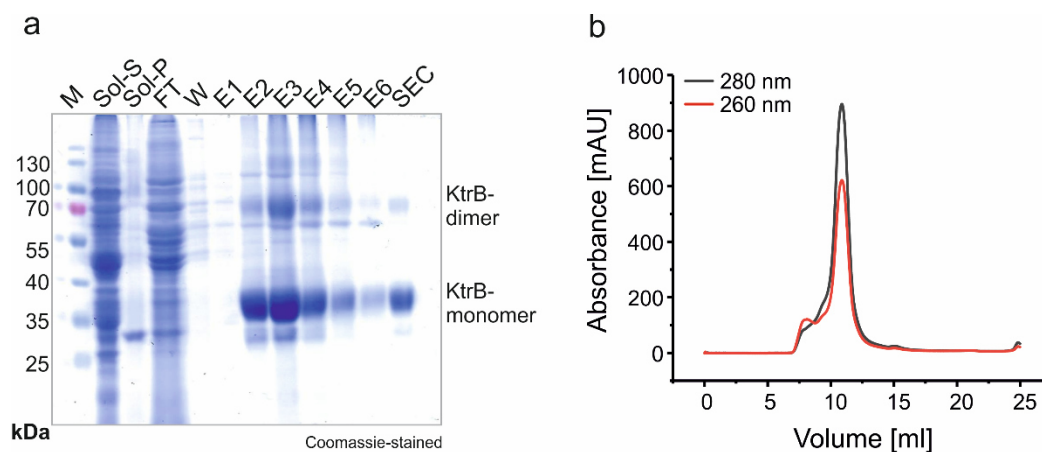


Figure 15 Purification of KtrB-3C-His₁₀ from *E. coli* strain LB2003. (a) 10 µl protein samples from each purification step were introduced to a 12% SDS-PAGE. The following samples were analyzed: supernatant after solubilization (Sol-S), the pellet after solubilization (Sol-P), the flow through (FT) and the wash step (W) after binding to the Ni²⁺-NTA resin, elution fractions (E1-E6) from the Ni²⁺-NTA resin, each eluted with 1/2x column volume and the main peak after size-exclusion chromatography (SEC). The predicted molecular mass for KtrB-3C-His₁₀ is 51.6 kDa, but the protein migrates at ~37 kDa. (b) Size exclusion chromatography was performed using a Superdex 200 Increase 10/300 GL column in basic ITC buffer, supplemented with 0.04% DDM. Absorbance was followed at 280 and 60 nm. The main peaks centered at an elution volume of 10.8 ml.

4.1.2 Purification of KtrB-3C-His₁₀ using styrene-maleic acid copolymer lipid particle (SMALP)

Identifying optimal conditions for membrane protein purification, from finding the right buffer conditions to suitable detergents, can be a challenging task. Detergents are the key players here. They are great tools to isolate membrane proteins for further studies since they create micelles that roughly mimic the natural conditions in the membrane. In recent years critical concerns were raised about using detergents. The reason is, that a lot of membrane proteins rely on lipid interaction for their function. These lipids are usually removed in the course of protein purification with detergents. Purifying membrane proteins without the need for detergents while preserving the proteins' natural lipid environment is therefore very desirable. The use of styrene-maleic acid copolymer (SMA) on natural membranes enables the extraction of small lipid discs containing membrane proteins (Knowles *et al.*, 2009; Jamshad *et al.*, 2011) and because of this property it has gained popularity among membrane protein researchers in the last years (Dörr *et al.*, 2014; Gulati *et al.*, 2014; Sun and Gennis, 2019).

To test this novel detergent-free method of purification and additionally investigate the integrity of the KtrB dimer, KtrB-3C-His₁₀ was purified from *E. coli* LB2003 membranes by the use of 2.5% SMA polymer Xiran® SL 30010 P20 (Polyscope). The protein was extracted via Ni²⁺-NTA and its purity was further improved by size-exclusion chromatography on a Superose 6 Increase 10/300 GL column. The purity of the protein was analyzed by SDS-PAGE showing two major fragments at apparent molecular weights of ~37 and ~70 kDa as well as higher

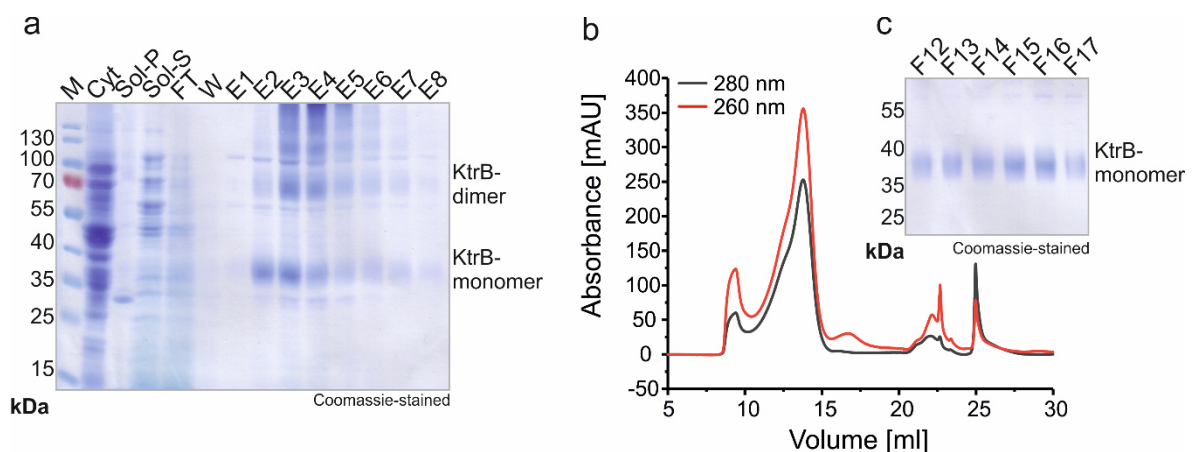


Figure 16 Purification of KtrB-3C-His₁₀ from *E. coli* strain LB2003 with SMAs. (a) 10 μ l protein samples from each purification step were introduced to a 12% SDS-PAGE. The following samples were analyzed: supernatant after solubilization (Sol-S), the pellet after solubilization (Sol-P), the flow through (FT) and the wash step (W) after binding to the Ni²⁺-NTA resin, elution fractions (E1-E6) from the Ni²⁺-NTA resin, each eluted with 1/2x column volume and the main peak after size-exclusion chromatography (SEC). The predicted molecular mass for KtrB-3C-His₁₀ is 51.6 kDa, but the protein migrates at ~37 kDa. (b) Size exclusion chromatography was performed using a Superose 6 Increase 10/300 GL column in LILBID buffer. The main peaks centered at an elution volume of 13.8 ml. Absorbance was followed at 280 and 60 nm. (c) Elution fractions F12-17 of KtrB/SMALP after size exclusion chromatography are shown in the 12% SDS-PAGE. Samples of 10 μ l were loaded.

oligomeric states referring to KtrB (Figure 16). One 0.5 ml fraction of the main peak was taken and concentrated to 50 μ l to address the integrity and the oligomeric state of KtrB in SMALPs using LILBID-MS.

4.2 Integrity of the KtrB dimer

Since the function of a protein depends on its structural integrity, KtrB purified with SMAs was investigated with LILBID-MS to determine its integrity and oligomeric state. In its native oligomeric state KtrB forms a functional dimer, which was also shown to be stable in detergent (Diskowski *et al.*, 2017; Schrecker, 2019). The oligomeric state and integrity of KtrB purified using SMALP was investigated and compared with detergent-purified KtrB. LILBID-MS spectra revealed populations of KtrB dimers in SMAs at low laser intensities and only KtrB monomers without SMALPs at high laser intensities (Figure 17). At low laser intensities a charge distribution of 1 to 5 for the KtrB dimer in SMAs was shown. The broad peaks correlate to a mass of approximately 166 kDa, which is about 62 kDa bigger than the dimer. A KtrB dimer without SMALPs was never observed, which can be attributed to the high binding affinity of the non-covalent interaction of the polymers and lipids wrapped around the protein.

Since the extraction of protein with SMALPs was so successful, a reconstitution of protein into liposomes for functional evaluation should be tried in the future.

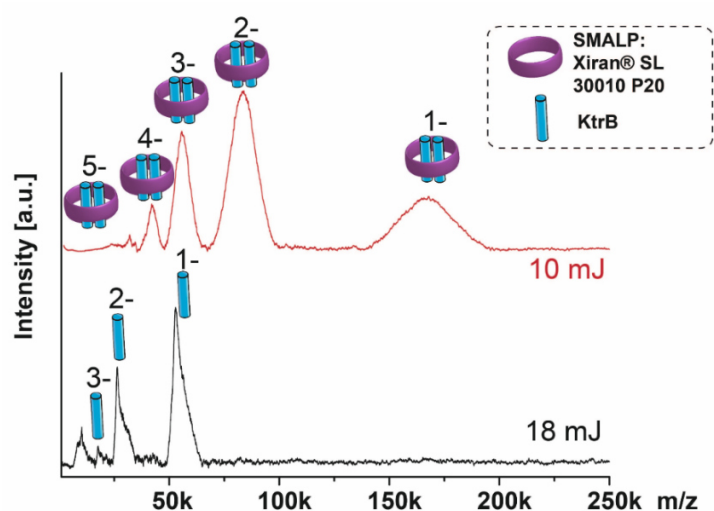


Figure 17 LILBID spectra of KtrB in SMALPs. Adapted from Hellwig *et al.* 2018. LILBID-MS spectra of KtrB/SMALP complex using a soft mode (low laser power, 10 mJ) and harsh mode (high laser power, 18 mJ) were compared. The soft laser mode yielded different charged states of the protein/SMALP-complex (indicated with 5-, 4-, 3-, 2- and 1-), while the harsh mode revealed different charged states of only the monomeric protein (indicated with 3-, 2- and 1- in orange). Sample preparation was performed by Vedrana Mikusevic, Institute of Biochemistry, Goethe-University Frankfurt. LILBID-MS analysis was performed by Dr. Oliver Peetz and Dr. Nils Hellwig, Institute of Physical and Theoretical Chemistry, Goethe-University Frankfurt.

4.3 Ion binding of KtrB-3C-His₁₀

Ion channels, as an imperative part of every lipid bilayer, are required to selectively discriminate between one ion over many others for binding and translocation. In this section the K⁺ channel subunit KtrB was investigated for its substrate specificity, since previous studies indicated a low K⁺ over Na⁺ selectivity (Tholema *et al.*, 2005; Hänel, Löchte, *et al.*, 2010). Ion binding was addressed with isothermal titration calorimetry (ITC).

4.3.1 Binding affinities of different cations to KtrB-3C-His₁₀

ITC experiments were performed to uncover which metal ions bind to KtrB. Specifically, cations from the first group of elements were investigated. These experiments should clarify once and for all which cation KtrB favors with what affinity in its atypical selectivity filter. For all ITC measurements, a basic ITC buffer with 200 mM choline chloride was used. The ITC titration buffers contained between 10 to 50 mM of LiCl, NaCl, KCl, RbCl or CsCl compensated to 200 mM of salt with choline chloride. The titration buffers were prepared to match the 200 mM choline chloride of the basic ITC buffer in which the protein is absorbed. Buffer to buffer control titrations are shown in Figure 18 a-d for each ion species. Binding affinities of KtrB towards each cation species were gained from three independent experiments, which were subsequently averaged. Mean data \pm SD are summarized in Table 8. Binding affinities for Na⁺, K⁺, Rb⁺, and Cs⁺ were obtained, while no binding was observed for Li⁺ (Supplement Figure 48). The affinities for the four binders were all in the low mM range, between 1.6 and 2.9 mM (Figure 18). Clear differences between Na⁺ and the other three cations were found. While the binding enthalpies for three of the alleged selectivity filter residents, K⁺, Rb⁺, and Cs⁺, were exothermic (\sim -4.5 kcal mol⁻¹), the binding of Na⁺ was obviously endothermic (\sim 3 kcal mol⁻¹) (Figure 18 e-h). This endothermic reaction of Na⁺ could reflect the high energy needed to dehydrate Na⁺. A small ion like Na⁺ is stronger hydrated than the group members below in the periodic table, it is therefore borderline kosmotropic, indicating that it would be unfavorable to dehydrate it (Collins, 1995). The binding affinity to K⁺ was expected to be significantly lower based on previously performed growth experiments in external potassium concentrations as low as 100 μ M (Tholema *et al.*, 2005; Hänel, Löchte, *et al.*, 2010). Based on this variance, the ITC experiments need to be critically examined and adjusted. I concluded that the low affinities could be a result of a lack of small cations, which under physiological conditions would be always present. The absence of small cations could have caused a destabilization of the protein. Consequently, the selectivity filter could be collapsed and have a changed affinity. Another possibility is that the low binding affinity reflects the binding of cations elsewhere in

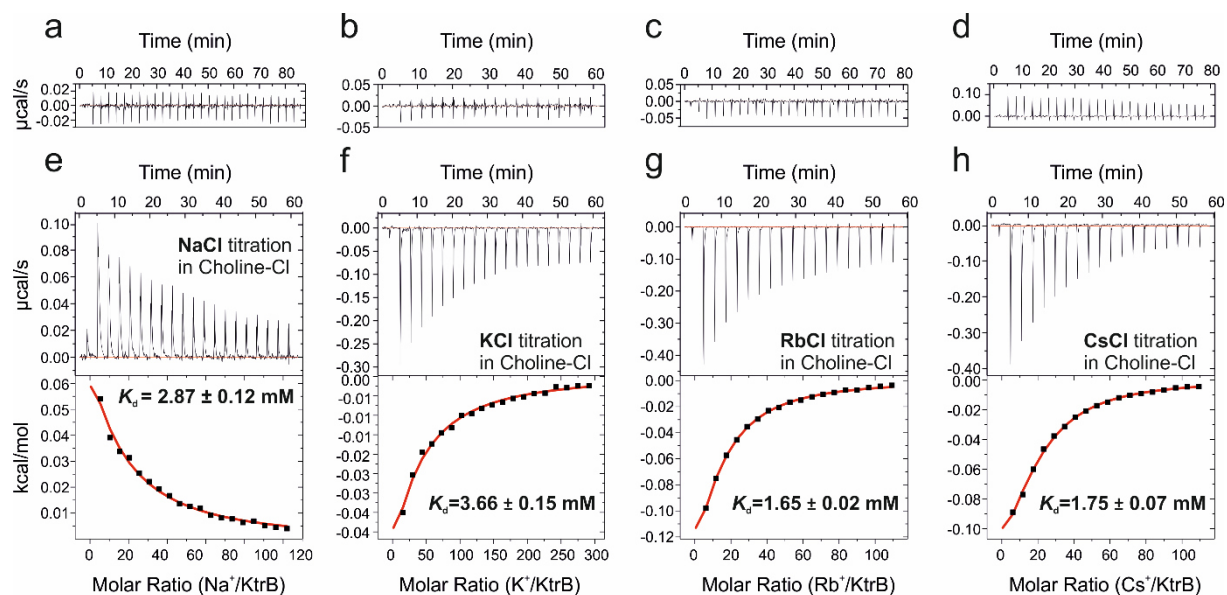


Figure 18 Binding affinity of monovalent cations to VaKtrB-3C-His₁₀ in choline chloride buffer examined by ITC. Adapted from Mikusevic *et al.* 2019. (a-d) Cation to buffer control titrations are shown above each cation to protein titration. For the cation to protein titrations the upper panels show the raw heat exchange data, associated with Na⁺ (e), K⁺ (f), Rb⁺ (g) or Cs⁺ (h) binding to detergent-solubilized VaKtrB-3C-His₁₀ in 200 mM choline chloride buffered with 20 mM Tris-HCl pH 7.5. The lower panels giving the integrated injection heat pulses, normalized per mole of injection, reveal different binding curves fitted by one-site binding model. K_D is given as mean values \pm SE. The data each represent an example of three independent experiments. Mean data \pm SD are summarized in Table 8.

the protein leading to its stabilization. A similar stabilization effect was shown for KcsA in the presence of certain small cations (Krishnan *et al.*, 2005). To address this concern, all measurements were repeated with LiCl replacing choline chloride in all buffers, since Li⁺ was the only ion for which no binding was detected in the initial measurements.

The basic ITC buffer containing the protein was adapted and is now comprised of 200 mM LiCl instead of choline chloride. The titration buffers contained between 5 and 50 mM NaCl, KCl, RbCl or CsCl compensated to 200 mM of salt with LiCl. Buffer to buffer titrations are again shown above the cation to protein titrations in Figure 19 a-d. The changed buffer conditions revealed considerably different binding affinities for KtrB as reflected by the data in Figure 19 e-h. Now the apparent affinity for Na⁺ is so low that it could not be measured. The affinities of Rb⁺ and Cs⁺ remained similar to the ones measured in the previous buffer conditions. Remarkably, the affinity for K⁺ towards KtrB increased drastically. The apparent K_D value decreased from 2.9 mM to approximately 91 μ M (cf. Figure 18, Figure 19 and Table 8) in the new buffer conditions, which is a factor of \sim 30. Hence, the small cation Li⁺ led to a modulated binding profile in which the binding of K⁺ was significantly preferred over all other tested cations. This could be a general effect of stabilizing the protein and/or hinting towards a modulatory role of small cations inside the SF. Li⁺ is a rather low abundant ion in nature. To investigate the modulatory effect of small cations further, a choline-based ITC buffer containing

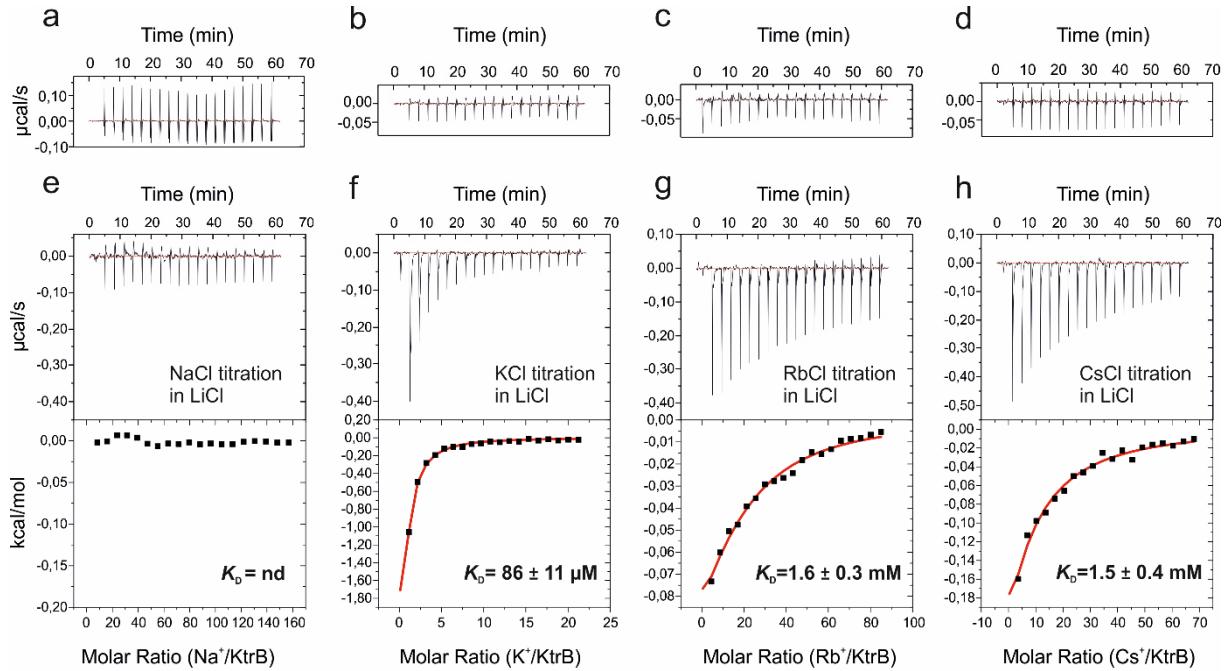


Figure 19 Binding affinity of monovalent cations to VaKtrB-3C-His₁₀ in lithium chloride buffer examined by ITC. Adapted from Mikusevic *et al.* 2019. (a-d) Cation to buffer control titrations are shown above each cation to protein titration. For the cation to protein titrations the upper panels show the raw heat exchange data, associated with Na⁺ (e), K⁺ (f), Rb⁺ (g) or Cs⁺ (h) binding to detergent-solubilized VaKtrB-3C-His₁₀ in 200 mM LiCl buffered with 20 mM Tris-HCl pH 7.5. The lower panels giving the integrated injection heat pulses, normalized per mole of injection, reveal different binding curves fitted by one-site binding model. K_D is given as mean values \pm SE. The data each represent an example of three independent experiments. Mean data \pm SD are summarized in Table 8.

the protein was supplemented with 5 mM NaCl and K⁺ titration experiments were carried out. Na⁺ is one of the most abundant cations in nature and it is known to stimulate K⁺ uptake through KtrAB. Similar to the LiCl-based buffer the presence of low millimolar NaCl concentrations led to a decreased K_D value to 260 μM (Figure 20). In conclusion, small cations like Li⁺ and particularly Na⁺ appear to modulate the architecture of the selectivity filter and probably the whole protein. This results in a significant selectivity for K⁺ over all other cations. The modest binding affinities of Rb⁺, Cs⁺ and potentially Na⁺ could be indicating that these ions do not bind to the selectivity filter at all. They could instead interact or bind unspecifically in the cavity making up the ion translocation pathway. To test for this hypothesis, I addressed the question whether all ions bind to the same, overlapping or different binding sites.

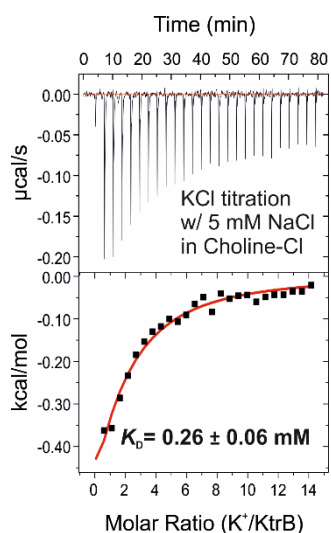


Figure 20 Binding affinity of K^+ to VaKtrB-3C-His₁₀ in the presence of NaCl. Adapted from Mikusevic *et al.* 2019. For the K^+ to protein titrations the upper panel shows the raw heat exchange data, associated with K^+ binding to detergent-solubilized VaKtrB-3C-His₁₀ in 195 mM choline chloride and 5 mM NaCl buffered with 20 mM Tris-HCl, pH 7.5. The lower panel displays the integrated injection heat pulses, normalized per mole of injection, fitted by one-site binding model. K_D is given as mean values \pm SE.

Table 8 Cation binding affinities to KtrB determined with ITC. Adapted from Mikusevic *et al.* 2019. The ionic radii r are shown in Å (Hill, 2001). ITC: K_D values were obtained from a fit to a single binding isotherm ($n = 3$).

Ions	r (Å)	K_D^{choline} (mM)	K_D^{lithium} (mM)
Li ⁺	0.60	nd	--
Na ⁺	0.95	1.8 ± 0.4	nd
K ⁺	1.33	2.9 ± 0.3	0.091 ± 0.012
Rb ⁺	1.48	1.9 ± 0.1	2.4 ± 0.2
Cs ⁺	1.69	1.6 ± 0.1	1.7 ± 0.3

nd: not detectable

4.3.2 Binding competition to the SF of KtrB

To test whether the low-affinity binders Na^+ , Rb^+ , and Cs^+ bind to the same or different sites in KtrB as the high-affinity binder K^+ , a cation competition assay using ITC was performed. For this assay, the total salt concentration of the ITC buffer was kept constant at 200 mM. The basic ITC buffer with LiCl containing KtrB was compensated with 50 mM of either NaCl, RbCl or CsCl. ITC titration buffer with 50 mM KCl was used for all experiments. The two bigger cations Rb^+ and Cs^+ utterly prohibited K^+ binding as shown in Figure 21 a and b. In the presence of 50 mM NaCl the apparent affinity for K^+ decreased more than 10-fold compared to its value in the presence of 5 mM NaCl ($K_D = 260 \mu\text{M}$) to a K_D of 1.8 mM (Figure 20 and Figure 21 c). However, even when raising the Na^+ concentration further to 200 mM, a concentration close to environmental conditions, the apparent affinity was still 3.5 mM for K^+ (Figure 21 d). This K_D suggests that the binding of K^+ is still preferred over the binding of Na^+ . In conclusion, all ions seem to bind to an identical or overlapping binding site likely localized in the selectivity filter as rationalized by the high binding affinity for K^+ . Na^+ appears to bind with an incomparably low affinity, making it immeasurable with ITC. Taken together, the ITC data show a clear preference of K^+ binding to KtrB over all other cations, a result previously anticipated.

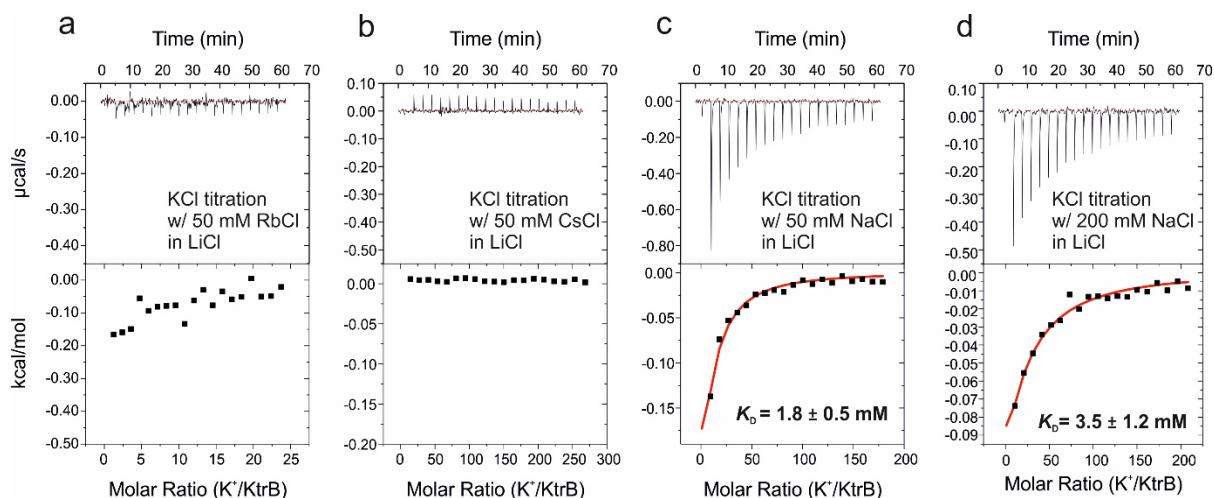


Figure 21 Ion binding competition examined by ITC. Adapted from Mikusevic *et al.* 2019. (a-d) Potassium to protein titration in the presence of different cations. (a-c) show KCl titration to protein solutions that contain 50 mM RbCl, CsCl or NaCl in 150 mM LiCl solution buffered with 20 mM Tris-HCl pH 7.5. (d) KCl titration to protein solution in 200 mM NaCl. The lower panels giving the integrated injection heat pulses, normalized per mole of injection, reveal different binding curves fitted by one-site binding model. K_D s are given as mean values \pm SE. The data each represent an example of three independent experiments.

4.4 Establishing functional assays to address ion translocation

Preferential K⁺ binding was determined by ITC, nevertheless, additional cations also showed the ability to bind to KtrB. Ion binding is a prerequisite for ion translocation, yet it is not a warranty. To address which ions are translocated by KtrB, two functional assays, namely SSM-based electrophysiology and a fluorescence-based transport assay, were established for KtrB in this thesis.

4.4.1 SSM-based electrophysiology

Measuring ion transporters and pumps with conventional electrophysiology techniques can be challenging since most of them rely on fast conductance only exhibited by channels. The channel-like subunit KtrB of the K⁺ uptake system KtrAB was believed to be slow based on whole-cell K⁺ uptake experiments. Furthermore, KtrAB was initially suggested to function as a K⁺/Na⁺ symporter (Tholema *et al.*, 1999). For this reason, SSM-based electrophysiology was selected as the method of choice to study ion translocation through KtrB. With the physically robust SSM an ensemble of electrogenic transporters can be measured at the same time. The method was already successfully applied studying electrogenic transporters (Seifert, Fendler and Bamberg, 1993; Pintschovius and Fendler, 1999; Garcia-Celma *et al.*, 2008; Bazzone *et al.*, 2013; Grewer *et al.*, 2013) and channels (Schulz *et al.*, 2009). Additionally, multiple conditions can be sequential tested to determine various kinetic parameters from transient currents. Similar to black lipid membranes (BLM) this method relies on capacitive coupling (Garcia-Celma *et al.*, 2007).

To perform SSM-based electrophysiology measurements, proteoliposomes containing KtrB had to be prepared and adsorbed to the established solid-supported membrane. Before each adsorption of proteoliposomes, the conductance and capacitance of the prepared SSM sensors were determined (Figure 22). The SSM sensor parameters were checked directly after mounting the cuvette, containing the sensor chip, and approximately 30 min after its assembly. During this incubation period the membranes were occasionally washed with NA buffer, containing 100 mM choline chloride, to check for their stability. The capacitance was determined applying triangular voltage (50 mV). The conductance of the membrane was gained by applying DC voltage (100 mV). Only membranes exhibiting parameters within the range were used for the SSM-based electrophysiology measurements. Table 9 shows the average values and deviation of conductance and capacitance of all membranes used during the course of this work. It demonstrates that the prepared membranes were well within the acceptable range showed by the small deviations.

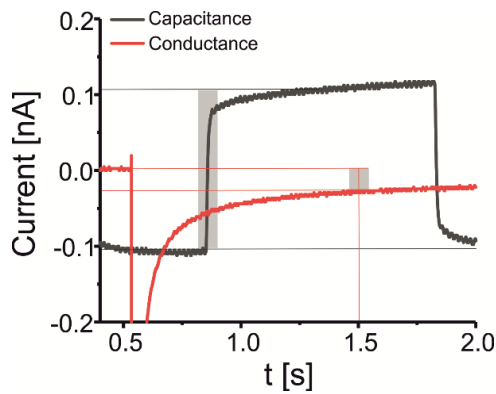


Figure 22 Exemplary measurements to determine the capacitance and conductivity of an SSM. Measured currents can be used to determine the capacitance and conductivity of the SSM. The conductance corresponds to the difference between the horizontal red lines. The capacitance corresponds to the difference between the horizontal black lines.

After the application of either empty control liposomes or proteoliposomes to the SSM sensor, transient currents were recorded by applying a 1.5 second simple solution exchange protocol [NA (0.5 s) – A (0.5 s) – NA (0.5 s)] shown in Figure 23. Background currents obtained with empty liposomes were reduced to a minimum by adjusting the buffer conditions. The basic SSM buffer for all solutions consisted of 50 mM Tris, 50 mM MES, 50 mM HEPES, 5 mM MgCl₂, 200 mM choline-Cl at a pH of 7.5. To suppress the effect of the background currents additional 200 mM choline-Cl were present in all working solutions. The basic SSM buffer was prepared in 1.25x composition and diluted 1/5 with 500 mM of the respective salts to guarantee the lowest possible background, since especially more kosmotropic ions cause big artefacts (Garcia-Celma *et al.*, 2007; Schulz, Garcia-Celma and Fendler, 2008). All tested buffer compositions are listed in Supplement Table 12 and all buffer measurements on empty liposomes are summarized in the Supplement Tables 13 to 19. Subsequently, the same solution exchange protocol with potassium chloride in the activating solution was applied to KtrB-containing liposomes (Figure 23). Currents significantly over background were determined at all KCl concentrations tested. In the course of this work LPRs of 5:1, 10:1 and 50:1 were used for SSM-based electrophysiology.

Table 9 Overview of the average values of capacitance C [nF] and conductance G [nS] and the corresponding deviations of the solid-supported membranes used during this work (n=37).

C [nF]	ΔC [nF]	G [nS]	ΔG [nS]
2.79	0.62	0.14	0.05

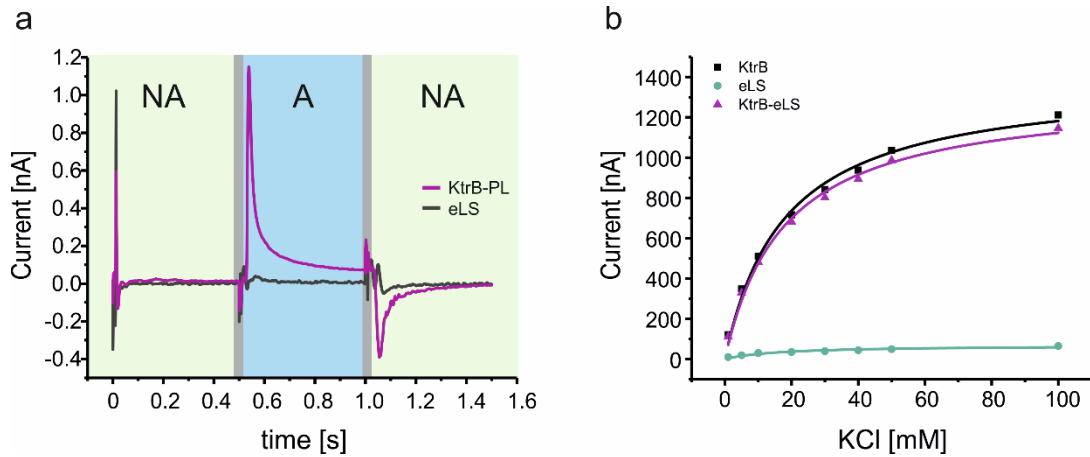


Figure 23 Flow protocol and K^+ concentration jumps of KtrB proteoliposomes (KtrB-PL) and control liposomes (LS) in comparison. (a) Recording of the transient currents from KtrB-containing liposomes (KtrB-PL) and empty liposomes (eLS) after a 100 mM choline chloride (NA, light green area) to KCl (A, light blue area) concentration jump. The areas, highlighted in light grey, mark the switching artifact of the valves. (b) Peak currents recorded of KtrB-PL and eLS at different KCl concentrations, respectively, are subtracted from each other. A Hyperbolic fit is used to determine the Michaelis-Menten constant.

4.4.2 Establishing fluorescence-based assay for studying KtrB

In a second approach a fluorescence-based assay was aimed for to determine the specificity of ion translocation by KtrB, complementing the SSM-based electrophysiology measurements. Initial trials using the membrane impermeable fluorescent dyes Sodium Green™ (SG) from Thermo Fisher Scientific and Asante Potassium Green-4 (APG-4) from Teflabs failed. This was mostly due to the hydrophobic nature for these dyes making them stick to the membrane. For this reason, a different approach was chosen using the membrane permeable pH-sensitive dye ACMA.

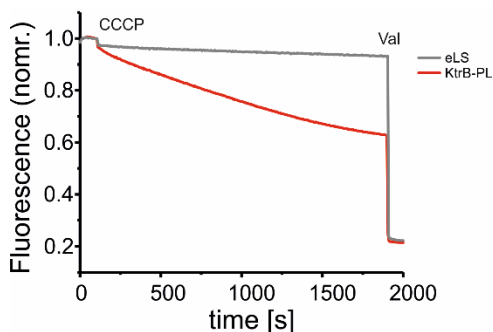


Figure 24 ACMA-based fluorescence assay after reconstitution. ACMA fluorescence is shown dependent on empty liposomes (eLS) and KtrB proteoliposomes (KtrB-PL). All liposomes were filled with 150 mM KCl, 20 mM HEPES pH 7.3. In grey eLS are shown, initially produced KtrB-PL are shown in red. Flux inducing H^+ ionophore carbonyl cyanide chlorophenyl-hydrazone (CCCP) and valinomycin (Val) additions are indicated.

ACMA fluorescence depends on its protonation and deprotonation states and can be used as an indirect readout of KtrB-mediated cation efflux from liposomes. The efflux of cations is balanced with the influx of H^+ using CCCP. As a result, cation efflux leads to H^+ -dependent quenching of ACMA fluorescence. KtrB-mediated K^+ efflux was successfully established in the

ACMA-based assay. Empty liposomes (eLS) and KtrB-containing liposomes (KtrB-PL; LPR 100:1) filled with KCl were prepared. The prepared empty liposomes were leak-proof and ACMA fluorescence quenching was only induced after the control addition of valinomycin (Figure 24, grey line in Figure 25).

In contrast, ACMA quenching dependent on the K^+ flux through KtrB was observed after CCCP addition (Figure 24, red line). However, most of the proteoliposomes did not contain any protein as shown by the control addition of valinomycin in the end to reach full ACMA quenching. The established fluorescence-based transport assay uncovered that the prepared proteoliposomes were not optimal. Therefore, the next logical step was to optimize the reconstitution and to better distribute the protein among all liposomes. To obtain a better distribution of protein in the liposomes two strategies were tried. First, freeze-thaw cycles and sonication could help to gain a more even distribution of protein in the liposomes. This approach led to a slight improvement, however still 50% of liposomes appeared to contain no protein (Figure 25, blue line). Second, a slower reconstitution was tried by reducing the amount of BioBeads per addition but including two more additions (section 3.7.4). In total six additions of 40 mg/ml and one last addition of 80 mg/ml of BioBeads resulted in a more homogeneous protein distribution among all liposomes, leading to efficient ACMA quenching (Figure 25, black line).

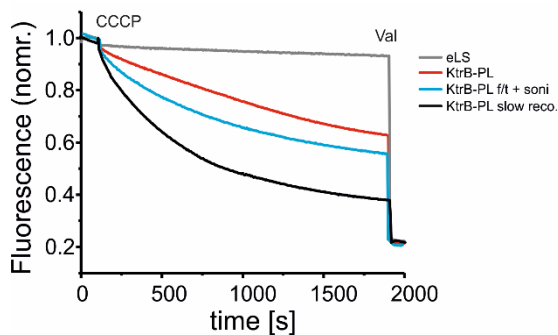


Figure 25 Optimization of the protein reconstitution into liposomes analyzed with the ACMA-based fluorescence assay ACMA fluorescence is shown dependent on eLS (grey) and KtrB-PL (red) and the same KtrB-PL after three freeze/thaw-cycles (f/t) and sonification (f/t + soni, blue). KtrB-PL after slow BioBead removal (slow reco., black) directly used after reconstitution without freezing. Flux inducing H^+ ionophore carbonyl cyanide chlorophenyl-hydrazone (CCCP) and valinomycin (Val) additions are indicated.

4.4.2.1 Optimization of liposome reconstitution

For all activity assays, liposomes with a consistent diameter and internal volumes were desirable. The size of the vesicles can be adapted with the use of polycarbonate filters with a defined size. All *E. coli* polar lipid liposomes were extruded through a 400 nm polycarbonate filter after 3 freeze-thaw cycles. After reconstitution again 3 freeze-thaw cycles were performed and the liposomes were extruded sequentially through 400, 200 and 100 nm polycarbonate filters. Nanoparticle tracking analysis based on light scattering of the liposomes following Brownian motion was used to determine the size of the liposomes as described in section 3.8.2. A viscosity of 1.55 cP was determined using 100 nm standard beads and the parameters

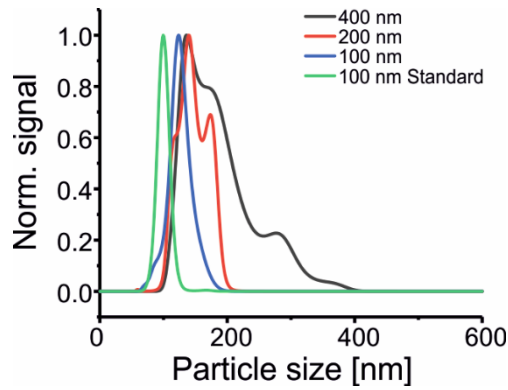


Figure 26 Size distribution of preformed liposomes determined with nanoparticle tracking. Standard beads with 100 nm were used to determine the viscosity of the buffer (green). A viscosity of 1.55 cP was determined for the used reconstitution buffer. Size distribution of vesicles extruded through a 400 nm polycarbonate filter are shown in black. The mean value of size distribution was determined as 187.9 nm \pm 56.8 nm. Size distribution of liposomes extruded through 200 nm filter have a mean size distribution of 146.6 nm \pm 23.5 nm. The mean size distribution of liposomes extruded through 100 nm 126.4 nm \pm 20.2 nm was determined.

were adjusted for all measurements. The liposome size profiles are shown in Figure 26. Since all liposomes were smaller than 400 nm, extrusion through polycarbonate filter of 400 or even 200 nm would not result in unilamellar vesicles. Consequently, all liposomes were sonicated before use for any assay to get homogeneous, small and unilamellar vesicles.

After gel filtration, some of the protein was reconstituted into *E. coli* polar lipid liposomes to investigate ion translocation using SSM-based electrophysiology or ACMA-based fluorescence assays. Lipid to protein ratios (LPR) of 5:1, 10:1, 50:1, or 100:1 were the aim of all reconstitutions. To confirm successful reconstitutions for all LPRs, a resolubilization assay was used. The rationale behind this is, only correctly reconstituted proteins can be resolubilized. Others precipitate during resolubilization. At all LPRs a reconstitution efficiency of \sim 80% was determined based on the signal intensities of the Coomassie-stained SDS-PAGE (Figure 27).

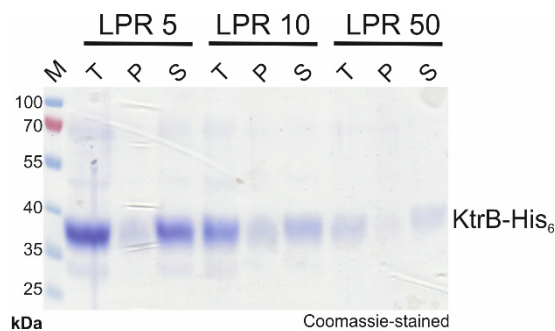


Figure 27 Reconstitution efficiency of KtrB-His₆. 40 μ l of proteoliposomes with a lipid concentration of 2 mg/ml at different lipid to protein ratios of 5, 10 and 50 (w/w) were resolubilized in 1% DDM. Half of each sample was used as positive control (KtrB-PL) the other half was submitted to a centrifugation step. Equal volumes of the positive control (T), the supernatant (S) and the resuspended pellet (P) were loaded on a 12% SDS PAGE. By evaluating the Coomassie-stained band intensities, the reconstitution efficiencies were estimated to approx. 80% using ImageJ.

4.5 Ion transport specificity of KtrB

4.5.1 Ion specificity of VaKtrB-His₆ explored with SSM-based electrophysiology

The ITC measurements showed that besides K⁺ also Rb⁺, Cs⁺ and to a lesser extent Na⁺ bind. To evaluate whether all these ions are also translocated through KtrB, at first SSM-based electrophysiology measurements were performed as introduced in the last chapter. All the monovalent cations tested by ITC (Li⁺, Na⁺, K⁺, Rb⁺, and Cs⁺) were also used in the SSM measurements. To define the substrate specificity, 100 mM concentration jumps were applied. Experiments were performed on the same sensor to permit a direct comparison of transient currents. Background currents were subtracted from the peak currents for evaluation. The background currents of empty liposomes are shown in Figure 28 a. Of the five tested cations, Li⁺ was the only one not resulting in transient currents bigger than the artefacts. SSM-based electrophysiology experiments were unable to show Li⁺ translocation, confirming the ITC measurements, where no binding was detected. Hence, Li⁺ is not a substrate of KtrB. Opposite to this, for all other cations transient currents were recorded (Figure 28 b). The signals showed clearly a correlation between the peak intensities and the ion sizes. The biggest peak current was observed for the biggest ion, in this case Cs⁺, while Rb⁺ gave a smaller signal followed by K⁺ and then Na⁺. The order of signal intensities increased with increasing ion size (Na⁺ < K⁺ < Rb⁺ < Cs⁺). The relative peak currents obtained from one set of measurements on the same sensor were normalized to the biggest peak current, namely Cs⁺ (Figure 28 c). This allowed averaging measurements from different sensors for analysis. The peak currents for Cs⁺ were twice as big as the ones of the natural substrate K⁺, indicating that Cs⁺ is the preferred substrate. However, the obtained currents not only differed in height but also in their shapes. While the currents for Cs⁺ and Rb⁺ showed a fast rise and decay resulting in very sharp signals, those of K⁺ and Na⁺ were surprisingly broad. Comparing the electrical charges by integrating the transient currents between 0.52 to 0.9 s resulted in a different ion preference. Normalizing the transient currents to the largest area under the curve reversed the order to Na⁺ > K⁺ > Rb⁺ > Cs⁺. The biggest overall electrical charge measured for Na⁺ and K⁺ suggested that these two ions are better translocated than Rb⁺ and particularly Cs⁺ (Figure 28 d). The decay times determined from 100 mM concentration jumps on KtrB-containing liposomes were in agreement with this conclusion. Usually, fast decay times (τ) like in the case of Cs⁺ (~9 ms) and Rb⁺ (~8 ms) suggest pre-steady state charge displacement (Table 10, LPR 5:1), indicative of either fast translocation or only binding, while slow decay times represent steady-state ion translocation (Zuber *et al.*, 2005; Wacker *et al.*, 2014; Bazzone *et al.*, 2017). The decay times of K⁺ and Na⁺ currents were determined to be ~15 ms and ~45 ms, respectively (Table 10, LPR 5:1). To further verify which of the ions are translocated, decay times at different LPRs of 5:1, 10:1 and 50:1 were compared (Table 10). In the case of just ion binding, the decay time

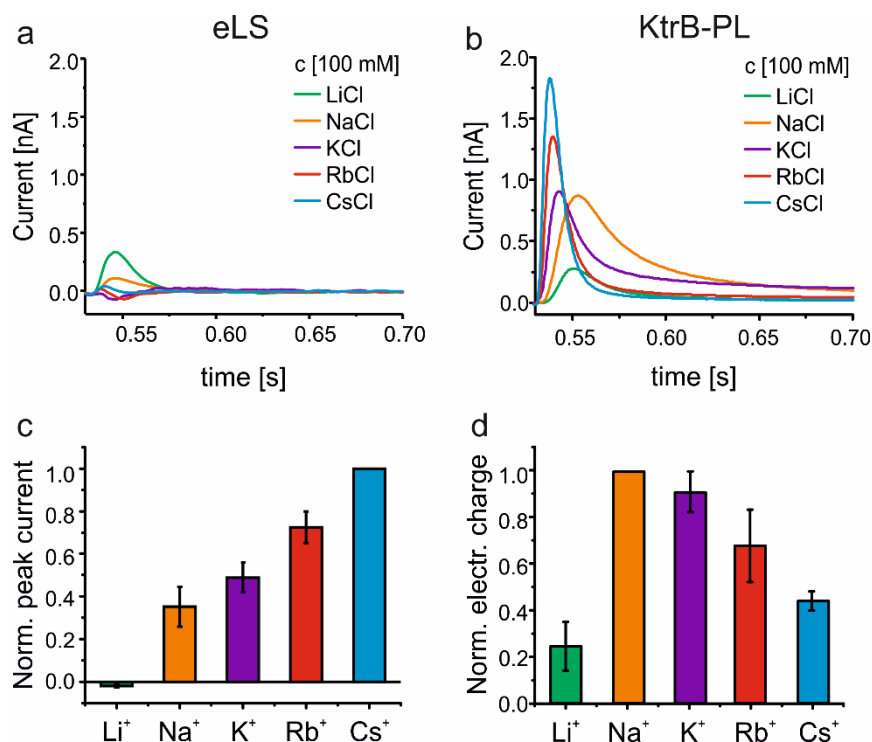


Figure 28 Ion specificity and electrogenic behavior of VaKtrB-His₆ analyzed using SSM-based electrophysiology. Adapted from Mikusevic *et al.* 2019. The results of the SSM-based experiments for the cations Li⁺, Na⁺, K⁺, Rb⁺ and Cs⁺ are shown in green, orange, purple, red and blue, respectively. Transient currents of (a) empty liposomes (eLS) and (b) KtrB-containing liposomes (KtrB-PL) are induced by 100 mM concentration jumps of LiCl, NaCl, KCl, RbCl and CsCl on one sensor. (c) To CsCl normalized peak currents of in (b) performed experiments are shown in a bar graph. All data are corrected by subtraction of empty liposome signals (\pm SD, n=3). (c) Bar graph of integrated transient currents (0.52-1 s) normalized to the biggest area (Na⁺). All data are corrected by subtraction of empty liposome signals (\pm SD, n=3).

should not be affected by decreasing the LPR, because the binding kinetics do usually not change in dependence of protein concentrations. Instead, in the case of ion transport, decay times should increase with decreasing protein concentrations because steady-state transport rates are reached slower at low protein concentrations. Proteoliposomes with LPRs of 50:1 and 10:1 were compared to the measurements performed with liposomes using a LPR of 5:1 and the half-maximal decay times were determined. With increasing LPR the decay times for concentration jumps with KCl increased from 15.2 via 17.5 to 44.5 ms, respectively. This effect could also be partly observed for Rb⁺, with decay times of 8.3, 11.7 and 15.6 ms, respectively. Changes were neither detected for the smallest ion, Na⁺, nor for the biggest ion, Cs⁺. Their decay times were in the range of 42 and 9.6 ms, respectively (Figure 29 and Table 10). Combining the analysis of the signal shapes and the decay times at different LPRs one could claim that K⁺ is in fact translocated, while data for the other three cations does not allow any clear conclusion about ion translocation.

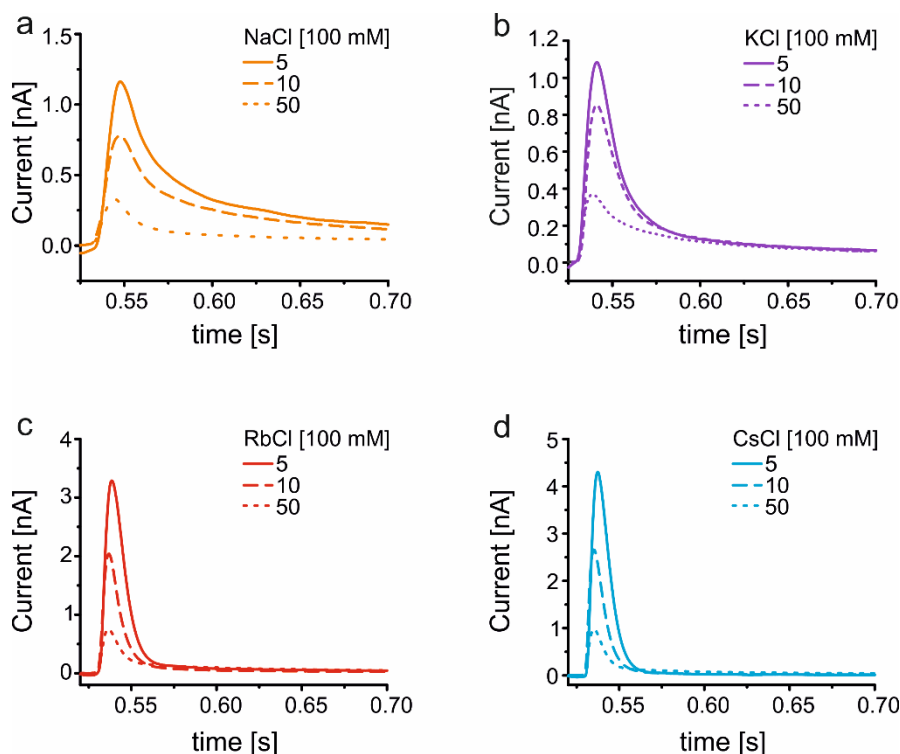


Figure 29 Ion specificity of electrogenic behavior of KtrB at different LPRs analyzed using SSM-based electrophysiology. Transient currents recorded upon 100 mM concentration jumps of NaCl, KCl, RbCl or CsCl at LPRs of 5:1, 10:1 and 50:1, respectively, are shown. The corresponding τ values for the decay times are shown in Table 10.

Table 10 Decay times of transient currents of different cations. Buffers containing 100 mM NaCl, KCl, RbCl or CsCl were used to record transient currents at different lipid to protein ratios (LPRs: 5:1, 10:1 and 50:1). The decay times of the transient currents are indicated as τ (\pm SD, $n=3$).

Decay time [ms]				
LPR	NaCl	KCl	RbCl	CsCl
5:1	45.2 \pm 3.0	15.2 \pm 2.9	8.3 \pm 0.5	9.2 \pm 2.3
10:1	47.5 \pm 15.5	17.5 \pm 3.5	11.7 \pm 4.8	10.0 \pm 3.0
50:1	35.4 \pm 9.5	44.5 \pm 3.0	15.6 \pm 3.3	9.5 \pm 1.1

4.5.2 Transport kinetics of VaKtrB-His₆ explored with SSM-based electrophysiology

In an attempt to further analyze the selectivity of KtrB regarding ion translocation, Michaelis-Menten constants K_M for the four cation species were determined. The Michaelis-Menten constant $K_M = (k_1^- + k_2)/k_1^+$ and the dissociation constant $K_D = k_1^-/k_1^+$ are identical, insignificantly small k_2 ($k_2 \ll k_1^-$). A small k_2 would be indicative of only binding. In contrast,

ion translocation most likely would result in a significant k_2 value because translocation is usually dependent on conformational changes and therefore slower than the initial binding. Hence, a K_M value larger than the K_D value determined by ITC would argue ion translocation. For determining the K_M values different NaCl, KCl, RbCl and CsCl concentrations ranging from 1 to 50 or 100 mM were used. Measurements were performed on the same sensor allowing the direct comparison of current profiles. Background currents were subtracted from the KtrB-generated currents for evaluation. The background currents of empty liposomes are shown in Figure 30 a-d, the KtrB-mediated currents are shown in Figure 30 e-h. To evaluate the relative peak currents, data measured on a minimum of three independent sensors were averaged and normalized to the highest peak current. By plotting the normalized currents and fitting with the Michaelis-Menten equation, K_M values for Na^+ , K^+ , Rb^+ , and Cs^+ were determined. The K_M value of Cs^+ obtained by SSM is congruent with the K_D acquired by ITC (cf. Figure 30 and Table 8 and TABLE 11). For Rb^+ a K_M of 5.9 mM was determined, which is marginally increased compared to its K_D of 2.5 mM (cf. Figure 19 c and Figure 30 g). A K_M of 35.5 mM was determined for Na^+ . This high K_M value could reflect the low binding affinity to Na^+ and would explain why a K_D could not be measured using ITC. A significantly large difference between K_M and K_D was observed for K^+ with values of 16.4 mM and 91 μM , respectively (Figure 19 b and Figure 30 f).

One could argue, that the high K_M value for K^+ again was caused by the lack of small cations. To test this hypothesis K^+ concentration jumps were repeated in the presence of 5 mM NaCl, since this concentration was sufficient to increase the binding affinity of KtrB to K^+ . However, SSM-based electrophysiology measurements resulted in a similar K_M value of 28.9 mM (Figure 31) suggesting that a second rate-limiting step is required for translocation. Also, whole-cell K^+ uptake studies confirm this assumption. The uptake of K^+ through KtrB into K^+ -depleted *E. coli* LB2003 cell is characterized by a K_M value in the low millimolar range, independent of the presence or absence of Na^+ ions (Kolesova, 2016). The elevated K_M values of K^+ and lesser of Rb^+ suggest that these ions are translocated through KtrB, while again Cs^+ most likely only binds. Whether Na^+ is translocated remains uncertain. Taken all SSM-based electrophysiology measurements together, only K^+ was identified to be translocated through KtrB, while all data suggest that Cs^+ is not translocated. The information on Na^+ and Rb^+ are inconclusive and a final claim of whether or not they are translocated cannot be made.

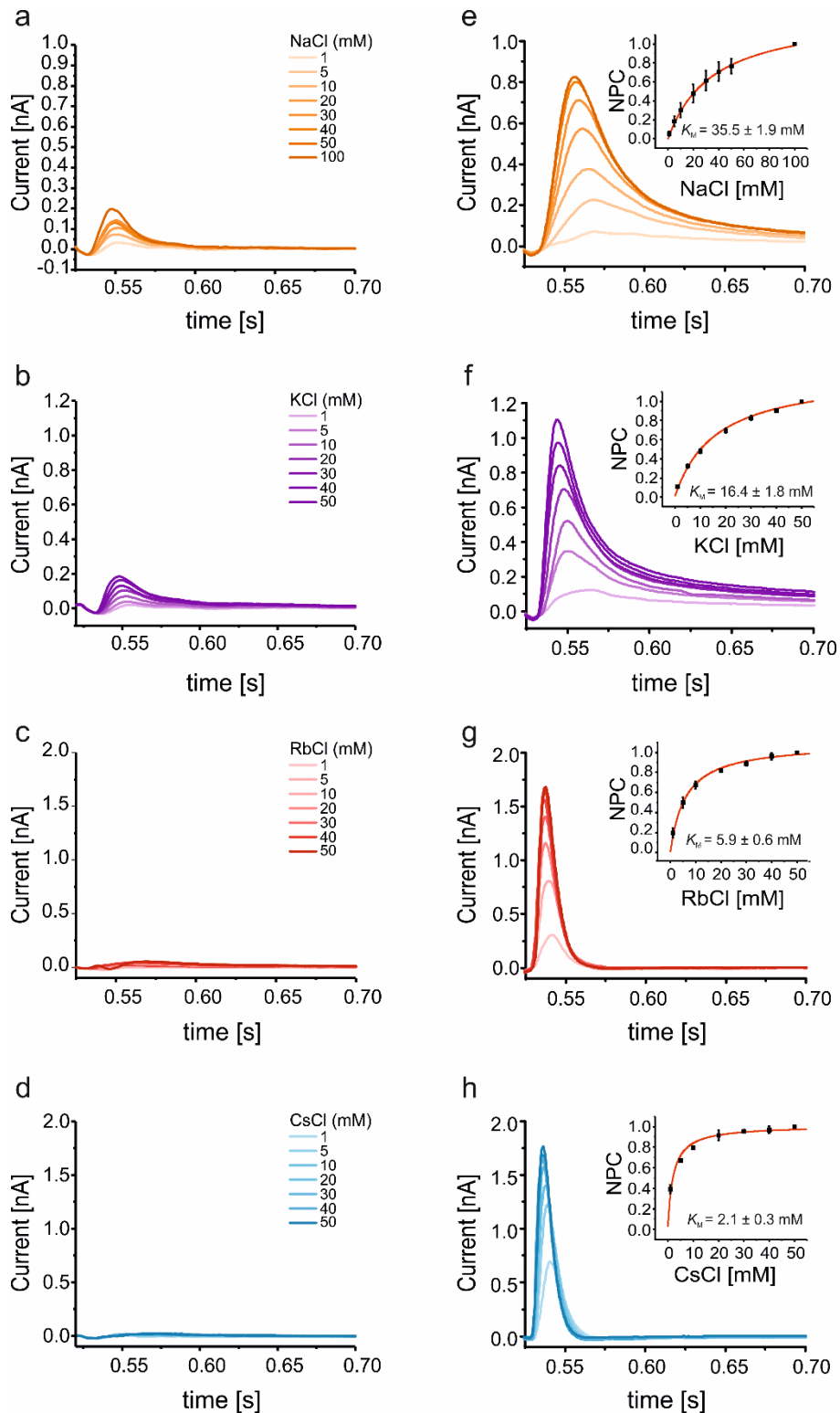


Figure 30 Exploring the transport kinetics of VaKtrB-His₆ with SSM-based electrophysiology. Adapted from Mikusevic *et al.* 2019. (a-h) Experiments for the cations Na⁺, K⁺, Rb⁺ and Cs⁺ are shown in orange, purple, red and blue, respectively. Concentration jumps with increasing salt concentration performed on (a-d) empty liposomes and (e-h) KtrB-containing proteoliposomes. Increasing salt concentrations are indicated by rising color intensities (1-50 or 100 mM). All data were corrected by subtraction of empty liposome signals. For determining the K_M values with OriginPro2017, peak currents were normalized (NPC) to the highest concentration jump during one set of measurements (\pm SEM, $n \geq 3$).

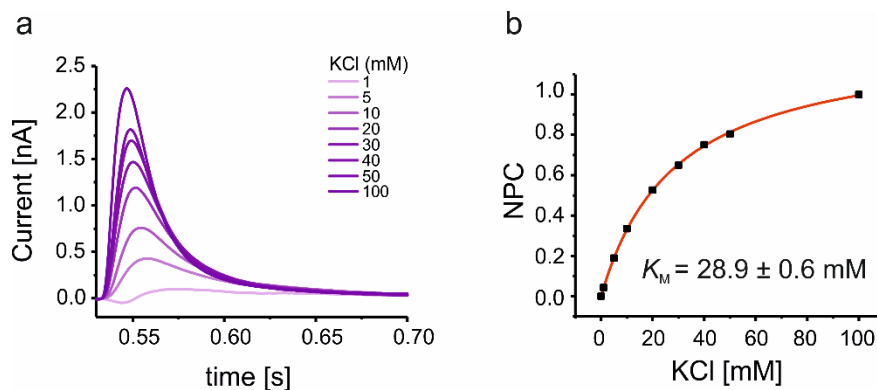


Figure 31 Exploring the transport kinetics of VaKtrB-His₆ in the presence of Na⁺ with SSM-based electrophysiology. Adapted from Mikusevic *et al.* 2019. (a) K⁺ concentration jumps with increasing K⁺ concentrations indicated by rising color intensities (1-100 mM) in the presence of 5 mM NaCl. All data were corrected by subtraction of empty liposome signals. For determining the K_M values with OriginPro2017, peak currents were normalized (NPC) to the highest concentration jump. The K_M value was determined to be 28.9 ± 0.6 mM ($n=1$) in the presence of NaCl.

Table 11 Michaelis-Menten constant obtained from SSM-based electrophysiology measurements of KtrB-PL. The ionic radii r are shown in Å [1]. SSM: K_M values obtained from the peak currents measured with SSM-based electrophysiology ($n \geq 3$).

Ion	r [Å]	K_M [mM]
Li ⁺	0.60	nd
Na ⁺	0.95	35.5 ± 1.9
K ⁺	1.33	16.4 ± 1.8
Rb ⁺	1.48	5.9 ± 0.6
Cs ⁺	1.69	2.1 ± 0.3

nd: not detectable

4.5.3 Evaluating ion translocation with the fluorescence-based ACMA assay

SSM-based electrophysiology was tremendously important to approach the question about preferred translocation of K^+ over Na^+ . Nevertheless, it remained challenging to distinguish between binding and translocation, especially for Na^+ . For this reason, the ACMA-based flux assay was established as an alternative *in vitro* assay. After this assay was successfully performed for K^+ , simultaneously prepared liposomes were loaded with either NaCl, KCl, RbCl or CsCl and diluted into a LiCl-containing buffer. Continuous ion efflux was triggered by CCCP addition. As anticipated from the initial experiments, the addition of CCCP had almost no effect on liposomes without KtrB and only the addition of ionophores (Valinomycin for K^+ , Rb^+ , Cs^+ and Selectophore IV for Na^+) led to the quenching of ACMA (Figure 32). Similarly, KtrB-containing liposomes loaded with CsCl did not result in a fluorescence decrease after CCCP addition. In contrast, fast fluorescence quenching was observed for liposomes charged with Na^+ , followed by those loaded with K^+ . Liposomes filled with RbCl resulted in modest ACMA quenching, suggesting very slow Rb^+ fluxes. In conclusion, the ACMA-based flux assay finally revealed a size-dependent ion permeation profile ($Na^+ > K^+ \gg Rb^+ \gg Cs^+$) for KtrB, where Na^+ , the smallest cation with lowest binding affinity, fluxes faster than all other cations.

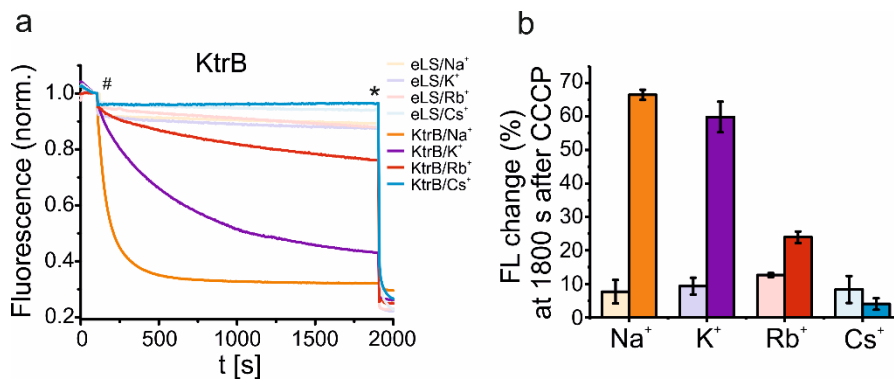


Figure 32 Ion permeability determined by ACMA-based cation flux assay. Adapted from Mikusevic *et al.* 2019. (a) KtrB-containing liposomes at a LPR of 100:1 loaded with NaCl (orange), KCl (purple), RbCl (red) or CsCl (blue) were diluted 1:20 into LiCl-based buffer. Empty liposomes filled with the respective cations are shown as a control (light colours). The addition of H^+ ionophore carbonyl cyanide chlorophenylhydrazone (CCCP) is indicated by the number sign (#). Consequently, the efflux of ions was accompanied by an intravesicular pH decrease, which quenched the fluorescent dye 9-amino-6-chloro-2-methoxyacridine (ACMA). Finally, for the normalization of all data, sodium ionophore IV (Nal IV) for NaCl-containing liposomes or valinomycin (Val) for all other intravesicular cations was added indicated by the asterisk (*). This induced protein-independent cation efflux leading to maximal ACMA quenching. (b) Fluorescence change (%) in proteoliposomes and empty liposomes at 1800 seconds after CCCP addition are shown in a bar graph ($n \geq 3$, \pm SD).

4.5.4 Competitive ion uptake through KtrB

The ACMA-based flux assay and the previous ITC data led to an apparent contradiction: While the ITC measurements showed, that K^+ binds with much higher affinity than Na^+ , the ACMA assay suggested that Na^+ is the preferred ion in translocation. However, so far only single ions were tested, while mixed ion conditions would be needed. If KtrB functions as a specific K^+ channel for the purpose of osmoadaptation, it should prefer the translocation of K^+ over Na^+ . Although, Na^+ is much more abundant in nature than K^+ . The *in vitro* assays do not allow for a direct distinction of the ions translocated. Instead, an *in vivo* K^+ uptake assay into K^+ and Na^+ -depleted cells was performed in the presence of competing Rb^+ and Na^+ concentrations (Figure 33). The uptake of K^+ in the presence of 50 mM Li^+ served as a positive control, because Li^+ was neither bound to nor was it translocated by KtrB. The presence of 50 mM Rb^+ completely abolished K^+ uptake into the cells. The 25-fold excess of Rb^+ outcompeted the binding of K^+ and also abolished its uptake. In contrast, a 25-fold excess of Na^+ had no inhibitory effect on the uptake of K^+ . The ~500-fold higher affinity for K^+ over Na^+ therefore favors the uptake of K^+ , classifying KtrB as a selective K^+ channel.

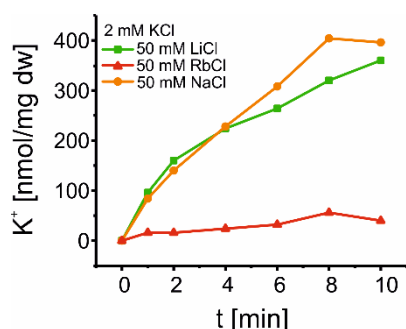


Figure 33 Competition for K^+ uptake by *E. coli* cells containing KtrB. Adapted from Mikusevic *et al.* 2019. The strain LB2003/pEL901 was grown and induced for *ktrB* expression with 0.02% L-arabinose. For the K^+ uptake experiment cells were suspended to 1 mg dw (dry weight)/ml of medium containing 200 mM HEPES-triethanolamine, pH 7.5, 0.2% glycerol, 0.02% L-arabinose and the indicated ions at 50 mM concentration. The suspension was shaken at room temperature. After 10 min, 2 mM KCl was added. For each data point a 1 ml sample was taken from the suspension, centrifuged through silicone oil and the cellular K^+ content was determined by flamephotometry.

4.6 Motifs responsible for ion selectivity

4.6.1 Converting the poorly conserved selectivity filter to -TVGYG-

The previous section showed that KtrB is surprisingly selective for K^+ over all tested monovalent cations, although it harbors a poorly conserved selectivity filter compared to for example tetrameric potassium channels. Besides the selectivity filter, KtrB holds an intramembrane loop that was previously demonstrated to act on ion gating (Hänelt, Löchte, *et al.*, 2010). This loop could, therefore, contribute to KtrB's selectivity. In the following section, the role of the selectivity filter and the intramembrane loop was evaluated.

In each M1-P-M2 motif of KtrB, only a single glycine residue of the canonical -TVYGY- signature sequence is conserved. Changing any of these four glycines to a serine resulted in decreased apparent affinities for K^+ , while the apparent affinity for Na^+ increased significantly. The KtrAB complex appeared to become notably unselective. So far, the reversed experiment, converting the selectivity filter sequence into the canonical sequence, has not been performed. For that reason, motifs -VTGLA-, -NAGFS-, -TAGFN- and -TVGLT- of domains D1 to D4, respectively, were mutated into the canonical -TVGYG- signature sequence. Each domain was mutated consecutively starting from P_{D1} through $P_{D1}P_{D2}P_{D3}P_{D4}$. To test the functionality of the variant, a complementation assay was performed using *E. coli* strain LB2003 transformed with plasmids encoding for the wild-type protein and KtrB_{TVGYG}, respectively (Figure 34). LB2003 growth was determined in K^+ minimal media with KCl concentrations of 0.5, 1, 3, 5, 7, 10, 30 and 115 mM (Epstein and Kim, 1971). Obviously, the -TVGYG- variant lost its ability to translocate potassium since no growth was observed below a concentration of 10 mM KCl. Simply exchanging the selectivity filter did not lead to an even more selective K^+ channel but instead inactivated KtrB. Likely, the non-symmetrical pore region is not compatible with the symmetrical filter sequence.

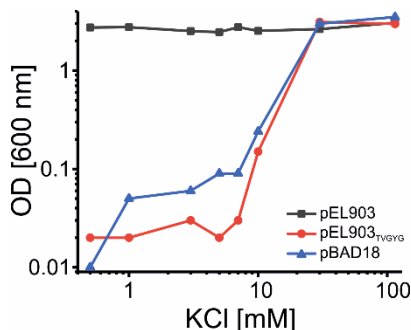


Figure 34 Complementation assay for the investigation of the K^+ uptake activity of protein variants. *E. coli* LB2003 containing VaKtrB-His₆ variants were grown overnight in minimal medium with glycerol as a carbon source at the K^+ concentrations indicated. The following plasmids were used: empty vector pBAD18 (blue); pEL903, coding for VaKtrB-His₆ (black) and pEL903_{TVGYG}, coding for VaKtrB_{TVGYG}-His₆ were the SF sequence in all four domains D1-D4 of the pore loops had been exchanged (red).

4.6.2 Modifying the intramembrane loop of KtrB

The intramembrane loop was previously shown to confine ion fluxes and was suggested to function as a gate in KtrB. It was thought to not affect ion selectivity, but only conductance. Mutations in the intramembrane loop resulted in increased K^+ uptake velocities, while neither the apparent affinity (K_M) nor the uptake of Na^+ were affected. The ACMA assay suggested a size-dependent ion translocation, in which the intramembrane loop could play an essential role. To elucidate this presumable role of the loop in size-selective ion translocation mutations within the intramembrane loop were investigated by the ACMA assay. A complete deletion of the intramembrane loop and a single substitution of glycine 316 to serine were chosen for evaluation. Both mutations resulted in strongly increased V_{max} values for K^+ uptake as shown by previous experiments (Hänelt, Löchte, *et al.*, 2010).

4.6.2.1 Purification of intramembrane loop variant

For the *in vitro* characterization of $VaKtrB_{G316S}$ and $VaKtrB_{\Delta 314-23}$ fair amounts of pure and stable protein were required. Consequently, $ktrB_{G316S-his_6}$ and $ktrB_{\Delta 314-23-his_6}$ were expressed under the control of an arabinose promotor in *E. coli* strain LB2003 transformed with the plasmids pEL903_G316S and pEL903_Δ314-23, respectively. Cells were grown in either K3 minimal medium or KML. After membrane preparation and solubilization with DDM, proteins were extracted via Ni^{2+} -NTA and their purity was further improved by size-exclusion chromatography (Figure 35 b+d). The purifications were analyzed by SDS-PAGE. Unfortunately, $KtrB_{\Delta 314-23}$ could not be purified to acceptable amounts. The protein appeared to be unstable, shown by the aggregation and degradation surrounding the main protein peak in SEC (Figure 35 b). In contrast, $KtrB_{G316S}$ could be successfully purified. Noticeable fragments were visible at apparent molecular weights of ~37 and ~70 kDa, corresponding to monomers and dimers of KtrB, respectively (Figure 35 a). The size-exclusion profile indicated high purity and homogeneity of the protein, optimal for further studies. Detergent-purified $KtrB_{G316S-His_6}$ was reconstituted for ACMA-based transport assays using the optimized protocol.

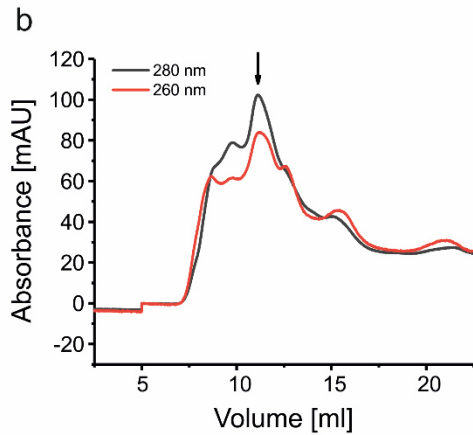
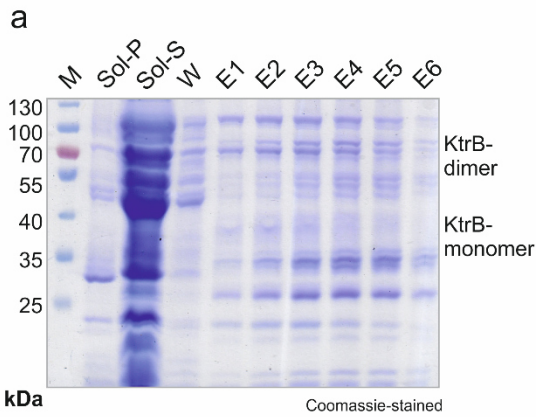
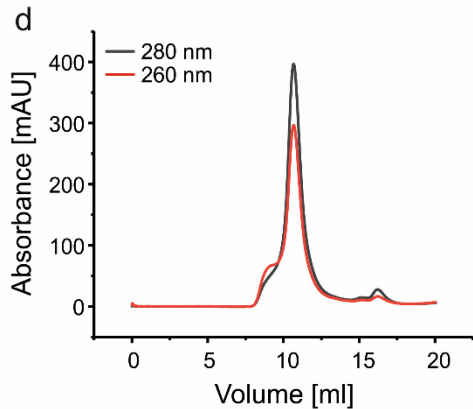
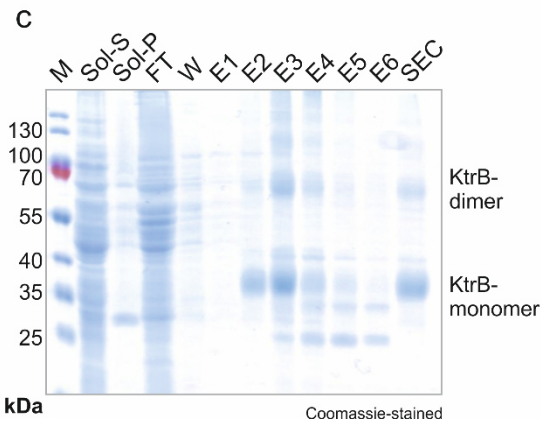
KtrB_{Δ314-23}-His₆KtrB_{G316S}-His₆

Figure 35 Purification of intramembrane loop variants KtrB_{G316S}-His₆ and KtrB_{Δ314-23}-His₆ from *E. coli* strain LB2003. (a+c) 10 μ l protein samples from each purification step were introduced to a 12% SDS-PAGE. The following samples were analyzed: supernatant after solubilization (Sol-S), the pellet after solubilization (Sol-P), the flow through (FT) and the wash step (W) after binding to the Ni²⁺-NTA resin, elution fractions (E1-E6) from the Ni²⁺-NTA resin, each eluted with 1/2x column volume and the main peak after size-exclusion chromatography (SEC). The predicted molecular mass for KtrB-His₆ is 50.5 kDa, but the protein migrates at ~37 kDa. (b+d) Size exclusion chromatography was performed using a Superdex 200 Increase 10/300 GL column in buffer W, supplemented with 0.04% DDM. The main peaks centered at an elution volume of 10.8 ml.

4.6.2.2 ACMA-based fluorescence assay with KtrB_{G316S}-containing liposomes

Variant KtrB_{G316S} showed a 5-fold increased V_{\max} compared to the wild-type in whole-cell K⁺ uptake measurements, while the uptake of Na⁺ was not affected (Hänelt, Löchte, *et al.*, 2010). Similarly, increased K⁺ currents using SSM-based electrophysiology were recorded suggesting a gain of function (Mikusevic, 2014). However, both previous approaches did not allow for any conclusion on how this mutation affects the activity of the protein. The here-established ACMA-based fluorescence assay allows the investigation of ion fluxes for all group 1 cations. This

should permit the answer of whether the intramembrane loop is responsible for the previously observed size-selective ion transport.

The ACMA flux assays of KtrB_{G316S}-containing liposomes performed as for the wild-type (section 4.5.3) are shown in Figure 36. When comparing the fluxes of the variant with the wild-type very different characteristics are visible: The variant presented extremely fast K⁺ fluxes, followed by Rb⁺ and Na⁺, while Cs⁺ remained impermeable. The decay rates of fluorescence quenching by Na⁺ fluxes were very similar between wild-type KtrB- and KtrB_{G316S}-containing liposomes. Contrary to this, the decay rates for Rb⁺ increased by a factor of 8 (1.6 ms⁻¹ vs. 12.6 ms⁻¹), while for K⁺ a 60-fold increase from 1.6 ms⁻¹ to 100 ms⁻¹ was identified. Hence, the intramembrane loop seems to restrict faster fluxes of K⁺ and Rb⁺. Showing that changing only one single amino acid drastically effects the open probability of the gate or its efficient closing. Na⁺ fluxes appear to be independent of the gate suggested by previous *in vivo* studies (Hänelt, Löchte, *et al.*, 2010). The only remaining uncertainty is, whether Cs⁺ would be able to pass through KtrB when the loop is deleted or whether it is always caught in the selectivity filter.

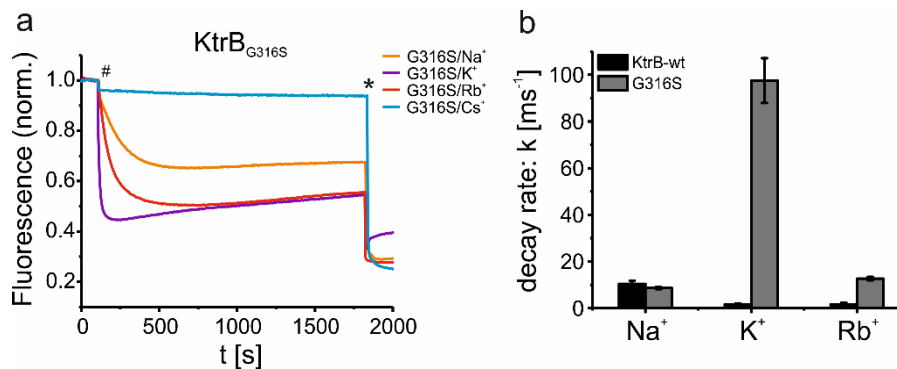


Figure 36 ACMA-based flux assay of KtrB_{G316S}-containing liposomes compared with those containing wt-KtrB. Adapted from Mikusevic *et al.* 2019. (a) KtrB_{G316S}-containing liposomes at a LPR of 100:1 loaded with NaCl (orange), KCl (purple), RbCl (red) or CsCl (blue) were diluted 1:20 into LiCl-based buffer. Experiments were performed as described in the text. (b) Decay rates ($k = 1/t_1$) for one-phase exponential decays of Na⁺, K⁺ and Rb⁺ traces of KtrB_{G316S}- and wt-KtrB-containing liposomes are shown in a bar graph ($n \geq 3$, \pm SD).

4.7 The role of Na⁺ for KtrAB

In previous whole-cell uptake experiments it was revealed that KtrB translocates K⁺ as well as Na⁺ (Tholema *et al.*, 2005; Hänelt, Löchte, *et al.*, 2010) with similar K_M values which led to the conclusion that it has a low ion selectivity. Here, it could be established that KtrB is in fact very selective for potassium and that this selectivity is achieved by the presence of Na⁺ itself. For the KtrAB system it was shown that the uptake of K⁺ entirely depends on the presence of Na⁺. In the present chapter the effect of Na⁺ on KtrB and KtrAB is further explored.

4.7.1 K⁺ currents of KtrB in the presence of small cations

In analogy to the adaptations made for the ITC measurements, SSM-based electrophysiology measurements were adapted. All the previous electrophysiology measurements assessing translocation were performed in almost complete absence of small cations. Only 5 mM Mg²⁺ was present in all working buffers. Therefore, new SSM-based electrophysiology experiments were carried out evaluating the influence of small monovalent cations. Potassium concentration jumps were performed after pre-incubation of KtrB-containing liposomes in the presence of either 5 mM LiCl, NaCl, KCl, RbCl or CsCl compensated with 95 mM choline-Cl. Between each new NA solution, the SSM sensor was washed multiple times and incubation for at least 5 min allowed a sufficient buffer/ion exchange. The measurements revealed remarkably high K⁺ currents in the presence of NaCl compared to measurements in the absence of additional ions (Figure 37 a). The K⁺ current increased almost two-fold. In contrast, Cs⁺ and Rb⁺ effectively blocked the K⁺ currents and K⁺ itself led to a reduced peak current, while Li⁺ showed not effect (Figure 37 a). Equal concentration jumps with Rb⁺ and Cs⁺ in the presence of 5 mM NaCl did not result in increased peak currents. Hence, the stimulatory effect was specific to K⁺ (Figure 37 b-c). To evaluate the Na⁺ effect further, different NaCl concentration between 0.1 and 100 mM were used for preincubation. While the currents initially increased with rising NaCl concentration until approximately 10 mM, they decreased again at concentrations higher than 10 mM NaCl. However, the signals were always at least as high as in the absence of Na⁺ (Figure 37 d-f). These data are consistent with the ITC measurements showing that low NaCl concentrations lead to an increase in K⁺ affinity, while higher concentrations lead to a decrease of affinity due to competitive ion binding. By plotting the peak currents against the respective NaCl concentration a half-maximal activating concentration (AC_{50}) of 0.54 mM was determined. The maximum signal enhancement was reached between 2.5 and 10 mM of NaCl (Figure 37 e). Knowing the AC_{50} , the question arose how and where Na⁺ binds to KtrB. Applying Na⁺ only in the NA buffer established a gradient across the membrane. To avoid this gradient, at first, equal concentrations of NaCl in both NA

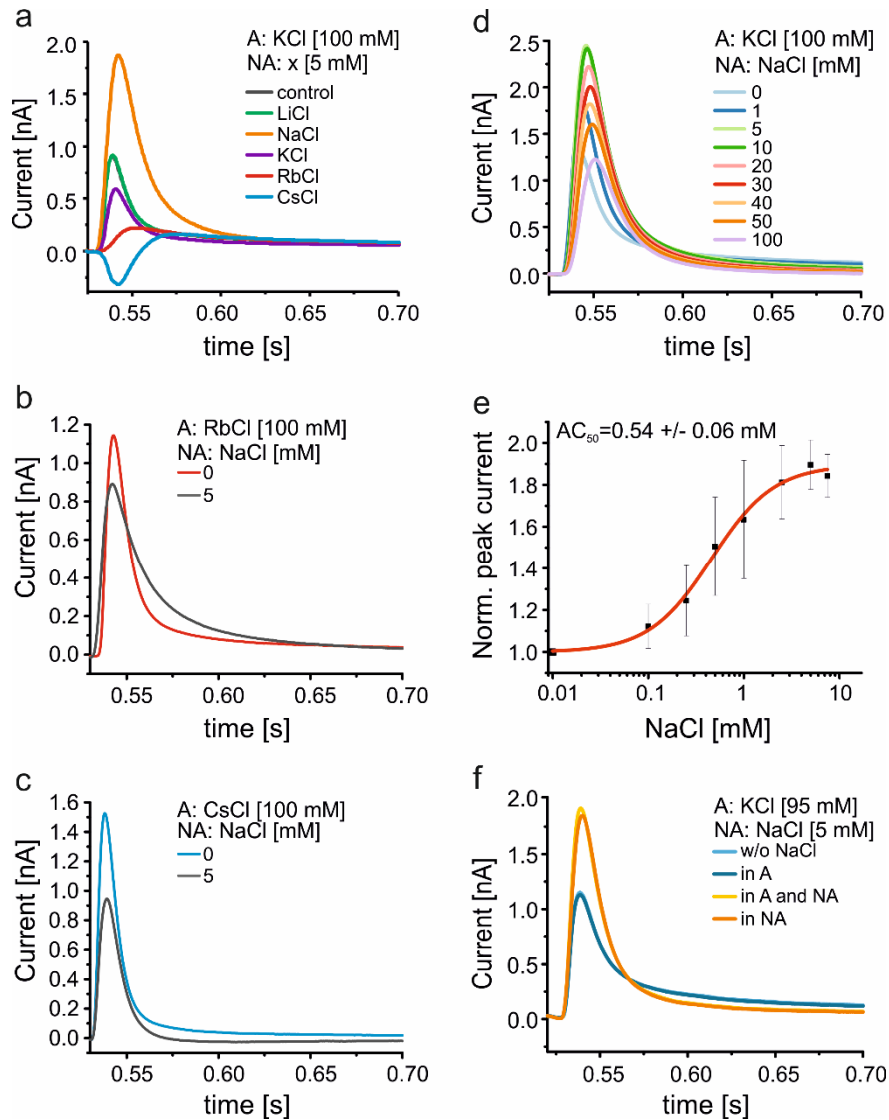


Figure 37 Na⁺-stimulated current of KtrB determined with SSM-based electrophysiology. (a) 100 mM K⁺-stimulated transient currents in the presence of 5 mM of either choline-Cl (grey, control), LiCl (green), NaCl (orange), KCl (purple), RbCl (red) or CsCl (blue). (b) 100 mM Rb⁺-stimulated transient currents in the presence of 5 mM choline-Cl or NaCl. (c) 100 mM Cs⁺-stimulated transient currents in the presence of 5 mM choline-Cl or NaCl. (d) Na⁺ concentration-dependent K⁺ currents obtained upon 100 mM KCl concentration jumps at different NaCl concentrations (0-100 mM) in the non-activating solution (NA). (e) Normalized peak currents of 100 mM KCl concentration jumps pre-incubated with 0-10 mM of NaCl. $AC_{50} = 0.54 \pm 0.06$ mM ($n=3$, \pm SD) determined by dose-response analysis with OriginPro 2017. (f) Transient currents recorded by inducing 95 mM KCl concentration jumps with either 5 mM NaCl in the activating (dark blue), the non-activating (orange), both solutions (yellow) or in the absence of NaCl (light blue).

and A solutions were applied resulting in similarly stimulated K⁺ currents. Thus, a Na⁺ K⁺ antiporter function of KtrB could be excluded. In fact, I found that the pre-incubation with Na⁺ in the NA solution was absolutely essential for increasing the transient current of K⁺, while Na⁺ solely in the A buffer did not stimulate KtrB (Figure 37 f). Moreover, an at least 5-minute-long pre-incubation with Na⁺-containing NA solution was required to achieve the maximal activation. I thus conclude, that Na⁺ diffused into the vesicular lumen and was bound to the cytosolic side

of KtrB. This hypothesis is supported by the notion that the Na^+ concentration leading to full stimulation is in good agreement with Na^+ concentrations found inside the cytoplasm of most bacteria (Castle, Macnab and Shulman, 1986). The stimulated currents could either indicate changes in K^+ binding or translocation. The previously mentioned K_M evaluation in the presence of 5 mM NaCl (Figure 31) and *in vivo* K^+ uptake experiments in the presence of 0.05-5 mM (Kolesova, 2016) suggested that K^+ translocation is not affected by the presence of Na^+ . It is more reasonable to assume that the increased currents reflect the increased affinity for K^+ in the presence of Na^+ . However, it is important to note, that this stimulatory effect was exclusive to the presence of Na^+ , while Li^+ had no stimulatory effect. It remains to be answered where in KtrB Na^+ binds and what the increased peak current actually reflects. Investigating the effect of Na^+ on KtrAB could further help.

4.7.2 Na^+ dependency of KtrAB

The uptake of K^+ by KtrAB has long been known to depend on Na^+ (Tholema *et al.*, 1999), without Na^+ the uptake of K^+ is impaired. This implies that Na^+ binding not only affects the affinity for K^+ , but also the regulation of gating in the complex. Current structural data suggests that KtrA does not affect the selectivity filter directly, but that it rather regulates gating via the intramembrane loop. It was further hypothesized that ATP binding to KtrA supports the active conformation of KtrB, while the closed conformation is retained by ADP binding (Szollosi *et al.*, 2016; Diskowski *et al.*, 2017). To understand the molecular role of Na^+ binding the kinetic parameters of K^+ in the presence of different Na^+ concentrations needed to be investigated. The SSM-based electrophysiology or ACMA-based flux assays would have been preferable. However, an *in vitro* assay could not be established. The reason is the composition of the purified complex: The purification yields a sandwiched complex of two octameric KtrA rings with the KtrB dimer wedged in between them (Diskowski *et al.*, 2017). This was shown to impair a sufficient reconstitution of the complex into liposomes (Stautz, 2016). Instead, a series of whole-cell K^+ uptake experiments was performed. The uptake of K^+ through KtrAB was determined in the presence of four different KCl concentrations (0.5, 1, 2, and 5 mM) in combination with four different NaCl concentrations (0, 0.05, 0.5, and 5 mM). Analyzing the uptake data shows a considerable gain in K^+ uptake upon increasing the Na^+ concentration (Figure 38 a). Determination of Michaelis-Menten kinetics were achieved for every Na^+ concentration. The data revealed that with increasing Na^+ concentrations the V_{\max} increased more than two-fold from 29 $\text{nmol}\cdot\text{min}^{-1}\cdot\text{mg}^{-1}$ in the absence of Na^+ to 66 $\text{nmol}\cdot\text{min}^{-1}\cdot\text{mg}^{-1}$ in the presence of 5 mM Na^+ (Figure 38 b). At the same time the K_M considerably decreased more than 20-fold from 1 mM to 37 μM (Figure 38 c). In the absence of Na^+ , KtrAB displayed similar

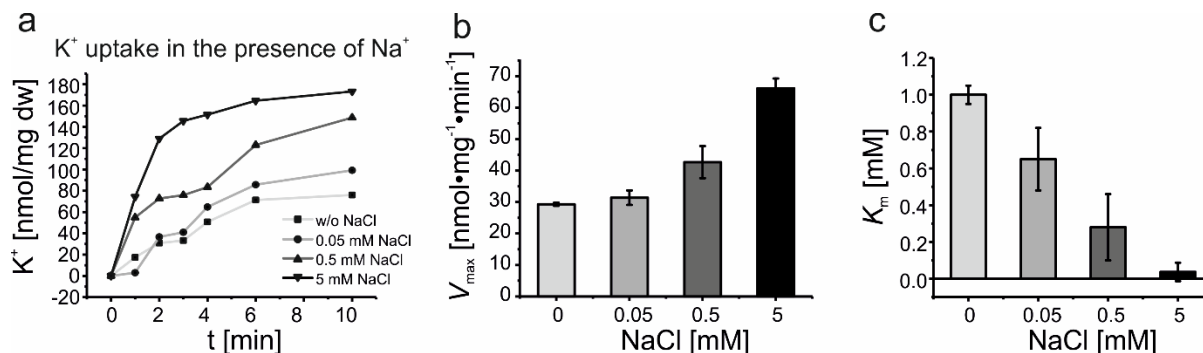


Figure 38 K⁺ uptake by *E. coli* cells containing KtrAB. Adapted from Mikusevic *et al.* 2019. The strain LB2003pKT84 was grown and induced for *ktrAB* expression with 0.02% L-arabinose. For the K⁺ uptake experiment, cells were suspended to 1 mg dw (dry weight)/ml of medium containing 200 mM HEPES-triethanolamine, pH 7.5, 0.2% glycerol, and 0.02% L-arabinose. The suspension was shaken at room temperature. (a) After 10 min, 2 mM KCl was added in the presence of the following NaCl concentrations: 0 mM; 0.05 mM; 0.5 mM; and 5 mM. For each data point a 1.0-ml sample was taken from the suspension, centrifuged through silicone oil and the cellular K⁺ content was determined by flame photometry. (b and c) K⁺ uptake experiments at different KCl concentrations in the presence of different NaCl concentrations were performed in triplicates. Subsequently, K_M and V_{max} depending on different NaCl concentration were determined ($n=3$, \pm SD). Uptake experiments and evaluation were performed by master student Natalie Kolesova, Institute of Biochemistry, Goethe-University Frankfurt under my supervision.

kinetics as KtrB alone (Kolesova, 2016). In conclusion, Na⁺ does not only modulate the affinity for K⁺, but it also influences K⁺ gating by KtrAB. The K_M value approaches the K_D for K⁺ binding suggesting that the rate-limiting step (k_2), the gating, was eliminated in the presence of Na⁺. It is likely, that Na⁺ maintained an active and open conformation of the KtrAB complex.

4.7.3 Potential second binding site for Na⁺

Since the presence of Na⁺ also affected gating in the KtrAB complex one can speculate that Na⁺ binding could take place close to the gating region or to the gating ring. Binding of Na⁺ to KtrA could not be confirmed by ITC measurements (Stautz, personal communication). Instead, MD simulations on KtrB's ion permeation were performed and a second unanticipated cation binding site was revealed with this untargeted approach (Figure 39). This simulation identified a region very close to the intramembrane loop, located in the part of KtrB undergoing the biggest structural rearrangements induced by ADP vs. ATP binding to KtrA. Residues contributing to this proposed binding site are Q93, E149, and N182. Obviously, the most important residue for cation binding would be the negatively charged E149. Consequently, E149, located in the membrane plane was mutated into a neutral leucine (L) or a positively charged lysine (K) to elucidate its functional role. Additionally, Q93 was mutated to a leucine. Further, a combination of both was created providing the double mutant Q93L/E149L. A complementation assay at different K⁺ concentrations (1, 3, 5, 7, 10, 30 and 115 mM) was used

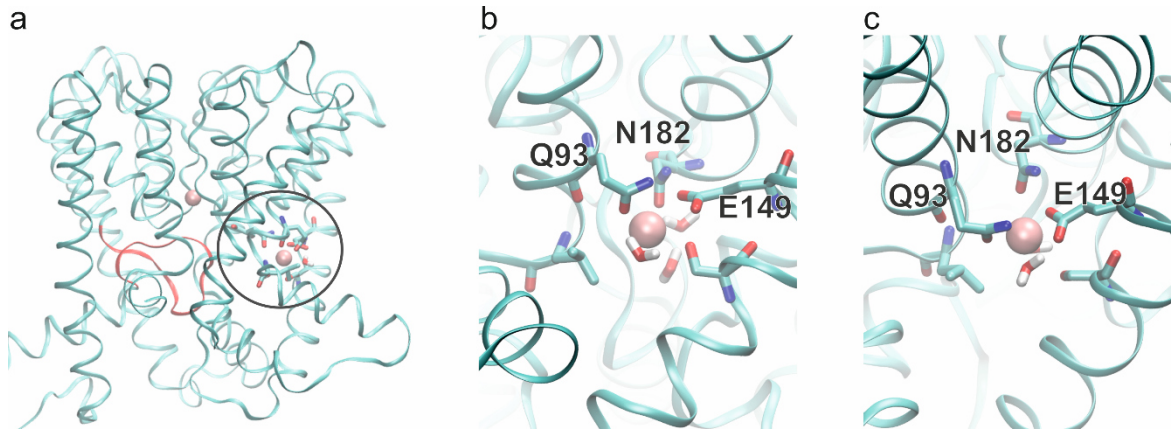


Figure 39 MD simulations revealed a second cation binding site within the membrane plane. (a) MD simulations on the influence of cations on the intramembrane loop (red) revealed a second binding site for cations within the membrane plane. It is located at the height of the intramembrane loop and (b-c) mainly formed by residues Q93, E149 and N182. MD simulations were performed by Dr. Ahmad Reza Mehdipour, Department of Theoretical Biophysics, Max Planck Institute of Biophysics in Frankfurt.

to investigate these mutations in KtrB and KtrAB (Figure 40). It was expected that cells expressing only KtrB variants would grow normally, because KtrB's translocation activity does not depend on Na^+ . Instead, for the KtrAB-expressing cells, a growth deficiency would be expected, if this is the Na^+ binding site. In fact, all variants presented normal growth behavior, except for two which showed a growth deficiency exclusively in KtrAB. These variants were E49K and Q93L. While all KtrB variants complemented growth of LB2003 at all concentrations, Q93L in KtrAB only restored growth at 7 mM K^+ or higher. E149K did not complement growth at any concentration tested with KtrAB. Only KtrAB-independent growth at ≥ 30 mM KCl was

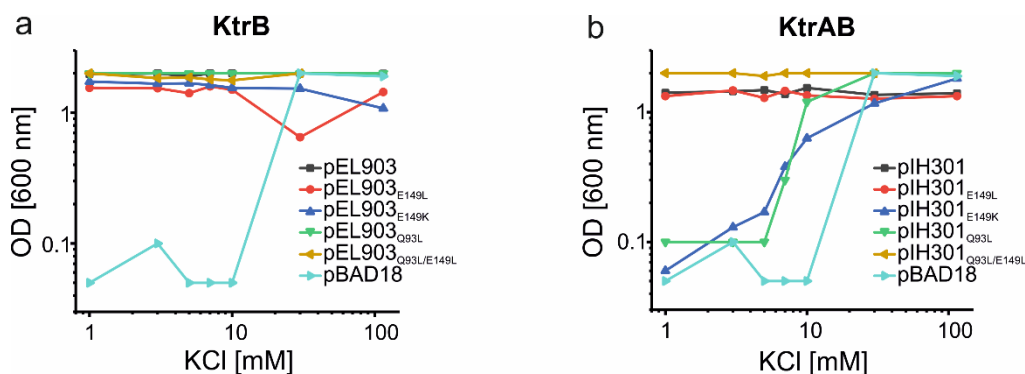


Figure 40 Complementation assay for the investigation of the K^+ uptake activity of different mutations in KtrB and KtrAB. *E. coli* LB2003, containing one of the KtrB or KtrAB variants, was grown overnight in minimal medium with glycerol as a carbon source at the K^+ concentrations indicated. The following plasmids were used: (a) pEL903, coding for VaKtrB-His₆ (black); pEL903_E149L, coding for VaKtrB_{E149L}-His₆ (red); pEL903_E149K, coding for VaKtrB_{E149K}-His₆ (blue); pEL903_Q93L, coding for VaKtrB_{Q93L}-His₆ (green); pEL903_Q93L/E149L, coding for VaKtrB_{Q93L/E149L}-His₆ (ocher); (b) pIH301, coding for His₁₀-VaKtrAB (black); pIH301_E149L, coding for His₁₀-VaKtrAB_{E149L} in KtrB (red); pIH301_E149K, coding for His₁₀-VaKtrAB_{E149K} in KtrB (blue); pIH301_Q93L, coding for His₁₀-VaKtrAB_{Q93L} in KtrB (green); pIH301_Q93L/E149L, coding for His₁₀-VaKtrAB_{Q93L/E149L} in KtrB (ocher); and the empty vector pBAD18 (light blue).

observed for E149K. Interestingly, the double mutation Q93L/E149L cancelled out the growth defect of Q93L alone behaving normally again. In conclusion, this region holds promising opportunities to explore the Na⁺-dependency of KtrAB in the future.

5. Discussion

The aim of this Ph.D. thesis was the functional investigation of the K⁺ uptake system KtrAB from *V. alginolyticus*. The main focus was put on the ion selectivity of the membrane-embedded KtrB subunit and its two key features involved in selective ion conductance: the non-canonical selectivity filter and the intramembrane loop just below the selectivity filter (Figure 41). These two features and their properties determine the thermodynamics and kinetics of cation binding and translocation by KtrAB. ITC measurements in this study revealed that the selectivity filter preferably binds K⁺ with micromolar affinity in comparison to Na⁺, Rb⁺, and Cs⁺, which only bind with millimolar affinities. Even though binding of K⁺ is favored, the translocation of these four ions was shown to be size-dependent by SSM-based electrophysiology in combination with ACMA-based flux assays. The size-dependent translocation follows the order Na⁺ > K⁺ > Rb⁺ > Cs⁺, best to worst. This order can be influenced towards preferred K⁺ translocation by mutations in the intramembrane loop, revealing the loop's involvement in size-selective translocation. Moreover, a third feature involved in ion selectivity was suggested by MD simulations: An additional cation binding site within the membrane plane, which could be related to the described Na⁺ dependency. In summary, this study sheds new light on the concept of selectivity and regulation of K⁺ translocation in subunit KtrB of the KtrAB complex.

5.1 Selectivity of KtrAB is a result of ion binding and translocation

Selective K⁺ conductance is usually provided by the backbone carbonyls of the -TVGYG-signature sequence conserved in almost all K⁺ channels (Heginbotham, Abramson and MacKinnon, 1992; Heginbotham *et al.*, 1994). The structure of KcsA from *Streptomyces lividans* (Doyle *et al.*, 1998; Zhou *et al.*, 2001) revealed four consecutive binding sites coordinating K⁺ ions stripped of water molecules as predicted beforehand (Hille, 1973; Neyton and Miller, 1988b, 1988a). It was further shown that touching any of the residues in the selectivity filter or the pore region has devastating effects on ion selectivity (Zhou and MacKinnon, 2004; Cheng *et al.*, 2011; Derebe *et al.*, 2011; Furini and Domene, 2013; Sauer *et al.*, 2013). This is the reason why KtrB and its homolog TrkH with their non-canonical selectivity filter sequences were regarded as unselective (Levin and Zhou, 2014). Both have a limited number of binding sites and only the middle glycine of the -TVGYG- sequence is conserved in KtrB (Cao *et al.*, 2011; Vieira-Pires, Szollosi and Morais-Cabral, 2013). So far, little was known about the selectivity of ion translocation of different cations through KtrB/KtrAB. Ion translocation by KtrB was known to be conferred through the selectivity filter and regulated by the intramembrane loop, which is controlled by KtrA (Tholema *et al.*, 1999,

2005; Hänel, Löchte, *et al.*, 2010). The homologues TrkH was shown to conduct Li^+ , Na^+ , K^+ , Rb^+ , and Cs^+ rather unselectively (Cao *et al.*, 2013). It was always assumed, that KtrB similarly to TrkH with the short selectivity filter is fairly unselective (Levin and Zhou, 2014).

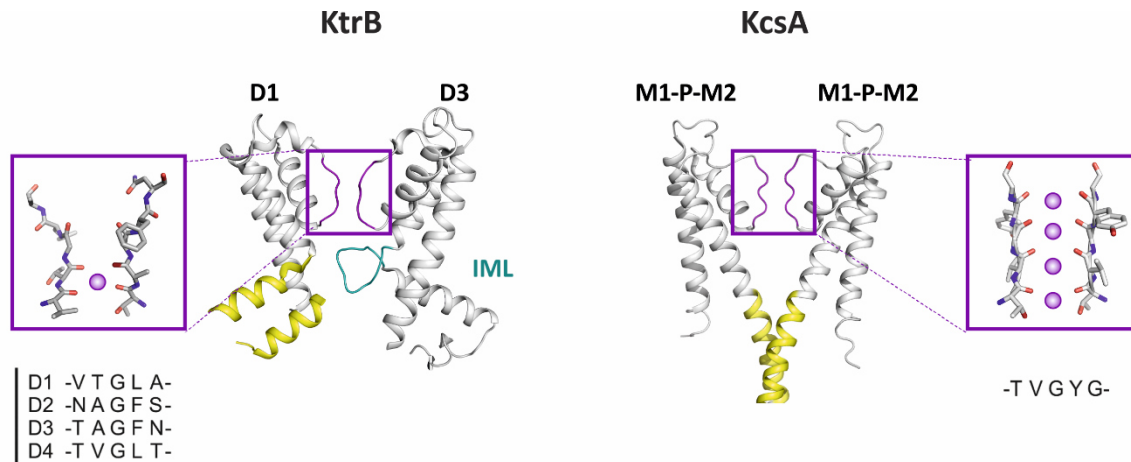


Figure 41 Ion permeation pathway and selectivity filter. Ribbon representation of one KtrB protomer (4J7C) and KcsA (PDB) highlighting the permeation pathway with the selectivity filter (purple box), the intramembrane loop (IML, green) and the “bundle crossing” (yellow). Domains D2 and D4 of KtrB are removed for clarity, and so are two of the KcsA subunits. Stick representations of the selectivity filters of KtrB (4J7C) and KcsA (1BL8), respectively are shown in the inset with the so far confirmed K^+ binding sites as purple spheres. The selectivity filter signature sequences of all four KtrB domains from *V. alginolyticus* in comparison to the signature sequence of KcsA are shown below.

In general, K^+ selective conductance depends on three main aspects, the architecture of the pore, the size of the cation and how much water it attracts and holds around itself. Initial ITC measurements revealed that Na^+ , K^+ , Rb^+ , and Cs^+ bind to KtrB seemingly unselective (Figure 18). This observation was consistent with previous assumptions made for the homologue TrkH (Cao *et al.*, 2013). In fact, these rather unselective binding properties of KtrB were demonstrated to be the result of an absence of small cations, which rendered the protein unstable. Consistently, previous studies on KcsA discovered that small cations are necessary for the stability of the tetramer (Krishnan *et al.*, 2005). Hence, all measurements were repeated by replacing choline-Cl with LiCl in all buffers, which had a drastic effect on the binding affinities (Figure 19). While the apparent affinities for Rb^+ and Cs^+ were unchanged compared to the previous measurements, surprisingly no binding of Na^+ could be detected. The most significant change was the apparent K_D obtained for K^+ , which decreased from 2.9 mM to 90 μM in the presence of LiCl. In conclusion, it seems that KtrB, despite its rather simple selectivity filter, preferably binds K^+ over all other tested cations.

For an ions to bind in the selectivity filter first the dehydration of the hydration shell is required (Doyle *et al.*, 1998; Zhou *et al.*, 2001). The dehydration of a small cation like Na^+ requires much more energy than the dehydration of bigger cations (Mähler and Persson, 2012). Small cations attract and hold the surrounding water molecules much firmer, which was proposed to be one

of the reasons why Na^+ entering a K^+ selectivity filter is usually unfavored (Biggin *et al.*, 2001; Song and Corry, 2009). This has become more evident since the first crystal structure of a Na^+ channel was determined, which showed a very wide Na^+ selectivity filter allowing the coordination of water molecules between the ion and the protein (Payandeh *et al.*, 2011; Sula *et al.*, 2017). Stripping water molecules of bigger ions, like Rb^+ and Cs^+ , is energetically easier. However, their big size makes it harder to fit them into the selectivity filter, which is probably the reason why their binding affinities towards KtrB are lower compared to the affinity for K^+ .

After an ion has been dehydrated it is coordinated in one of the four selectivity filter binding sites in canonical selectivity filters, each provided by eight backbone carbonyl oxygens (Zhou *et al.*, 2001) mimicking the first hydration shell optimized for a K^+ ion (Thomas, Jayatilaka and Corry, 2007). Na^+ prefers a different coordination number of five to six oxygen atoms (Harding, 2002). However, a binding site for Na^+ or Li^+ was identified in the canonical selectivity filter in the plane between S3 and S4 (Thompson *et al.*, 2009). This B-site was shown to constrain the binding and conductance of K^+ (Shrivastava *et al.*, 2002; Thomas, Jayatilaka and Corry, 2007). ITC competition experiments also showed that all four ions compete for selectivity filter binding in KtrB (Figure 21) and that the two bigger cations, Rb^+ and Cs^+ , can block K^+ binding and translocation at concentrations 10-fold above their binding affinities (Figure 21 and Figure 33). At physiological concentrations, even the smaller Na^+ reduced the binding affinity of K^+ to KtrB, suggesting that Na^+ can also bind to KtrB with low binding affinity. All these data points towards the fact that KtrB, like most proteins, is inherently flexible (Zaccai, 2000) and that KtrB's pore and selectivity filter are not as rigid as always painted since they can accommodate all cations. Nevertheless, the ITC data also imply that K^+ is still preferred over Na^+ at equilibrium concentrations. Multiple laboratory experiments on different K^+ channels all come to the same conclusion that K^+ ions are preferred over Na^+ ion at equilibrium (Neyton and Miller, 1988a; Korn and Ikeda, 1995; Baukowitz and Yellen, 1996; Ogielska and Aldrich, 1999; Åqvist and Luzhkov, 2000; Zhou *et al.*, 2001; Krishnan *et al.*, 2005; Noskov and Roux, 2006; Bhate *et al.*, 2010; Piasta, Theobald and Miller, 2011; Liu, Bian and Lockless, 2012), which is understood to be the reason for selectivity. The simplest explanation for selectivity is the thermodynamic advantage for K^+ over other cations in the selectivity filter.

A classical K^+ selectivity filter consists of four consecutive K^+ binding sites (KcsA, Figure 41). The number of sites was shown to be essential for selective and fast conductance (Figure 4). Based on the number of binding sites, a multi-ion mechanism was proposed, which depends on maximally dehydrated K^+ being efficiently translocated by direct Coulomb knock-on (Köpfer *et al.*, 2014; Kopec *et al.*, 2018). This particular mechanism of K^+ over Na^+ selectivity is believed to be best achieved by selectivity filters with four binding sites. A reduced number of binding sites leads to a poor K^+ over Na^+ conductance. For example, NaK channels with only 2 binding

sites were shown to non-selectively conduct K^+ and Na^+ even though they exhibit a K^+ over Na^+ binding preference at equilibrium (Liu and Lockless, 2013; Kopec *et al.*, 2018). KtrB has instead of four consecutive binding sites only one, where eight carbonyl backbone oxygens can coordinate one K^+ ion. In agreement, SSM-based electrophysiology and ACMA-based flux assays suggested a size-selective translocation and not the preference of potassium ions (Figure 28 and Figure 32). Surprisingly fast Na^+ fluxes were observed followed by slower K^+ and very slow Rb^+ fluxes, while Cs^+ did not flux at all through KtrB as shown by the ACMA assay. This means that the smallest cation fluxes faster than all other cations with the order $Na^+ > K^+ > Rb^+ > Cs^+$, as also indicated by integrated transient currents obtained with SSM-based electrophysiology. This observation would be in principle in good agreement with the expected low selectivity for less than four consecutive binding sites (Liu and Lockless, 2013; Sauer *et al.*, 2013; Kopec *et al.*, 2018). Whether in this case, Na^+ fluxes through KtrB in a hydrated state is unknown. Nevertheless, Na^+ fluxes must be taken with precaution, since K^+ is completely missing in the experiment. For other K^+ channels it is known that they can conduct Na^+ in the absence of K^+ (Korn and Ikeda, 1995; Kiss, LoTurco and Korn, 1999; Wang, Zhang and Fedida, 2000; Valiyaveetil *et al.*, 2006; Zhenyu *et al.*, 2013; Kopec *et al.*, 2018). In the absence of K^+ , the selectivity filter is collapsed, allowing the flux of Na^+ together with water (Kopec *et al.*, 2018). In agreement with this are the results from competition experiments with KtrB using SSM-based electrophysiology and whole-cell K^+ uptake, which further showed that high Na^+ concentrations inhibited neither K^+ transient currents nor K^+ uptake (cf. Figure 33 and Figure 37). Following the argumentation of the importance of the number of binding sites for the selective conductivity this could suggest that KtrB contains indeed more than one binding site. For the homologous TrkH, for which initially only one binding site was shown, two additional binding sites have been proposed by MD simulations (Domene and Furini, 2012). Similarly, KtrB could have additional binding sites. However, attempts to simulate ion conductance and additional binding sites with MD failed, probably due to a collapsed selectivity filter structure (Dr. Ahmad Reza Mehdipour, personal communication). Apparently contrary to the results obtained here are the results obtained in single-channel recording of TrkAH, showing similar conductivities for K^+ , Rb^+ , and Cs^+ , while a slower conductance was observed for Na^+ and Li^+ (Cao *et al.*, 2013). However, in that study the open probabilities for the different cations were never examined. Therefore, the efficiency of ion translocation is still unknown. Whether the selectivity filter of KtrB has more than just one binding site needs to be answered in the future. Taken together, the prerequisite of preferred K^+ binding and translocation is met by KtrB. The next hurdle for the cation to overcome is the intramembrane loop. Its role will be discussed in the following section 5.2.

5.2 Size restriction by the intramembrane loop in KtrB

Typically, most 2TM/P K⁺ channels have added to the selectivity filter a bundle crossing gate, which creates a constriction on the intracellular side (Uysal *et al.*, 2009). This gate is formed by either helix M2 in for example KcsA (Perozo, Marien Cortes and Cuello, 1998; Liu, Sompornpisut and Perozo, 2001; Blunck *et al.*, 2006) or helix S6 of the core domain of voltage-gated K⁺ channels (Liu *et al.*, 1997; del Camino and Yellen, 2001). This bundle crossing gate was shown to be crucial for efficient ion translocation in K⁺ channels (Liu *et al.*, 1997; Jiang, Lee, Chen, Cadene, Brian T Chait, *et al.*, 2002). This usually hydrophobic part of the helical bundle crossing creates a steric hindrance for K⁺ ions (del Camino and Yellen, 2001; Kitaguchi, Sukhareva and Swartz, 2004). In KtrB as well as TrkH the M2 helices are broken and the lower segments point away from the central axis of the pore (Figure 9). Therefore, the characteristic intracellular constriction is not present. Both proteins have, alternatively to the bundle crossing gate, a bulky non-helical segment in the middle of broken helix D3M2, which constricts the permeation pathway, known as the intramembrane loop (Hänelt, Löchte, *et al.*, 2010; Vieira-Pires, Szollosi and Morais-Cabral, 2013). While the bundle crossing gate is mostly hydrophobic (Uysal *et al.*, 2009), the intramembrane loop is generally hydrophilic in both KtrB and TrkH (Figure 42 a). In KtrB, this gatekeeper is flanked with glycines and contains several polar residues, mostly serines, and threonines. Furthermore, in KtrB as well as TrkH the C-terminal end of the intramembrane loop is formed by a conserved, positively charged amino acid, lysine (K) or arginine (R), pointing in the cavity. Another highly conserved positive amino acid in this region is an arginine residue located in D4M2 of KtrB (Vieira-Pires, Szollosi and Morais-Cabral, 2013). It was suggested that the polar and charged residues between the cavity and the intramembrane loop could contribute the stability of the loop (Levin and Zhou, 2014). Opening the ion pathway to the intracellular side requires the full hydration of the cavity, which is influenced by the flexibility and characteristics of the intramembrane loop (Diskowski *et al.*, 2017). KtrA was proposed to regulate ion fluxes by influencing the intramembrane loop. An ATP/ADP-induced conformational change of KtrA was shown to trigger the release of helix D1M2 opposite from the intramembrane loop (Figure 9). It was shown, that this conformational change consequently allows the loop to move freely (Diskowski *et al.*, 2017). *In vitro* investigations of this gatekeeping loop in only KtrB clearly show that it limits ion fluxes (Figure 36). This is in agreement with previous studies (Hänelt, Löchte, *et al.*, 2010; Hänelt, Wunnicke, *et al.*, 2010). In KtrB alone, the speed of ion translocation could be altered by mutations in the loop. Adding a more polar residue, by replacing a glycine for serine at position 316, led to increased fluxes of K⁺ and Rb⁺. Possible explanations are that the intramembrane loop adopts a more open position, that the serine residue helps with the rehydration of the ion, or both. Interestingly, neither the Na⁺ nor the Cs⁺ fluxes are influenced by the mutations (Figure 36).

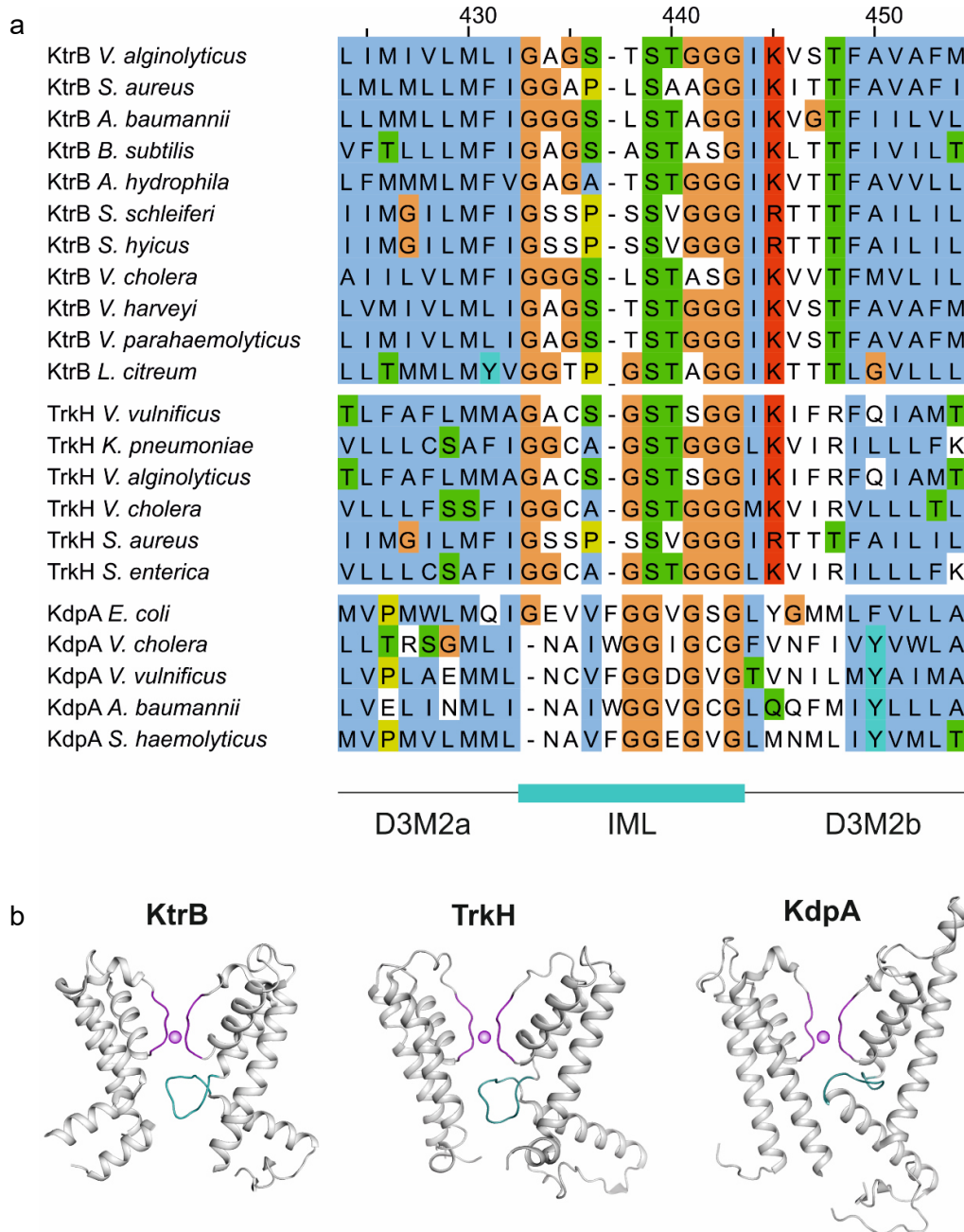


Figure 42 Sequence alignments of the intramembrane loop (IML) of KtrB, TrkH and KdpA. (a) A sequence alignment of KtrB, TrkH and KdpA proteins was generated by Clustal Omega and adjusted by Jalview. Amino acid sequences of the following organisms are shown: *Vibrio alginolyticus* (*V. alginolyticus*), *Staphylococcus aureus* (*S. aureus*), *Acinetobacter baumannii* (*A. baumannii*), *Bacillus subtilis* (*B. subtilis*), *Aeromonas hydrophila* (*A. hydrophila*), *Staphylococcus schleiferi* (*S. schleiferi*), *Staphylococcus hyicus* (*S. hyicus*), *Vibrio cholera* (*V. cholera*), *Vibrio harveyi* (*V. harveyi*), *Vibrio parahaemolyticus* (*V. parahaemolyticus*), *Leuconostoc citreum* (*L. citreum*), *Vibrio vulnificus* (*V. vulnificus*), *Klebsiella pneumoniae* (*K. pneumoniae*), *Salmonella enterica* (*S. enterica*), *Escherichia coli* (*E. coli*) and *Staphylococcus haemolyticus* (*S. haemolyticus*). The Clustal X color scheme was used to examine conservation: Hydrophobic residues are highlighted in blue, polar residues are green, glycines are orange, positive residues are highlighted in red, and prolines are highlighted in yellow. Non-conserved residues are uncolored. (b) D1 and D3 of KtrB, TrkH and KdpA (grey) showing the selectivity filter (purple) and the intramembrane loop (teal) in comparison.

Cs⁺ is probably arrested in the selectivity filter and cannot permeate. The question is, why is the permeation of the small Na⁺ not affected? Considering efficient ion translocation,

rehydration of the cation is necessary. Typically, K^+ channels like KcsA have an aqueous cavity on the intracellular side (Doyle *et al.*, 1998). In KtrB, the intramembrane loop obstructs the ion permeation pathway. Depending on the position of the loop in KtrB, the cavity is either more or less filled with water, as shown in both KtrB alone (Figure 43) and in the complex (Diskowski *et al.*, 2017). For KtrAB, the position of the loop was shown to be dependent on the extended helix D1M2 regulated by conformational changes of KtrA (Diskowski *et al.*, 2017). Na^+ might just not be influenced by this, because the cavity could be already big enough to accommodate a hydrated Na^+ ion. The position of the loop possibly obstructs bigger ions, which, when fully hydrated, may take up more space in the cavity under the selectivity filter. This hypothesis is supported by whole-cell K^+ and Na^+ uptake experiments with different KtrB $_{\Delta}$ loop mutants showing only increased K^+ uptake rates while the Na^+ uptake was not affected (Hänelt, Löchte, *et al.*, 2010). It needs to be shown whether decreasing the polarity of the intramembrane loop or its surrounding region can generally decrease cation fluxes and possibly also influence Na^+ permeation. However, a far bigger enigma is the influence of Na^+ on K^+ uptake through KtrB and the role of KtrA in triggering these fast fluxes.

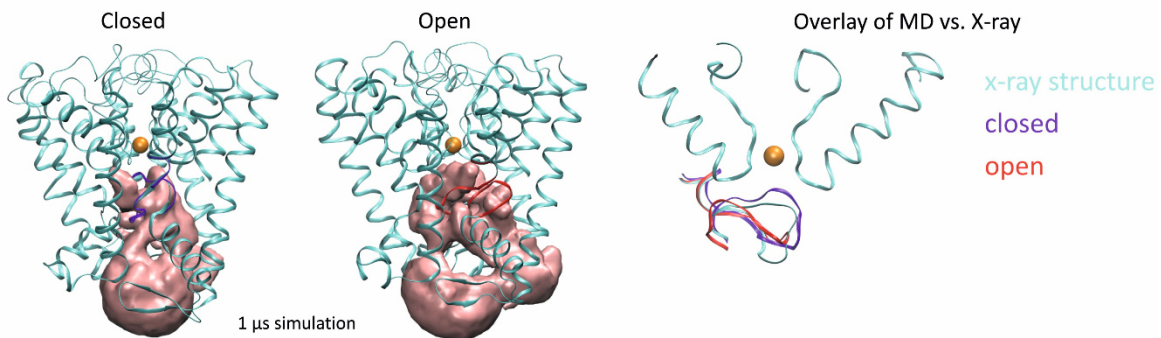


Figure 43 Comparison of the simulated closed and open state of KtrB's intramembrane loop. MD simulations on the flexibility of the intramembrane loop show a closed (purple, left) or open (red, center) state in comparison with the loop positions in the x-ray structure (right, modeled on pdb: 4J7C) in a 1 μ s simulation. The intramembrane loop impedes on the hydration of the cavity below the selectivity filter. MD simulations were performed by Dr. Ahmad Reza Mehdipour, Department of Theoretical Biophysics, Max Planck Institute of Biophysics in Frankfurt.

5.3 Na^+ dependency of KtrAB

It has long been known that Na^+ aids fast K^+ fluxes through KtrAB, while K^+ uptake through KtrB alone is not influenced by Na^+ (Tholema *et al.*, 1999). Two concepts for Na^+ -dependent K^+ translocation have been discussed for KtrAB. The first concept assumed that Na^+ acts as a co-substrate in a symporter-like fashion (Tholema *et al.*, 1999). This has been proposed for another SKT member, HKT1. This eukaryotic protein was termed a Na^+/K^+ symporter (Rubio, Gassmann and Schroeder, 1995; Rubio *et al.*, 1999). However, when critically examining this

data, it was shown that already 100 mM NaCl had an inhibitory effect on K⁺ uptake (Rubio, Gassmann and Schroeder, 1995; Rubio *et al.*, 1999), which would rather be in agreement with an unselective channel than with a symporter activity. For KtrAB, the symport concept was excluded by the fact that the uptake of K⁺ is dependent on Na⁺, but the uptake of Na⁺ is independent of K⁺ (Kolesova, 2016). A symporter would, however, require a strict coupling. The second concept suggested the allosteric coupling of Na⁺ binding to either KtrA or KtrB for gating. Only recently binding of Na⁺ to the cytoplasmic gating ring KtrA at physiological conditions was excluded by ITC measurements (Janina Stautz, personal communication). By investigating the effect of Na⁺ on K⁺ uptake through KtrAB, it became evident that only 5 mM NaCl increased the K_M for K⁺ binding from ~1 mM to ~35 μ M, which is close to the K_D determined for K⁺ binding to KtrB. Further, the doubled V_{max} indicates an enhanced open probability of the gate. After untargeted MD simulations found a potential second binding site within KtrB, the main residues coordinating this site were investigated by mutational studies. The binding site is formed by residues Q93, E149, and N182 located in D1M2, D2M1, and D2P, respectively. The asparagine is located only one residue N-terminally away of the selectivity filter sequence -NAGFA-. Sequence alignments showed that all three residues are highly conserved (Figure 44). Furthermore, this region is not only close to the selectivity filter but also to the intramembrane loop and extended helix D1M2, which in KtrAB protrudes into the KtrA gating ring. The most important evidence that this 2nd binding site might be linked to the Na⁺ dependency of KtrAB was given by the mutational study combined with growth experiments in *E. coli* LB2003 shown in sections 4.7.3. Neutralizing the negatively charged E149 with L could mimic the presence of Na⁺ and was shown not to affect growth. A radical mutation of the same residues to lysine led to a growth defect only in KtrAB, but not in the Na⁺-independent KtrB. Replacing the polar Q93 with the apolar leucine had the same effect, but here, the coordination of the Na⁺ ion could be impaired. Combining the neutralizing mutant E149L and the reduced coordination site Q93L restored strain growth, probably because Na⁺ binding was not necessary anymore because of the mimicked neutral charge from the leucine residue. Finally, the gained data provide a first hint on where the Na⁺ binding site could be localized. It seems to be plausible and in agreement with its effect on only KtrAB, since it is closely located to the gating region which is regulated by structural changes in KtrA. However, of course, further structural and functional assays are required confirming this site. Importantly, the assays to study ion fluxes through KtrAB have been established in this thesis.

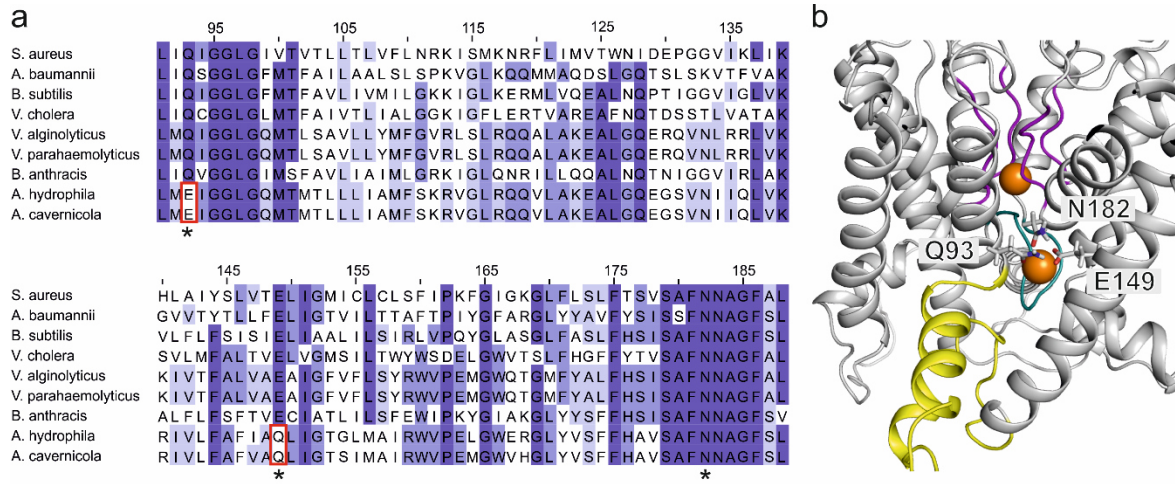


Figure 44 Sequence alignment showing conservation of the potential second binding site. (a) A sequence alignment for KtrB was generated by Clustal Omega and adjusted by Jalview. KtrB amino acid sequences of the following organisms are compared: *Vibrio alginolyticus* (*V. alginolyticus*), *Staphylococcus aureus* (*S. aureus*), *Acinetobacter baumannii* (*A. baumannii*), *Bacillus subtilis* (*B. subtilis*), *Vibrio cholera* (*V. cholera*), *V. parahaemolyticus*, *Aeromonas hydrophila* (*A. hydrophila*), *Bacillus anthracis* (*B. anthracis*) and *Aeromonas cavernicola* (*A. cavernicola*). The Percentage Identity color scheme with dark blue (>80%), blue (>60%), light blue (>40%), and colorless (<40%) indicate the conservation of residues from high to low, respectively. Amino acids corresponding to the second binding site are highly conserved and marked by the asterisk. (b) Location of the second binding site amino acids (Q93, E149, and N182) in relation to the selectivity filter in purple, the intramembrane loop in teal, and helix D1M2b in yellow. Ions located in the selectivity filter and the second binding site are shown in orange.

6. Directories

6.1 List of abbreviations

Abbreviations	Meaning
AC	Alternating current
ACMA	9-Amino-6-Chloro-2-Methoxyacridine
ADP	Adenosine diphosphate
APG-4	Assante Potassium Green-4 (fluorescent dye)
APS	Ammonium persulfate
ATP	Adenosine triphosphate
A solution	Activating solution
<i>B. subtilis</i>	<i>Bacillus subtilis</i>
Ba²⁺	Barium ion
BCA	Bicinchoninic acid
BLM	Black lipid membrane
c-di-AMP	Cyclic-di-adenosine monophosphate
CCCP	Carbonylcyanid- <i>m</i> -chlorophenylhydrazon
CNG	Cyclic nucleotide-gated
Cs⁺	Cesium ion
D	Domain
DC	Direct current
DDM	Dodecyl- β -d-maltopyranosid
DNA	Deoxyribonucleic acid
DPhyPC	1,2 Diphytanoyl-sn-glycero-3-Phosphatidylcholin
<i>E. coli</i>	<i>Escherichia coli</i>
EDTA	Ethylenediaminetetraacetic acid
eLS	Empty (control) liposomes
HEPES	4-(2-hydroxyethyl)-1-piperazineethanesulfonic acid
IMAC	Immobilized metal ion affinity chromatography
ITC	Isothermal titration calorimetry
K⁺	Potassium ion
K_D	Equilibrium dissociation constant
K_M	Michaelis-Menten-constant
Ktr	Potassium (K ⁺) transporter
KP_i	Potassium phosphate
Li⁺	Lithium ion
LILBID-MS	Laser induced liquid bead ion desorption-mass spectrometry
LPR	Lipid to protein ratio
M (TM)	Transmembrane helix
MD	Molecular dynamics

MES	2-(N-morpholino)ethanesulfonic acid
M1-P-M2 domain	Transmembrane-P loop-transmembrane domain
Na⁺	Sodium ion
NA solution	Non activating solution
NAD⁺/NADH	Nicotinamide adenine dinucleotide
Ni²⁺-NTA	Nickle-nitrilotriacetic acid
OD₆₀₀	Optical density measured at 600 nm
P-loop/-helix	Pore-loop/-helix
PCR	Polymerase chain reaction
P_{DX}	Pore loop of domain X
PL	Proteoliposomes
PMSF	Phenylmethylsulfonyl fluoride
Rb⁺	Rubidium ion
RCK	Regulator of potassium conductance
RT	Room temperature
SAM	Self-assembling monolayer
SD	Standard deviation
SDS-PAGE	Sodium dodecyl sulfate-polyacrylamide gel electrophoresis
SEC	Size-exclusion chromatography
SEM	Standard error of the mean
SF	Selectivity filter
SG	Sodium Green™ (fluorescent dye)
SKT	Superfamily of potassium transporters
SMA	Styrene-maleic acid
SMALP	Styrene-maleic acid lipid nano-particles
SSM	Solid supported membrane
TEMED	Tetramethylethylenediamine
TM (M)	Transmembrane helix
Tris	Tris-hydroxymethyl-aminomethan
<i>V. alginolyticus</i>	<i>Vibrio alginolyticus</i>
VaKtrB	KtrB from <i>Vibrio alginolyticus</i>
Val	Valinomycin
w/v	Weight per volume
w/w	Weight per weight ratio

7. References

- Adler, S. and Fraley, D. S. (1977) 'Potassium and intracellular pH', *Kidney International*, 11(6), pp. 433–442. doi: 10.1038/ki.1977.61.
- Alam, A. and Jiang, Y. (2009a) 'High-resolution structure of the open NaK channel', *Nature Structural & Molecular Biology*, 16(1), pp. 30–34. doi: 10.1038/nsmb.1531.
- Alam, A. and Jiang, Y. (2009b) 'Structural analysis of ion selectivity in the NaK channel', *Nature Structural & Molecular Biology*, 16(1), pp. 35–41. doi: 10.1038/nsmb.1537.
- Alberts, B., Wilson, J. H. and Hunt, T. (2008) 'Molecular biology of the cells', *Molecular biology of the cell, 5th edn*, Garland Science, New York.
- Albright, R. A. *et al.* (2006) 'The RCK Domain of the KtrAB K⁺ Transporter: Multiple Conformations of an Octameric Ring', *Cell*, 126(6), pp. 1147–1159. doi: 10.1016/j.cell.2006.08.028.
- Altendorf, K. *et al.* (1998) 'Structure and function of the Kdp-ATPase of *Escherichia coli*', *Acta Physiologica Scandinavica, Supplement*, 163(643), pp. 137–146.
- Altendorf, K. and Epstein, W. (1994) 'Kdp-atpase of *Escherichia coli*', *Cellular Physiology and Biochemistry*, 4(3–4), pp. 160–168. doi: 10.1159/000154719.
- Åqvist, J. and Luzhkov, V. (2000) 'Ion permeation mechanism of the potassium channel', *Nature*, 404(6780), pp. 881–884. doi: 10.1038/35009114.
- Ashcroft, F., Gadsby, D. and Miller, C. (2009) 'Introduction. The blurred boundary between channels and transporters', *Philosophical Transactions of the Royal Society B: Biological Sciences*, 364(1514), pp. 145–147. doi: 10.1098/rstb.2008.0245.
- Bakker, E. P. and Mangerich, W. E. (1981) 'Interconversion of components of the bacterial proton motive force by electrogenic potassium transport.', *Journal of bacteriology*, 147(3), pp. 820–6. Available at: <http://www.ncbi.nlm.nih.gov/pubmed/6268609>.
- Bakker, E. P. and Mangerich, W. E. (1983) 'The effects of weak acids on potassium uptake by *Escherichia coli* K-12 inhibition by low cytoplasmic pH.', *Biochimica et biophysica acta*, 730(2), pp. 379–86. doi: 10.1016/0005-2736(83)90355-3.
- Bamberg, E. *et al.* (1979) 'Photocurrents generated by bacteriorhodopsin on planar bilayer membranes', *Biophysics of Structure and Mechanism*, 5(4), pp. 277–292. doi: 10.1007/BF02426663.
- Bangham, A. D., Standish, M. M. and Watkins, J. C. (1965) 'Diffusion of univalent ions across the lamellae of swollen phospholipids.', *Journal of molecular biology*, 13(1), pp. 238–52. doi: 10.1016/s0022-2836(65)80093-6.
- Bartolomtnei, G. *et al.* (2009) 'Electrogenic ion pumps investigated on a solid supported membrane: Comparison of current and voltage measurements', *Langmuir*, 25(18), pp. 10925–10931. doi: 10.1021/la901469n.
- Baukrowitz, T. and Yellen, G. (1996) 'Use-dependent blockers and exit rate of the last ion from the multi-ion pore of a K⁺ channel', *Science*, 271(5249), pp. 653–656. doi: 10.1126/science.271.5249.653.
- Bazzone, A. *et al.* (2013) 'Introduction to solid supported membrane based

- electrophysiology', *Journal of Visualized Experiments*, (75), pp. 1–11. doi: 10.3791/50230.
- Bazzone, A. *et al.* (2016) 'pH regulation of electrogenic sugar/H⁺ symport in MFS sugar permeases', *PLoS ONE*, 11(5), pp. 1–17. doi: 10.1371/journal.pone.0156392.
- Bazzone, A. *et al.* (2017) 'A Loose Relationship: Incomplete H⁺/Sugar Coupling in the MFS Sugar Transporter GlcP', *Biophysical Journal*. Biophysical Society, 113(12), pp. 2736–2749. doi: 10.1016/j.bpj.2017.09.038.
- Bazzone, A. (2017) *Mechanismen des Zucker-Transports: Vergleichende elektrophysiologische Untersuchungen an Transportern der major facilitator superfamily*. Johann Wolfgang Goethe-University Frankfurt.
- Bazzone, A., Barthmes, M. and Fendler, K. (2017) 'SSM-Based Electrophysiology for Transporter Research.', *Methods in enzymology*, 594, pp. 31–83. doi: 10.1016/bs.mie.2017.05.008.
- Becker, D. *et al.* (2007) 'The conserved dipole in transmembrane helix 5 of KdpB in the *Escherichia coli* KdpFABC P-type ATPase is crucial for coupling and the electrogenic K⁺-translocation step', *Biochemistry*, 46(48), pp. 13920–13928. doi: 10.1021/bi701394h.
- Bellamacina, C. R. (1996) 'The nicotinamide dinucleotide binding motif: a comparison of nucleotide binding proteins.', *The FASEB Journal*, 10(11), pp. 1257–1269. doi: 10.1096/fasebj.10.11.8836039.
- Berry, S. *et al.* (2003) 'Potassium uptake in the unicellular cyanobacterium *Synechocystis* sp. strain PCC 6803 mainly depends on a Ktr-like system encoded by slr1509 (ntpJ)', *FEBS Letters*, 548, pp. 53–58. doi: 10.1016/S0014-5793(03)00729-4.
- Bezannilla, F. and Armstrong, C. M. (1972) 'Negative conductance caused by entry of sodium and cesium ions into the potassium channels of squid axons', *Journal of General Physiology*, 60(5), pp. 588–608. doi: 10.1085/jgp.60.5.588.
- Bhate, M. P. *et al.* (2010) 'Conformational dynamics in the selectivity filter of KcsA in response to potassium ion concentration.', *Journal of Molecular Biology*, 401(2), pp. 155–66. doi: 10.1016/j.jmb.2010.06.031.
- Biggin, P. C. *et al.* (2001) 'Potassium and sodium ions in a potassium channel studied by molecular dynamics simulations', *Biochimica et Biophysica Acta - Biomembranes*, 1510(1–2), pp. 1–9. doi: 10.1016/S0005-2736(00)00345-X.
- Biggin, P. C., Roosild, T. and Choe, S. (2000) 'Potassium channel structure: Domain by domain', *Current Opinion in Structural Biology*, 10(4), pp. 456–461. doi: 10.1016/S0959-440X(00)00114-7.
- Blunck, R. *et al.* (2006) 'Detection of the opening of the bundle crossing in KcsA with fluorescence lifetime spectroscopy reveals the existence of two gates for ion conduction', *Journal of General Physiology*, 128(5), pp. 569–581. doi: 10.1085/jgp.200609638.
- Booth, I. A. N. R. (1985) 'Regulation of Cytoplasmic pH in Bacteria', *Microbiological Reviews*, 49(4), pp. 359–378.
- Bramkamp, M., Gassel, M. and Altendorf, K. (2004) 'FITC Binding Site and p-Nitrophenyl Phosphatase Activity of the Kdp-ATPase of *Escherichia coli*', *Biochemistry*, 43(15), pp. 4559–4567. doi: 10.1021/bi030198a.

- Bretschneider, F. and de Weille, J. R. (2006) *Introduction to Electrophysiological Methods and Instrumentation*. 1st edn. Amsterdam: Elsevier.
- del Camino, D. and Yellen, G. (2001) 'Tight Steric Closure at the Intracellular Activation Gate of a Voltage-Gated K⁺ Channel', *Neuron*, 32(4), pp. 649–656. doi: 10.1016/S0896-6273(01)00487-1.
- Cao, Y. *et al.* (2011) 'Crystal structure of a potassium ion transporter, TrkH', *Nature*. Nature Publishing Group, 471(7338), pp. 336–341. doi: 10.1038/nature09731.
- Cao, Y. *et al.* (2013) 'Gating of the TrkH ion channel by its associated RCK protein TrkA', *Nature*. Nature Publishing Group, 496(7445), pp. 317–322. doi: 10.1038/nature12056.
- Castle, A. M., Macnab, R. M. and Shulman, R. G. (1986) 'Measurement of intracellular sodium concentration and sodium transport in *Escherichia coli* by ²³Na nuclear magnetic resonance', *Journal of Biological Chemistry*, 261(7), pp. 3288–3294.
- Cheng, W. W. L. *et al.* (2011) 'Mechanism for selectivity-inactivation coupling in KcsA potassium channels', *Proceedings of the National Academy of Sciences of the United States of America*, 108(13), pp. 5272–5277. doi: 10.1073/pnas.1014186108.
- Coetzee, W. A. *et al.* (1999) 'Molecular diversity of K⁺ channels', *Annals of the New York Academy of Sciences*, 868, pp. 233–285. doi: 10.1111/j.1749-6632.1999.tb11293.x.
- Collins, K. D. (1995) 'Sticky ions in biological systems.', *Proceedings of the National Academy of Sciences of the United States of America*, 92(12), pp. 5553–7. doi: 10.1073/pnas.92.12.5553.
- Cordero-Morales, J. F. *et al.* (2006) 'Molecular determinants of gating at the potassium-channel selectivity filter.', *Nature Structural & Molecular Biology*, 13(4), pp. 311–8. doi: 10.1038/nsmb1069.
- Cordero-Morales, J. F. *et al.* (2011) 'A multipoint hydrogen-bond network underlying KcsA C-type inactivation', *Biophysical Journal*. Biophysical Society, 100(10), pp. 2387–2393. doi: 10.1016/j.bpj.2011.01.073.
- Corrigan, R. M. *et al.* (2013) 'Systematic identification of conserved bacterial c-di-AMP receptor proteins', *Proceedings of the National Academy of Sciences of the United States of America*. doi: 10.1073/pnas.1300595110.
- Corrigan, R. M. and Gründling, A. (2013) 'Cyclic di-AMP: Another second messenger enters the fray', *Nature Reviews Microbiology*. Nature Publishing Group, 11(8), pp. 513–524. doi: 10.1038/nrmicro3069.
- Derebe, M. G. *et al.* (2011) 'Tuning the ion selectivity of tetrameric cation channels by changing the number of ion binding sites', *Proceedings of the National Academy of Sciences of the United States of America*, 108(2), pp. 598–602. doi: 10.1073/pnas.1013636108.
- Dibrova, D. V *et al.* (2015) 'Ancient Systems of Sodium/Potassium Homeostasis as Predecessors of Membrane Bioenergetics.', *Biochemistry. Biokhimiia*, 80(5), pp. 495–516. doi: 10.1134/S0006297915050016.
- Dimroth, P. (1980) 'A new sodium-transport system energized by the decarboxylation of oxaloacetate', *FEBS Letters*, 122(2), pp. 234–236. doi: 10.1016/0014-5793(80)80446-7.
- Diskowski, M. *et al.* (2015) 'Functional diversity of the superfamily of K⁺ transporters to meet

- various requirements', *Biological Chemistry*, 396(9–10), pp. 1003–1014. doi: 10.1515/hsz-2015-0123.
- Diskowski, M. *et al.* (2017) 'Helical jackknives control the gates of the double-pore K⁺ uptake system KtrAB', *eLife*, 6, pp. 1–21. doi: 10.7554/eLife.24303.
- Domene, C. and Furini, S. (2012) 'Molecular dynamics simulations of the TrkH membrane protein', *Biochemistry*, 51(8), pp. 1559–1565. doi: 10.1021/bi201586n.
- Donowitz, M., Ming Tse, C. and Fuster, D. (2013) 'SLC9/NHE gene family, a plasma membrane and organellar family of Na⁺/H⁺ exchangers', *Molecular Aspects of Medicine*, 34(2–3), pp. 236–251. doi: 10.1016/j.mam.2012.05.001.
- Dörr, J. M. *et al.* (2014) 'Detergent-free isolation, characterization, and functional reconstitution of a tetrameric K⁺ channel: The power of native nanodiscs', *Proceedings of the National Academy of Sciences of the United States of America*, 111(52), pp. 18607–18612. doi: 10.1073/pnas.1416205112.
- Doyle, D. A. *et al.* (1998) 'The structure of the potassium channel: Molecular basis of K⁺ conduction and selectivity', *Science*, 280(5360), pp. 69–77. doi: 10.1126/science.280.5360.69.
- Durell, S. R. *et al.* (1999) 'Evolutionary relationship between K⁺ channels and symporters', *Biophysical Journal*, 77(2), pp. 775–788. doi: 10.1016/S0006-3495(99)76931-6.
- Durell, S. R., Bakker, E. P. and Guy, H. R. (2000) 'Does the KdpA subunit from the high affinity K⁺-translocating P-type KDP-ATPase have a structure similar to that of K⁺ channels?', *Biophysical Journal*, 78(1), pp. 188–99. doi: 10.1016/S0006-3495(00)76584-2.
- Egwolf, B. and Roux, B. (2010) 'Ion Selectivity of the KcsA Channel: A Perspective from Multi-Ion Free Energy Landscapes', *Journal of Molecular Biology*, 401(5), pp. 831–842. doi: 10.1016/j.jmb.2010.07.006.
- Epstein, W. and Kim, B. S. (1971) 'Potassium transport loci in *Escherichia coli* K-12.', *Journal of Bacteriology*, 108(2), pp. 639–44.
- Evans, H. J. and Sorger, G. J. (1966) 'Role of Mineral Elements with Emphasis on the Univalent Cations', *Annual Review of Plant Physiology*, 17(1), pp. 47–76. doi: 10.1146/annurev.pp.17.060166.000403.
- Fahr, A., Läger, P. and Bamberg, E. (1981) 'Photocurrent kinetics of purple-membrane sheets bound to planar bilayer membranes', *The Journal of Membrane Biology*, 60(1), pp. 51–62. doi: 10.1007/BF01870832.
- Fendler, K. *et al.* (1993) 'Pre-steady-state charge translocation in NaK-ATPase from eel electric organ.', *The Journal of General Physiology*, 102(4), pp. 631–666. doi: 10.1085/jgp.102.4.631.
- Furini, S. and Domene, C. (2013) 'K⁺ and Na⁺ conduction in selective and nonselective ion channels via molecular dynamics simulations', *Biophysical Journal*. Biophysical Society, 105(8), pp. 1737–1745. doi: 10.1016/j.bpj.2013.08.049.
- Gadsby, D. C. (2009) 'Ion channels versus ion pumps: The principal difference, in principle', *Nature Reviews Molecular Cell Biology*, 10(5), pp. 344–352. doi: 10.1038/nrm2668.
- Garcia-Celma, J. J. *et al.* (2007) 'Specific anion and cation binding to lipid membranes

- investigated on a solid supported membrane', *Langmuir*, 23(20), pp. 10074–10080. doi: 10.1021/la701188f.
- Garcia-Celma, J. J. *et al.* (2008) 'Rapid activation of the melibiose permease MelB immobilized on a solid-supported membrane', *Langmuir*, 24(15), pp. 8119–8126. doi: 10.1021/la800428h.
- Garcia-Celma, J. J. *et al.* (2010) 'Delineating electrogenic reactions during lactose/H⁺ symport', *Biochemistry*, 49(29), pp. 6115–6121. doi: 10.1021/bi100492p.
- Garcia-Celma, J., Szydelko, A. and Dutzler, R. (2013) 'Functional characterization of a CIC transporter by solid-supported membrane electrophysiology', *Journal of General Physiology*, 141(4), pp. 479–491. doi: 10.1085/jgp.201210927.
- Geertsma, E. R. *et al.* (2008) 'Membrane reconstitution of ABC transporters and assays of translocator function', *Nature Protocols*, 3(2), pp. 256–266. doi: 10.1038/nprot.2007.519.
- Geertsma, E. R. and Dutzler, R. (2011) 'A versatile and efficient high-throughput cloning tool for structural biology', *Biochemistry*, 50(15), pp. 3272–3278. doi: 10.1021/bi200178z.
- Goldman, D. E. (1943) 'Potential, Impedance, and Rectification in Membranes', *The Journal of General Physiology*, 27(1), pp. 37–60.
- Goldstein, S. A. N. *et al.* (1998) 'Sequence and function of the two P domain potassium channels: Implications of an emerging superfamily', *Journal of Molecular Medicine*, 76(1), pp. 13–20. doi: 10.1007/s001090050186.
- Grabov, A. (2007) 'Plant KT/KUP/HAK potassium transporters: Single family - Multiple functions', *Annals of Botany*, 99(6), pp. 1035–1041. doi: 10.1093/aob/mcm066.
- Grewer, C. *et al.* (2013) 'Electrophysiological Characterization of Membrane Transport Proteins', *Annual Review of Biophysics*, 42(1), pp. 95–120. doi: 10.1146/annurev-biophys-083012-130312.
- Gries, C. M. *et al.* (2013) 'The Ktr potassium transport system in *Staphylococcus aureus* and its role in cell physiology, antimicrobial resistance and pathogenesis', *Molecular Microbiology*, 89(4), pp. 760–773. doi: 10.1111/mmi.12312.
- Guidotti, G. (1972) 'The composition of biological membranes.', *Archives of internal medicine*, 129(2), pp. 194–201. doi: 10.1001/archinte.1972.00320020038003.
- Gulati, S. *et al.* (2014) 'Detergent-free purification of ABC (ATP-binding-cassette) transporters.', *The Biochemical journal*, 461(2), pp. 269–78. doi: 10.1042/BJ20131477.
- Guzman, L. M. *et al.* (1995) 'Tight regulation, modulation, and high-level expression by vectors containing the arabinose PBAD promoter.', *Journal of Bacteriology*, 177(14), pp. 4121–30. doi: 10.1128/jb.177.14.4121-4130.1995.
- Hänelt, I., Löchte, S., *et al.* (2010) 'Gain of function mutations in membrane region M2C2 of KtrB open a gate controlling K⁺ transport by the KtrAB system from *Vibrio alginolyticus*', *Journal of Biological Chemistry*, 285(14), pp. 10318–10327. doi: 10.1074/jbc.M109.089870.
- Hänelt, I., Wunnicke, D., *et al.* (2010) 'Membrane region M2C2 in subunit KtrB of the K⁺ uptake system KtrAB from *Vibrio alginolyticus* forms a flexible gate controlling K⁺ flux: An electron paramagnetic resonance study', *Journal of Biological Chemistry*, 285(36), pp. 28210–28219. doi: 10.1074/jbc.M110.139311.

- Hänelt, I. *et al.* (2011) 'KtrB, a member of the superfamily of K⁺ transporters', *European Journal of Cell Biology*, 90(9), pp. 696–704. doi: 10.1016/j.ejcb.2011.04.010.
- Harding, M. M. (2002) 'Metal-ligand geometry relevant to proteins and in proteins: sodium and potassium.', *Acta crystallographica. Section D, Biological crystallography*, 58(Pt 5), pp. 872–4. doi: 10.1107/s0907444902003712.
- Hastings, D. F. and Gutknecht, J. (1978) 'Potassium and turgor pressure in plants', *Journal of Theoretical Biology*, 73(2), pp. 363–366. doi: 10.1016/0022-5193(78)90197-2.
- Heginbotham, L. *et al.* (1994) 'Mutations in the K⁺ channel signature sequence', *Biophysical Journal*, 66(4), pp. 1061–1067. doi: 10.1016/S0006-3495(94)80887-2.
- Heginbotham, L., Abramson, T. and MacKinnon, R. (1992) 'A functional connection between the pores of distantly related ion channels as revealed by mutant K⁺ channels.', *Science (New York, N.Y.)*, 258(5085), pp. 1152–5. doi: 10.1126/science.1279807.
- Hibino, H. *et al.* (2010) 'Inwardly rectifying potassium channels: Their structure, function, and physiological roles', *Physiological Reviews*, 90(1), pp. 291–366. doi: 10.1152/physrev.00021.2009.
- Hille, B. (1973) 'Potassium Channels in Myelinated Nerve: Selective permeability to small cations', *The Journal of General Physiology*, 61(6), pp. 669–686. doi: 10.1085/jgp.61.6.669.
- Hille, B., Armstrong, C. M. and MacKinnon, R. (1999) 'Ion channels: From idea to reality', *Nature Medicine*, 5(10), pp. 1105–1109. doi: 10.1038/13415.
- Hite, R. K. *et al.* (2015) 'Cryo-electron microscopy structure of the Slo2.2 Na⁺-activated K⁺ channel', *Nature*, 527(7577), pp. 198–203. doi: 10.1038/nature14958.
- Hite, R. K., Tao, X. and MacKinnon, R. (2017) 'Structural basis for gating the high-conductance Ca²⁺-activated K⁺ channel', *Nature*. Nature Publishing Group, 541(7635), pp. 52–57. doi: 10.1038/nature20775.
- Hodgkin, A. L. and Horowicz, P. (1959) 'The influence of potassium and chloride ions on the membrane potential of single muscle fibres', *The Journal of Physiology*, 148(1), pp. 127–160. doi: 10.1113/jphysiol.1959.sp006278.
- Hodgkin, A. L. and Huxley, F. (1952a) 'A quantitative description of membrane current and its application to conduction and excitation in nerve.', *The Journal of Physiology*, 117(4), pp. 500–44. doi: 10.1113/jphysiol.1952.sp004764.
- Hodgkin, A. L. and Huxley, F. (1952b) 'Currents carried by Sodium and Potassium Ions through the Membrane of the Giant Axon of Loligo', *Journal of Physiology*, pp. 449–472. doi: 10.1113/jphysiol.1952.sp004717.
- Hodgkin, A. L. and Huxley, F. (1952c) 'Movement of Sodium and Potassium Ions during Nervous Activity', *Cold Spring Harbor Symposia on Quantitative Biology*. doi: 10.1101/SQB.1952.017.01.007.
- Hodgkin, A. L. and Huxley, F. (1952d) 'The dual effect of membrane potential on sodium conductance in the giant axon of Loligo.', *Journal of Physiology*, pp. 497–506.
- Hodgkin, A. L. and Katz, B. (1948) 'The effect of sodium ions on the electrical activity of the giant axon of the squid', *The Journal of Physiology*, 108(1), pp. 37–77. doi: 10.1113/jphysiol.1949.sp004310.

- Hodgkin, A. L. and Keynes, R. D. (1955) 'The potassium permeability of a giant nerve fibre', *The Journal of Physiology*, (1949), pp. 61–88.
- Holtmann, G. *et al.* (2003) 'KtrAB and KtrCD: Two K⁺ Uptake Systems in *Bacillus subtilis* and Their Role in Adaptation to Hypertonicity', *Society*, 185(4), pp. 1289–1298. doi: 10.1128/JB.185.4.1289.
- Hope, M. J. *et al.* (1985) 'Production of large unilamellar vesicles by a rapid extrusion procedure: characterization of size distribution, trapped volume and ability to maintain a membrane potential.', *Biochimica et biophysica acta*, 812(1), pp. 55–65. doi: 10.1016/0005-2736(85)90521-8.
- Hou, S. *et al.* (2010) 'Zn²⁺ activates large conductance Ca²⁺-activated K⁺ channel via an intracellular domain', *Journal of Biological Chemistry*, 285(9), pp. 6434–6442. doi: 10.1074/jbc.M109.069211.
- Huang, C. S., Pedersen, B. P. and Stokes, D. L. (2017) 'Crystal structure of the potassium-importing KdpFABC membrane complex', *Nature*. Nature Publishing Group, 546(7660), pp. 681–685. doi: 10.1038/nature22970.
- Imai, S. *et al.* (2010) 'Structural basis underlying the dual gate properties of KcsA', *Proceedings of the National Academy of Sciences of the United States of America*, 107(14), pp. 6216–6221. doi: 10.1073/pnas.0911270107.
- Jamshad, M. *et al.* (2011) 'Surfactant-free purification of membrane proteins with intact native membrane environment.', *Biochemical Society transactions*, 39(3), pp. 813–8. doi: 10.1042/BST0390813.
- Jiang, Y. *et al.* (2001) 'Structure of the RCK domain from the E. coli K⁺ channel and demonstration of its presence in the human BK channel.', *Neuron*, 29(3), pp. 593–601. doi: 10.1016/s0896-6273(01)00236-7.
- Jiang, Y., Lee, A., Chen, J., Cadene, M., Chait, Brian T., *et al.* (2002) 'Crystal structure and mechanism of a calcium-gated potassium channel', *Nature*, 417(6888), pp. 515–522. doi: 10.1038/417515a.
- Jiang, Y., Lee, A., Chen, J., Cadene, M., Chait, Brian T., *et al.* (2002) 'The open pore conformation of potassium channels.', *Nature*, 417(6888), pp. 523–6. doi: 10.1038/417523a.
- Kamb, A., Tanouye, M. A. and Tseng-Crank, J. (1988) 'Multiple Products of the Drosophila Shaker Gene May Contribute to Potassium Channel Diversity', 1, pp. 421–430.
- Kaplan, J. H. (2002) 'Biochemistry of Na,K-ATPase', *Annual Review of Biochemistry*, 71(1), pp. 511–535. doi: 10.1146/annurev.biochem.71.102201.141218.
- Kato, N. *et al.* (2007) 'Role of positively charged amino acids in the M2D transmembrane helix of Ktr/Trk/HKT type cation transporters', *Channels*, 1(3), pp. 161–171. doi: 10.4161/chan.4374.
- Kim, D. M. and Nimigean, C. M. (2016) 'Voltage-gated potassium channels: A structural examination of selectivity and gating', *Cold Spring Harbor Perspectives in Biology*, 8(5), pp. 1–19. doi: 10.1101/cshperspect.a029231.
- Kim, H. *et al.* (2015) 'Structural studies of potassium transport protein KtrA regulator of conductance of K⁺ (RCK) C domain in complex with cyclic diadenosine monophosphate (c-di-AMP)', *Journal of Biological Chemistry*, 290(26), pp. 16393–16402. doi:

10.1074/jbc.M115.641340.

Kim, I. and Allen, T. W. (2011) 'On the selective ion binding hypothesis for potassium channels.', *Proceedings of the National Academy of Sciences of the United States of America*, 108(44), pp. 17963–8. doi: 10.1073/pnas.1110735108.

Kiss, L., LoTurco, J. and Korn, S. J. (1999) 'Contribution of the selectivity filter to inactivation in potassium channels.', *Biophysical journal*, 76(1 Pt 1), pp. 253–63. doi: 10.1016/S0006-3495(99)77194-8.

Kitaguchi, T., Sukhareva, M. and Swartz, K. J. (2004) 'Stabilizing the closed S6 gate in the shaker Kv channel through modification of a hydrophobic seal', *Journal of General Physiology*, 124(4), pp. 319–332. doi: 10.1085/jgp.200409098.

Knowles, T. J. *et al.* (2009) 'Membrane proteins solubilized intact in lipid containing nanoparticles bounded by styrene maleic acid copolymer.', *Journal of the American Chemical Society*, 131(22), pp. 7484–5. doi: 10.1021/ja810046q.

Kolesova, N. (2016) *Investigation of substrate binding properties of the Ktr system*. Johann Wolfgang Goethe-University.

Kong, C. *et al.* (2012) 'Distinct gating mechanisms revealed by the structures of a multi-ligand gated K⁺ channel', *eLife*, 2012(1), pp. 1–20. doi: 10.7554/eLife.00184.

Kopec, W. *et al.* (2018) 'Direct knock-on of desolvated ions governs strict ion selectivity in K⁺ channels', *Nature Chemistry*. Springer US, 10(8), pp. 813–820. doi: 10.1038/s41557-018-0105-9.

Köpfer, D. A. *et al.* (2014) 'Ion permeation in K⁺ channels occurs by direct Coulomb knock-on', *Science*, 346(6207), pp. 352–355. doi: 10.1126/science.1254840.

Korn, S. J. and Ikeda, S. R. (1995) 'Permeation selectivity by competition in a delayed rectifier potassium channel.', *Science (New York, N.Y.)*, 269(5222), pp. 410–2. doi: 10.1126/science.7618108.

Krishnan, M. N. *et al.* (2005) 'Functional role and affinity of inorganic cations in stabilizing the tetrameric structure of the KcsA K⁺ channel.', *The Journal of general physiology*, 126(3), pp. 271–83. doi: 10.1085/jgp.200509323.

Kroll, R. G. and Booth, I. R. (1983) 'The relationship between intracellular pH, the pH gradient and potassium transport in *Escherichia coli*.', *The Biochemical journal*, 216(3), pp. 709–16. doi: 10.1042/bj2160709.

Kröning, N. *et al.* (2007) 'ATP Binding to the KTN/RCK subunit KtrA from the K⁺-uptake system KtrAB of *Vibrio alginolyticus*: Its role in the formation of the KtrAB complex and its requirement in vivo', *Journal of Biological Chemistry*, 282(19), pp. 14018–14027. doi: 10.1074/jbc.M609084200.

Kubo, Y. *et al.* (1993) 'Primary structure and functional expression of a mouse inward rectifier potassium channel.', *Nature*, 362(6416), pp. 127–133.

Van der Laan, M., Gaßel, M. and Altendorf, K. (2002) 'Characterization of amino acid substitutions in KdpA, the K⁺-binding and -translocating subunit of the KdpFABC complex of *Escherichia coli*', *Journal of Bacteriology*, 184(19), pp. 5491–5494. doi: 10.1128/JB.184.19.5491-5494.2002.

- Labro, A. J. and Snyders, D. J. (2012) 'Being flexible: The voltage-controllable activation gate of Kv channels', *Frontiers in Pharmacology*, 3 SEP(September), pp. 1–12. doi: 10.3389/fphar.2012.00168.
- Laemmli, U. K. (1970) 'Cleavage of structural proteins during the assembly of the head of bacteriophage T4.', *Nature*, 227(5259), pp. 680–5. doi: 10.1038/227680a0.
- Lasic, D. D. (1988) 'The mechanism of vesicle formation', *Biochemical Journal*, 256(1), pp. 1–11. doi: 10.1042/bj2560001.
- Leive, L. (1968) 'Studies on the permeability change produced in coliform bacteria by ethylenediaminetetraacetate.', *Journal of Biological Chemistry*, 243(9), pp. 2373–2380.
- Lesage, F. *et al.* (1996) 'TWIK-1, a ubiquitous human weakly inward rectifying K⁺ channel with a novel structure', *The EMBO journal*, 15(5), pp. 1004–1011. doi: 10.1002/j.1460-2075.1996.tb00437.x.
- Levin, E. J. and Zhou, M. (2014) 'Recent progress on the structure and function of the TrkH/KtrB ion channel', *Current Opinion in Structural Biology*. Elsevier Ltd, 27, pp. 95–101. doi: 10.1016/j.sbi.2014.06.004.
- Lineweaver, H. and Burk, D. (1934) 'The Determination of Enzyme Dissociation Constants', *Journal of the American Chemical Society*, 56(3), pp. 658–666. doi: 10.1021/ja01318a036.
- Liu, J. *et al.* (2017) 'Coupling between distant biofilms and emergence of nutrient time-sharing', *Science*, 356(6338), pp. 638–642. doi: 10.1126/science.aah4204.
- Liu, S., Bian, X. and Lockless, S. W. (2012) 'Preferential binding of K⁺ ions in the selectivity filter at equilibrium explains high selectivity of K⁺ channels', *The Journal of General Physiology*, 140(6), pp. 671–679. doi: 10.1085/jgp.201210855.
- Liu, S. and Lockless, S. W. (2013) 'Equilibrium selectivity alone does not create K⁺-selective ion conduction in K⁺ channels', *Nature Communications*, 4, pp. 1–7. doi: 10.1038/ncomms3746.
- Liu, Y. *et al.* (1997) 'Gated access to the pore of a voltage-dependent K⁺ channel.', *Neuron*, 19(1), pp. 175–84. doi: 10.1016/s0896-6273(00)80357-8.
- Liu, Y., Jurman, M. E. and Yellen, G. (1996) 'Dynamic rearrangement of the outer mouth of a K⁺ channel during gating', *Neuron*, 16(4), pp. 859–867. doi: 10.1016/S0896-6273(00)80106-3.
- Liu, Y. S., Sompornpisut, P. and Perozo, E. (2001) 'Structure of the KcsA channel intracellular gate in the open state', *Nature Structural Biology*, 8(10), pp. 883–887. doi: 10.1038/nsb1001-883.
- Lockless, S. W., Zhou, M. and MacKinnon, R. (2007) 'Structural and thermodynamic properties of selective ion binding in a K⁺ channel', *PLoS Biology*, 5(5), pp. 1079–1088. doi: 10.1371/journal.pbio.0050121.
- Love, J. C. *et al.* (2005) *Self-assembled monolayers of thiolates on metals as a form of nanotechnology*, *Chemical Reviews*. doi: 10.1021/cr0300789.
- MacKinnon, R. (1991) 'Determination of the subunit stoichiometry of a voltage-activated potassium channel.', *Nature*, 350(6315), pp. 232–5. doi: 10.1038/350232a0.

- Mackinnon, R. (2003) 'Potassium channels', *FEBS Letters*, 555(1), pp. 62–65. doi: 10.1016/S0014-5793(03)01104-9.
- Mähler, J. and Persson, I. (2012) 'A study of the hydration of the alkali metal ions in aqueous solution', *Inorganic Chemistry*, 51(1), pp. 425–438. doi: 10.1021/ic2018693.
- Marty, A. *et al.* (1986) '9-amino-2-methoxy-6-chloroacridine monocation fluorescence analysis by phase-modulation fluorometry', *European Biophysics Journal*, 13(4), pp. 251–257. doi: 10.1007/BF00260372.
- McCoy, J. G. and Nimigean, C. M. (2012) 'Structural correlates of selectivity and inactivation in potassium channels.', *Biochimica et biophysica acta*, 1818(2), pp. 272–85. doi: 10.1016/j.bbamem.2011.09.007.
- Meury, J. and Kepes, A. (1981) 'The Regulation of Potassium Fluxes for the Adjustment and Maintenance of Potassium Levels in *Escherichia coli*', *European Journal of Biochemistry*, 119(1), pp. 165–170. doi: 10.1111/j.1432-1033.1981.tb05589.x.
- Meury, J., Robin, A. and Monnier-Champeix, P. (1985) 'Turgor-controlled K⁺ fluxes and their pathways in *Escherichia coli*', *European Journal of Biochemistry*, 151(3), pp. 613–619. doi: 10.1111/j.1432-1033.1985.tb09148.x.
- Mikusevic, V. (2014) *Solid-supported membrane-based electrophysiology measurements on the B subunit of the K⁺ uptake system VaKtrAB*. Johann Wolfgang Goethe-University Frankfurt.
- Mitchell, P. (1961) 'Coupling of Phosphorylation to Electron and Hydrogen Transfer by a Chemi-Osmotic type of Mechanism', *Nature*, 191(4784), pp. 144–148. doi: 10.1038/191144a0.
- Morais-Cabral, J. H., Zhou, Y. and MacKinnon, R. (2001) 'Energetic optimization of ion conduction rate by the K⁺ selectivity filter.', *Nature*, 414(6859), pp. 37–42. doi: 10.1038/35102000.
- Morgner, N. *et al.* (2007) 'A novel approach to analyze membrane proteins by laser mass spectrometry: from protein subunits to the integral complex.', *Journal of the American Society for Mass Spectrometry*, 18(8), pp. 1429–38. doi: 10.1016/j.jasms.2007.04.013.
- Nakamura, T. *et al.* (1998) 'KtrAB, a new type of bacterial K⁺-uptake system from *Vibrio alginolyticus*', *Journal of Bacteriology*, 180(13), pp. 3491–3494.
- Nanatani, K. *et al.* (2015) 'Comparative analysis of *kdp* and *ktr* mutants reveals distinct roles of the potassium transporters in the model cyanobacterium *Synechocystis* sp. strain PCC 6803', *Journal of Bacteriology*, 197(4), pp. 676–687. doi: 10.1128/JB.02276-14.
- Nernst, W. (1889) 'Die elektromotorische Wirksamkeit der Ionen.', *Zeitschrift für Physikalische Chemie*, 4U(1), pp. 129–181.
- Neumcke, B. and Läuger, P. (1969) 'Nonlinear electrical effects in lipid bilayer membranes. II. Integration of the generalized Nernst-Planck equations.', *Biophysical journal*, 9(9), pp. 1160–70. doi: 10.1016/S0006-3495(69)86443-X.
- Neyton, J. and Miller, C. (1988a) 'Discrete Ba²⁺ block as a probe of ion occupancy and pore structure in the high-conductance Ca²⁺-activated K⁺ channel.', *The Journal of general physiology*, 92(5), pp. 569–86. doi: 10.1085/jgp.92.5.569.

- Neyton, J. and Miller, C. (1988b) 'Potassium blocks barium permeation through a calcium-activated potassium channel.', *The Journal of general physiology*, 92(5), pp. 549–67. doi: 10.1085/jgp.92.5.549.
- Nimigeon, C. M. and Allen, T. W. (2011) 'Origins of ion selectivity in potassium channels from the perspective of channel block', *Journal of General Physiology*, 137(5), pp. 405–413. doi: 10.1085/jgp.201010551.
- Noskov, S. Y., Bernéche, S. and Roux, B. (2004) 'Control of ion selectivity in potassium channels by electrostatic and dynamic properties of carbonyl ligands', *Nature*, 431(7010), pp. 830–834. doi: 10.1038/nature02943.
- Noskov, S. Y. and Roux, B. (2006) 'Ion selectivity in potassium channels', *Biophysical Chemistry*, 124(3), pp. 279–291. doi: 10.1016/j.bpc.2006.05.033.
- Ochrombel, I. *et al.* (2011) 'Impact of improved potassium accumulation on pH homeostasis, membrane potential adjustment and survival of *Corynebacterium glutamicum*', *Biochimica et Biophysica Acta - Bioenergetics*. Elsevier B.V., 1807(4), pp. 444–450. doi: 10.1016/j.bbabi.2011.01.008.
- Ogielska, E. M. and Aldrich, R. W. (1999) 'Functional consequences of a decreased potassium affinity in a potassium channel pore. Ion interactions and C-type inactivation', *Journal of General Physiology*, 113(2), pp. 347–358. doi: 10.1085/jgp.113.2.347.
- Padan, E. and Schuldiner, S. (1993) 'Na⁺/H⁺ antiporters, molecular devices that couple the Na⁺ and H⁺ circulation in cells.', *Journal of bioenergetics and biomembranes*, 25(6), pp. 647–69. doi: 10.1007/bf00770252.
- Parsegian, A. (1969) 'Energy of an ion crossing a low dielectric membrane: solutions to four relevant electrostatic problems.', *Nature*, 221(5183), pp. 844–6. doi: 10.1038/221844a0.
- Patiño-Ruiz, M. *et al.* (2017) 'Competition is the basis of the transport mechanism of the NhaB Na⁺/H⁺ exchanger from *Klebsiella pneumoniae*', *PLoS ONE*, 12(7), pp. 1–19. doi: 10.1371/journal.pone.0182293.
- Patiño-Ruiz, M., Fendler, K. and Călinescu, O. (2019) 'Mutation of two key aspartate residues alters stoichiometry of the NhaB Na⁺/H⁺ exchanger from *Klebsiella pneumoniae*', *Scientific Reports*, 9(1), pp. 1–15. doi: 10.1038/s41598-019-51887-2.
- Payandeh, J. *et al.* (2011) 'The crystal structure of a voltage-gated sodium channel', *Nature*. Nature Publishing Group, 475(7356), pp. 353–359. doi: 10.1038/nature10238.
- Perozo, E., Marien Cortes, D. and Cuello, L. G. (1998) 'Three-dimensional architecture and gating mechanism of a K⁺ channel studied by EPR spectroscopy', *Nature Structural Biology*, 5(6), pp. 459–469. doi: 10.1038/nsb0698-459.
- Piasta, K. N., Theobald, D. L. and Miller, C. (2011) 'Potassium-selective block of barium permeation through single KcsA channels', *Journal of General Physiology*, 138(4), pp. 421–436. doi: 10.1085/jgp.201110684.
- Pinner, E. *et al.* (1993) 'Physiological role of NhaB, a specific Na⁺/H⁺ antiporter in *Escherichia coli*', *Journal of Biological Chemistry*, 268(3), pp. 1729–1734.
- Pintschovius, J. and Fendler, K. (1999) 'Charge translocation by the Na⁺/K⁺-ATPase investigated on solid supported membranes: rapid solution exchange with a new technique.', *Biophysical Journal*, 76(2), pp. 814–26. doi: 10.1016/S0006-3495(99)77245-0.

- Pintschovius, J., Fendler, K. and Bamberg, E. (1999) 'Charge translocation by the Na⁺/K⁺-ATPase investigated on solid supported membranes: Cytoplasmic cation binding and release', *Biophysical Journal*, 76(2), pp. 827–836. doi: 10.1016/S0006-3495(99)77246-2.
- Pintschovius, J., Seifert, K. and Fendler, K. (1997) 'Electrogenic reactions of Na⁺/K⁺-ATPase investigated on solid supported membranes', *Annals of the New York Academy of Sciences*, 834, pp. 361–363. doi: 10.1111/j.1749-6632.1997.tb52271.x.
- Pongs, O. *et al.* (1988) 'Shaker encodes a family of putative potassium channel proteins in the nervous system of *Drosophila*.', *The EMBO journal*, 7(4), pp. 1087–96. Available at: <http://www.ncbi.nlm.nih.gov/pubmed/2456921>.
- Purves, D. *et al.* (2001) 'Electrical Signals of Nerve Cells', in *Neuroscience*. Sunderland, MA, USA: Sinauer Associates, Inc., pp. 31–43.
- Roosild, T. P. *et al.* (2002) 'A mechanism of regulating transmembrane potassium flux through a ligand-mediated conformational switch', *Cell*, 109(6), pp. 781–791. doi: 10.1016/S0092-8674(02)00768-7.
- Rozov, A. *et al.* (2019) 'Importance of potassium ions for ribosome structure and function revealed by long-wavelength X-ray diffraction', *Nature Communications*. Springer US, 10(1), pp. 1–12. doi: 10.1038/s41467-019-10409-4.
- Rubio, F. *et al.* (1999) 'Genetic selection of mutations in the high affinity K⁺ transporter HKT1 that define functions of a loop site for reduced Na⁺ permeability and increased Na⁺ tolerance', *Journal of Biological Chemistry*, 274(11), pp. 6839–6847. doi: 10.1074/jbc.274.11.6839.
- Rubio, F., Gassmann, W. and Schroeder, J. I. (1995) 'Sodium-driven potassium uptake by the plant potassium transporter HKT1 and mutations conferring salt tolerance.', *Science*, 270(5242), pp. 1660–3. doi: 10.1126/science.270.5242.1660.
- Ryan, D. P. *et al.* (2010) 'Mutations in a potassium channel (Kir2.6) causes susceptibility to thyrotoxic hypokalemic periodic paralysis', *Cell*, 140(1), pp. 88–98. doi: 10.1016/j.cell.2009.12.024.
- Sambrook, J., Fritsch, E. F. and Maniatis, T. (1989) 'Molecular Cloning: A Laboratory Manual', in *Molecular Cloning: A Laboratory Manual*. 2nd edn. Cold Spring Harbor: Cold Spring Harbor Laboratory Press, pp. 49–55.
- Saraste, M. (1999) 'Oxidative phosphorylation at the fin de siecle', *Science*, 283(5407), pp. 1488–1493. doi: 10.1126/science.283.5407.1488.
- Sauer, D. B. *et al.* (2013) 'Sodium and potassium competition in potassium-selective and non-selective channels', *Nature Communications*. Nature Publishing Group, 4(May), pp. 1–9. doi: 10.1038/ncomms3721.
- Schrecker, M. (2019) *Exploring the structural and mechanistic basis of K⁺ translocation by the KtrAB system*. Johann Wolfgang Goethe-University.
- Schrecker, M., Wunnicke, D. and Hänel, I. (2019) 'How RCK domains regulate gating of K⁺ channels', *Biological Chemistry*, 400(10), pp. 1303–1322. doi: 10.1515/hsz-2019-0153.
- Schultz, S. G., Epstein, W. and Solomon, A. K. (1963) 'Cation Transport in *Escherichia coli*. Iv. Kinetics of Net K Uptake.', *The Journal of general physiology*, 47, pp. 329–346. doi: 10.1085/jgp.47.2.329.

- Schulz, P. *et al.* (2009) 'Measuring ion channels on solid supported membranes', *Biophysical Journal*. Biophysical Society, 97(1), pp. 388–396. doi: 10.1016/j.bpj.2009.04.022.
- Schulz, P., Garcia-Celma, J. J. and Fendler, K. (2008) 'SSM-based electrophysiology', *Methods*. Elsevier Inc., 46(2), pp. 97–103. doi: 10.1016/j.ymeth.2008.07.002.
- Seifert, K., Fendler, K. and Bamberg, E. (1993) 'Charge transport by ion translocating membrane proteins on solid supported membranes', *Biophysical Journal*, 64(2), pp. 384–391. doi: 10.1016/S0006-3495(93)81379-1.
- Sherman, J. M., Holm, G. E. and Albus, W. R. (1922) 'Effects in bacterial growth', pp. 583–588.
- Shrivastava, I. H. *et al.* (2002) 'K⁺ versus Na⁺ ions in a K channel selectivity filter: A simulation study', *Biophysical Journal*. Elsevier, 83(2), pp. 633–645. doi: 10.1016/S0006-3495(02)75197-7.
- Smith, P. K. *et al.* (1985) 'Measurement of protein using bicinchoninic acid', *Analytical Biochemistry*, 150(1), pp. 76–85. doi: 10.1016/0003-2697(85)90442-7.
- Song, C. and Corry, B. (2009) 'Intrinsic ion selectivity of narrow hydrophobic pores', *Journal of Physical Chemistry B*, 113(21), pp. 7642–7649. doi: 10.1021/jp810102u.
- Starkus, J. G. *et al.* (1997) 'Ion conduction through C-type inactivated Shaker channels.', *The Journal of General Physiology*, 110(5), pp. 539–50. doi: 10.1085/jgp.110.5.539.
- Stautz, J. (2016) *Regulation and organisation of KtrAB in the lipid bilayer in vivo and in vitro*. Johann Wolfgang Goethe-University.
- Stock, C. *et al.* (2018) 'Cryo-EM structures of KdpFABC suggest a K⁺ transport mechanism via two inter-subunit half-channels', *Nature Communications*. Springer US, 9(1), pp. 1–10. doi: 10.1038/s41467-018-07319-2.
- Stratford, J. P. *et al.* (2019) 'Electrically induced bacterial membrane-potential dynamics correspond to cellular proliferation capacity', *Proceedings of the National Academy of Sciences of the United States of America*, 116(19), pp. 9552–9557. doi: 10.1073/pnas.1901788116.
- Stumpe, S. and Bakker, E. P. (1997) 'Requirement of a large K⁺-uptake capacity and of extracytoplasmic protease activity for protamine resistance of *Escherichia coli*.', *Archives of microbiology*, 167(2–3), pp. 126–36.
- Su, Z. *et al.* (2016) 'Novel cell-free high-throughput screening method for pharmacological tools targeting K⁺ channels', *Proceedings of the National Academy of Sciences of the United States of America*, 113(20), pp. 5748–5753. doi: 10.1073/pnas.1602815113.
- Suelter, C. H. (1970) 'Enzymes activated by monovalent cations', *Science*, 168(3933), pp. 789–795. doi: 10.1126/science.168.3933.789.
- Sula, A. *et al.* (2017) 'The complete structure of an activated open sodium channel', *Nature Communications*. Nature Publishing Group, 8, pp. 1–9. doi: 10.1038/ncomms14205.
- Sulkowski, E. (1989) 'The saga of IMAC and MIT.', *BioEssays*, 10(5), pp. 170–5. doi: 10.1002/bies.950100508.
- Sun, C. and Gennis, R. B. (2019) 'Single-particle cryo-EM studies of transmembrane proteins

- in SMA copolymer nanodiscs.', *Chemistry and physics of lipids*, 221, pp. 114–119. doi: 10.1016/j.chemphyslip.2019.03.007.
- Szollosi, A. *et al.* (2016) 'Dissecting the Molecular Mechanism of Nucleotide-Dependent Activation of the KtrAB K⁺ Transporter', *PLoS Biology*, 14(1), pp. 1–21. doi: 10.1371/journal.pbio.1002356.
- Taglicht, D., Padan, E. and Schuldiner, S. (1993) 'Proton-sodium stoichiometry of NhaA, an electrogenic antiporter from *Escherichia coli*', *Journal of Biological Chemistry*, 268(8), pp. 5382–5387.
- Tao, X., Hite, R. K. and MacKinnon, R. (2017) 'Cryo-EM structure of the open high-conductance Ca²⁺-activated K⁺ channel', *Nature*. Nature Publishing Group, 541(7635), pp. 46–51. doi: 10.1038/nature20608.
- Teixeira-Duarte, C. M., Fonseca, F. and Morais-Cabral, J. H. (2019) 'Activation of a nucleotide-dependent RCK domain requires binding of a cation cofactor to a conserved site.', *eLife*. doi: 10.7554/eLife.50661.
- Tempel, B. L., Jan, Y. N. and Jan, L. Y. (1988) 'Cloning of a probable potassium channel gene from mouse brain.', *Nature*, 332(6167), pp. 837–9. doi: 10.1038/332837a0.
- Tolema, N. *et al.* (1999) 'Change to alanine of one out of four selectivity filter glycines in KtrB causes a two orders of magnitude decrease in the affinities for both K⁺ and Na⁺ of the Na⁺ dependent K⁺ uptake system KtrAB from *Vibrio alginolyticus*', *FEBS Letters*, 450(3), pp. 217–220. doi: 10.1016/S0014-5793(99)00504-9.
- Tolema, N. *et al.* (2005) 'All four putative selectivity filter glycine residues in KtrB are essential for high affinity and selective K⁺ uptake by the KtrAB system from *Vibrio alginolyticus*', *Journal of Biological Chemistry*, 280(50), pp. 41146–41154. doi: 10.1074/jbc.M507647200.
- Thomas, M., Jayatilaka, D. and Corry, B. (2007) 'The Predominant Role of Coordination Number in Potassium Channel Selectivity', *Biophysical Journal*, 93(8), pp. 2635–2643. doi: 10.1529/biophysj.107.108167.
- Thompson, A. N. *et al.* (2009) 'Mechanism of potassium-channel selectivity revealed by Na⁺ and Li⁺ binding sites within the KcsA pore', *Nature Structural & Molecular Biology*, 16(12), pp. 1317–1324. doi: 10.1038/nsmb.1703.
- Tivey, D. R., Simmons, N. L. and Aiton, J. F. (1985) 'Role of passive potassium fluxes in cell volume regulation in cultured HeLa cells', *The Journal of Membrane Biology*, 87(2), pp. 93–105. doi: 10.1007/BF01870656.
- Tokuda, H. and Unemoto, T. (1982) 'Characterization of the respiration-dependent Na⁺ pump in the marine bacterium *Vibrio alginolyticus*', *Journal of Biological Chemistry*, 257(17), pp. 10007–10014.
- Uysal, S. *et al.* (2009) 'Crystal structure of full-length KcsA in its closed conformation', *Proceedings of the National Academy of Sciences of the United States of America*, 106(16), pp. 6644–6649. doi: 10.1073/pnas.0810663106.
- Valiyaveetil, F. I. *et al.* (2006) 'Ion selectivity in a semisynthetic K⁺ channel locked in the conductive conformation', *Science*, 314(5801), pp. 1004–1007. doi: 10.1126/science.1133415.

- Varma, S. and Rempe, S. B. (2007) 'Tuning ion coordination architectures to enable selective partitioning.', *Biophysical Journal*, 93(4), pp. 1093–9. doi: 10.1529/biophysj.107.107482.
- Vieira-Pires, R. S., Szollosi, A. and Morais-Cabral, J. H. (2013) 'The structure of the KtrAB potassium transporter', *Nature*, 496(7445), pp. 323–328. doi: 10.1038/nature12055.
- Voet, D. and Voet, J. G. (2011) *Biochemistry*. 4th ed. Hoboken, NJ, USA: John Wiley & Sons.
- Wacker, T. *et al.* (2014) 'Direct observation of electrogenic NH₄⁺ transport in ammonium transport (Amt) proteins', *Proceedings of the National Academy of Sciences of the United States of America*, 111(27), pp. 9995–10000. doi: 10.1073/pnas.1406409111.
- Wang, Z., Zhang, X. and Fedida, D. (2000) 'Regulation of transient Na⁺ conductance by intra- and extracellular K⁺ in the human delayed rectifier K⁺ channel Kv1.5.', *The Journal of physiology*, 523 Pt 3, pp. 575–91. doi: 10.1111/j.1469-7793.2000.00575.x.
- Wolfersberger, M. G. (1994) 'Uniporters, symporters and antiporters.', *The Journal of experimental biology*, 196, pp. 5–6.
- Zaccai, G. (2000) 'How soft is a protein? A protein dynamics force constant measured by neutron scattering.', *Science*, 288(5471), pp. 1604–7. doi: 10.1126/science.288.5471.1604.
- Zhenyu, X. *et al.* (2013) 'First Characterization of Bacterial Pathogen, *Vibrio alginolyticus*, for Porites andrewsi White Syndrome in the South China Sea', *PLoS ONE*, 8(9), pp. 1–8. doi: 10.1371/journal.pone.0075425.
- Zhou, M. and MacKinnon, R. (2004) 'A mutant KcsA K⁺ channel with altered conduction properties and selectivity filter ion distribution', *Journal of Molecular Biology*, 338(4), pp. 839–846. doi: 10.1016/j.jmb.2004.03.020.
- Zhou, Y. *et al.* (2001) 'Chemistry of ion coordination and hydration revealed by a K⁺ channel-Fab complex at 2.0 Å resolution', *Nature*, 414(6859), pp. 43–48. doi: 10.1038/35102009.
- Zhou, Y. and MacKinnon, R. (2003) 'The occupancy of ions in the K⁺ selectivity filter: charge balance and coupling of ion binding to a protein conformational change underlie high conduction rates.', *Journal of molecular biology*, 333(5), pp. 965–75. doi: 10.1016/j.jmb.2003.09.022.
- Zuber, D. *et al.* (2005) 'Kinetics of charge translocation in the passive downhill uptake mode of the Na⁺/H⁺ antiporter NhaA of *Escherichia coli*', *Biochimica et Biophysica Acta (BBA) - Bioenergetics*, 1709(3), pp. 240–250. doi: 10.1016/j.bbabi.2005.07.009.

8. Supplement

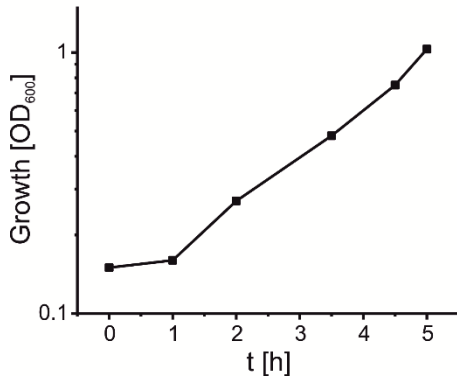


Figure 45 Growth curve of *E. coli* strain LB2003 carrying pEL903. Growth of *E. coli* LB2003 carrying plasmid pEL903, coding for KtrB-His₆, in K3 medium is shown. Expression of *ktrB-His₆* is induced from the start with 0.02% L-arabinose.

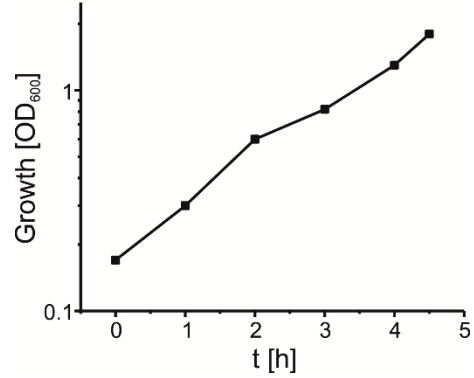


Figure 47 Growth curve of *E. coli* strain LB2003 carrying pEL903_G316S. Growth of *E. coli* LB2003pEL903_G316S in K3 medium is shown, producing KtrB_{G316S}-His₆. Induction from the start with 0.02%.

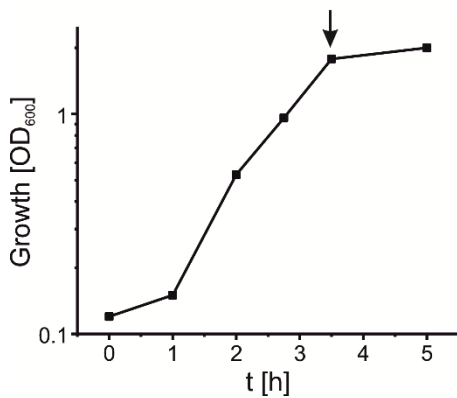


Figure 46 Growth curve of *E. coli* strain LB2003pBKtrB-C3H. Growth of *E. coli* LB2003 carrying plasmid pBKtrB-C3H, coding for KtrB-3C-His₁₀, in KML medium is shown. Expression of *ktrB-3C-His₁₀* was induced with 0.02% L-arabinose as indicated by the arrow.

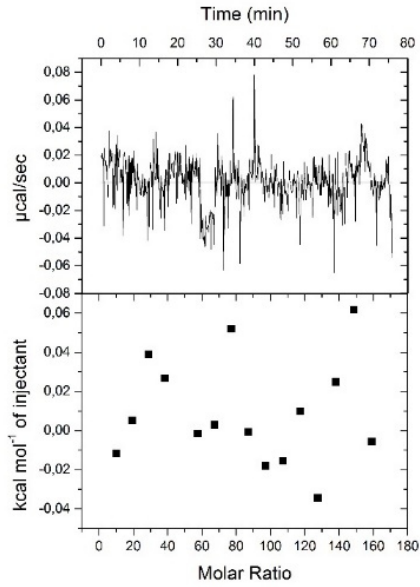


Figure 48 Binding affinity of LiCl to VaKtrB-His₆ examined by ITC. LiCl to detergent-solubilized VaKtrB-His₆ titrations is shown as raw heat exchange data in the upper panels. Titration buffer contained 30 mM LiCl 75 mM NaCl and 20 mM Tris-HCl pH 7.5. ITC titrations performed by Marina Schrecker.

Table 12 All non-activating and activating solution combinations used in SSM-based electrophysiology. The basis buffer for all solutions consisted of 50 mM Tris, 50 mM MES, 50 mM HEPES, 5 mM MgCl₂, 200 mM choline-Cl at a pH of 7.5. The basis buffer was prepared in 1.25x composition and diluted 1/5 with 500 mM of the respective salts.

<u>NA solutions</u>		<u>A solutions</u>	
Compensation salt	Active salt	Compensation salt	Active salt
100 mM choline-Cl	-	-	100 mM LiCl
100 mM choline-Cl	-	-	100 mM NaCl
100 mM choline-Cl	-	-	100 mM KCl
100 mM choline-Cl	-	-	100 mM RbCl
100 mM choline-Cl	-	-	100 mM CsCl
100 mM choline-Cl	-	99 mM choline-Cl	1 mM KCl
100 mM choline-Cl	-	95 mM choline-Cl	5 mM KCl
100 mM choline-Cl	-	90 mM choline-Cl	10 mM KCl
100 mM choline-Cl	-	80 mM choline-Cl	20 mM KCl
100 mM choline-Cl	-	70 mM choline-Cl	30 mM KCl
100 mM choline-Cl	-	60 mM choline-Cl	40 mM KCl
100 mM choline-Cl	-	50 mM choline-Cl	50 mM KCl
100 mM choline-Cl	-	99 mM choline-Cl	1 mM NaCl
100 mM choline-Cl	-	95 mM choline-Cl	5 mM NaCl
100 mM choline-Cl	-	90 mM choline-Cl	10 mM NaCl
100 mM choline-Cl	-	80 mM choline-Cl	20 mM NaCl
100 mM choline-Cl	-	70 mM choline-Cl	30 mM NaCl
100 mM choline-Cl	-	60 mM choline-Cl	40 mM NaCl
100 mM choline-Cl	-	50 mM choline-Cl	50 mM NaCl
100 mM choline-Cl	-	99 mM choline-Cl	1 mM RbCl
100 mM choline-Cl	-	95 mM choline-Cl	5 mM RbCl
100 mM choline-Cl	-	90 mM choline-Cl	10 mM RbCl
100 mM choline-Cl	-	80 mM choline-Cl	20 mM RbCl
100 mM choline-Cl	-	70 mM choline-Cl	30 mM RbCl
100 mM choline-Cl	-	60 mM choline-Cl	40 mM RbCl
100 mM choline-Cl	-	50 mM choline-Cl	50 mM RbCl
100 mM choline-Cl	-	99 mM choline-Cl	1 mM CsCl
100 mM choline-Cl	-	95 mM choline-Cl	5 mM CsCl
100 mM choline-Cl	-	90 mM choline-Cl	10 mM CsCl
100 mM choline-Cl	-	80 mM choline-Cl	20 mM CsCl
100 mM choline-Cl	-	70 mM choline-Cl	30 mM CsCl
100 mM choline-Cl	-	60 mM choline-Cl	40 mM CsCl
100 mM choline-Cl	-	50 mM choline-Cl	50 mM CsCl
95 mM choline-Cl	5 mM NaCl	-	100 mM KCl
95 mM choline-Cl	5 mM NaCl	99 mM choline-Cl	1 mM KCl
95 mM choline-Cl	5 mM NaCl	95 mM choline-Cl	5 mM KCl
95 mM choline-Cl	5 mM NaCl	90 mM choline-Cl	10 mM KCl
95 mM choline-Cl	5 mM NaCl	80 mM choline-Cl	20 mM KCl
95 mM choline-Cl	5 mM NaCl	70 mM choline-Cl	30 mM KCl
95 mM choline-Cl	5 mM NaCl	60 mM choline-Cl	40 mM KCl
95 mM choline-Cl	5 mM NaCl	50 mM choline-Cl	50 mM KCl

Table 13 to 19 show the obtained peak currents, average peak currents and deviations for SSM measurements on control liposomes with different chloride salt concentrations.

Table 13 Peak currents obtained for LiCl concentration jumps on control liposomes.

LiCl [mM]	I [pA]	I [pA]2	I [pA]3	Ø(I [pA])	Δ (I[pA])
100	317	485	420	407	85
50	166	242	220	209	39
40	141	191	180	171	26
30	101	153	145	133	28
20	68	95	106	90	20
10	31	60	73	55	22
5	14	26	29	23	8
1	1	15	24	13	12

Table 14 Peak currents obtained for NaCl concentration jumps on control liposomes.

NaCl [mM]	I [pA]	I [pA]2	I [pA]3	Ø(I [pA])	Δ (I[pA])
100	93	88	197	126	62
50	68	59	113	80	29
40	61	45	99	68	28
30	49	39	81	56	22
20	41	33	60	45	14
10	29	21	38	29	9
5	12	13	24	16	7
1	3	6	13	7	5

Table 15 Peak currents obtained for KCl concentration jumps on control liposomes.

KCl [mM]	I [pA]	I [pA]2	I [pA]3	Ø(I [pA])	Δ (I[pA])
100	41	108	46	65	37
50	37	71	40	49	19
40	35	61	36	44	15
30	35	49	35	40	8
20	31	44	39	38	7
10	26	34	29	30	4
5	19	24	14	19	5
1	9	13	8	10	3

Table 16 Peak currents obtained for RbCl concentration jumps on control liposomes.

RbCl [mM]	I [pA]	I [pA]2	I [pA]3	Ø(I [pA])	Δ (I[pA])
100	57	69	184	103	70
50	49	73	64	62	12
40	47	65	11	41	27
30	44	82	9	45	37
20	35	80	16	44	33
10	27	79	20	42	32
5	12	45	11	23	19

1	5	38	0	14	21
---	---	----	---	----	----

Table 17 Peak currents obtained for CsCl concentration jumps on control liposomes.

CsCl [mM]	I [pA]	I [pA]2	I [pA]3	Ø(I [pA])	Δ (I[pA])
100	43	60	55	53	9
50	32	48	35	38	9
40	30	43	31	35	7
30	28	39	27	31	7
20	24	35	27	29	6
10	22	27	21	23	3
5	18	17	18	18	1
1	13	7	9	10	3

Table 18 Peak currents obtained from 100 mM KCl concentration jumps in the presence of 5 mM X chloride salt on control liposomes.

A [100 mM]	NA [5 mM]	I [pA]	I [pA]2	I [pA]3	Ø(I [pA])	Δ (I[pA])
KCl	NaCl	46	41	48	45.00	3.61
KCl	KCl	40	34	42	38.67	4.16
KCl	RbCl	42	33	45	40.00	6.24
KCl	CsCl	47	42	51	46.67	4.51
KCl	LiCl	51	42	58	50.33	8.02

Table 19 Peak currents obtained from measurements on control liposomes (n=4).

100 [mM]	Ø (I [pA])	Δ (I[pA])
LiCl	230	40
NaCl	120	37
KCl	76	35
RbCl	-18	58
CsCl	22	66

9. Acknowledgments

Foremost, I would like to express my deepest gratitude to my supervisor, Jun. Prof. Dr. Inga Hänelt, for allowing me to stay and work in her laboratory on the KtrAB project. I am sincerely grateful to you for your expertise, understanding, motivation, patience, and your immense knowledge. Your guidance, opinion and constructive criticism helped me write this thesis. I could not have wished for a better mentor for my Ph.D. thesis!

I would like to express my sincere appreciation to Prof. Dr. Klaus Fendler from the Max Planck Institute of Biophysics for introducing me to SSM-based electrophysiology and allowing me to work in his laboratory. I am very grateful that he is my TRAM supervisor and a member of my Ph.D. committee. Thank you very much for all the advice, guidance, and enjoyable and productive collaboration.

I am most grateful to the mass spectrometry collaborators, Jun. Prof. Dr. Nina Morgner, Dr. Nils Hellwig and Dr. Oliver Peetz from the Institute of Physical and Theoretical Chemistry at the Goethe-University Frankfurt, for their expertise in LILBID-MS. I would like to thank you for a very successful cooperation!

My sincere thank-you goes to Prof. Dr. Gerhard Hummer and Dr. Ahmad Reza Mediphour from the Max Planck Institute of Biophysics for the MD simulations. Thank you for the excellent collaboration!

Furthermore, I would like to thank Jun. Prof. Dr. Eric Geertsma for being my TRAM supervisor. I am thankful for your support and counselling during the years!

A big thank-you goes to Dr. Dorith Wunnicke-Kortz for taking the time and proofreading this thesis. Dorith, I am forever grateful for all your help!

I thank Prof. Dr. Robert Tampé and PD Dr. Ruper Abele for the valuable advice and their great support throughout the years. Of course, my gratitude goes to all the Tampé and Abele group members for creating a friendly and welcoming environment.

My heartfelt thanks go out to my KtrAB-partners-in-crime Marina Schrecker, Janina Stautz Dorith Wunnicke-Kortz. Thank you for cheering me on, helping me through hard times, and celebrating each accomplishment. Without your motivation and encouragement, I would not be where I am right now.

Special thanks must go to Dr. Miyer Patiño-Ruiz for the friendly and extremely valuable introduction to SSM technology, but also to Dr. Andre Bazzone and Dr. Octavian Călinescu.

They taught me all the tricks of the SSM setup and were always there when I had a question. Thank you all for the wonderful atmosphere!

I would also like to thank all the students that contributed to the Ktr project: Natalie Kolesova, Janina Stautz, Jakob Silberberg, Paula Holzhüter, Jonatan Menger, and Yvonne Hellmich.

There are no words to express how much it meant to me to have been a member of the Hänelt Lab. Thank you for your kindness and inspiration over the many years: Marina, Charlott, Dorith, Igor, Janina, Yvonne, Michael, and all the current and former students. We had so much fun together!

Ein ganz besonderer Dank gilt meiner Familie für die Unterstützung, vor allem aber meiner Schwester Kati, die mir die letzten Jahre immer zur Seite stand. Danke, dass du immer für mich da bist!

Posebna zahvala mojoj mami koja je uvijek vjerovala u mene. Volim te najviše na svijetu!

10. CV

Personal Information

Name	Vedrana Mikušević
Academic Degree	Master of Science
Date of Birth	29 th December 1987
Place of Birth	Zagreb (former SFR Yugoslavia)
Nationality	Croatian

Education

11/2014 – present	Goethe University in Frankfurt, Germany PhD in Biochemistry, with Inga Hänelt Thesis Title ' <i>Physiological role of Na⁺ and nucleotide binding for K⁺ translocation via the KtrAB system</i> '
10/2012 – 11/2014	Goethe University in Frankfurt, Germany MSc in Molecular Biology, with Inga Hänelt Thesis Title ' <i>Solid-supported membrane-based electrophysiology measurements on the B subunit of the K⁺ uptake system VaKtrAB</i> '
10/2007 – 10/2012	Goethe University in Frankfurt, Germany BSc in Chemistry, with Gunter P. Eckert (now in Gießen) Thesis Title in German: ' <i>Untersuchungen zum Zusammenhang zwischen mitochondrialer Schwellung und Membranfluidität</i> ', English translation: ' <i>Investigation of the correlation of mitochondrial swelling and membrane fluidity</i> '
09/2004 – 06/2007	Philipp-Reis-Schule in Friedrichsdorf, Germany Upper secondary education with advanced courses in Biology and Chemistry

Publications

Vedrana Mikusevic, Marina Schrecker, Miyer Patiño-Ruiz, Klaus Fendler and Inga Hänelt. 2019. '*A channel profile report of the unusual K⁺ channel KtrB.*' *Journal of General Physiology*

Marina Diskowski, Ahmad Reza Mehdipour, Dorith Wunnicke, Deryck J Mills, **Vedrana Mikusevic**, Natalie Bärland, Jan Hoffmann, Nina Morgner, Heinz-Jürgen Steinhoff, Gerhard Hummer, Janet Vonck and Inga Hänelt. 2017. '*Helical jackknives control the gates of the double-pore K⁺ uptake system KtrAB.*' *eLife*.

Igor Tascón, Joana S. Sousa, Robin A. Corey, Deryck J. Mills, David Griwatz, Nadine Aumüller, **Vedrana Mikusevic**, Phillip J. Stansfeld, Janet Vonck and Inga Hänelt. 2020. '*Structural basis of the proton-coupled potassium transport in the KUP family.*' *Nature Communications*. In press.

Nils Hellwig, Oliver Peetz, Zainab Ahdash, Igor Tascón, Paula J. Booth, **Vedrana Mikusevic**, Marina Diskowski, Argyris Politis, Yvonne Hellmich, Inga Hänelt, Eamonn Reading and Nina Morgner. 2018. '*Native mass spectrometry goes more native: Investigation of membrane protein complexes directly from SMALPs.*' *Chemical Communications*.

Marina Diskowski, **Vedrana Mikusevic**, Charlott Stock, and Inga Hänel. 2015. *'Functional diversity of the superfamily of K⁺ transporters to meet various requirements.'* Biological Chemistry.

Work Experience and Teaching

- 11/2014 - present **Teaching assistant, Goethe University in Frankfurt, Germany**
- Undergraduate practical course: Cellular Biochemistry
 - Undergraduate lecture: Gene Expression and Regulation
 - Bachelor/Master internship supervisor (5)
 - Master thesis supervisor (2)
- 08/2017 **International Summer School 2017 in Hirschegg, Austria**
- Organization, fundraising and invitation of speakers
- 05/2011 - 04/2014 **Student worker, Continental AG in Frankfurt, Germany**
R&D Process and Quality Management in Passive Safety & Sensorics
- Analysing, optimizing and mapping engineering processes in STAGES
 - Provision and training of PTC Integrity on an international level

Conferences and Workshops

- 11/2014 - present **Workshops offered by the Integrated Research Training Group 'TRAM' in Frankfurt, Germany**
Basics of scientific work, statistics, poster design, oral scientific presentation, scientific writing, voice and speech training, biotech project management, GxP intensive course
- 06/2019 **GRC/GRS 'Mechanisms of Membrane Transport' in New London, NH, USA**
Poster on *'A channel profile report of the channel subunit KtrB'*
Discussion Leader for the GRS
- 03/2019 **Collaborative Research Center (CRC) 807 Conference in Obergurgl, Austria**
Talk on *'A channel profile report of the simple K⁺ translocation subunit KtrB'*
- 06/2017 **GRC/GRS 'Mechanisms of Membrane Transport' in New London, NH, USA**
Poster on *'Subunit KtrB confers Na⁺ dependency to the K⁺ uptake system KtrAB'*
Discussion Leader for the GRS
- 04/2017 **SCIENCEPLUS-Workshop by GOLIN Wissenschaftsmanagement in Frankfurt, Germany**
'Team Work & Leadership in & outside Academia: Team Player – Key Player – Head Coach'
- 03/2017 **Workshop on GMO law and Biological Safety in Heidelberg, Germany**

- 02/2016 **GRC/GRS 'Ligand Recognition and Molecular Gating' in Lucca (Barga), Italy**
Poster on '*Ion selectivity of the channel-like subunit KtrB*'
- 10/2016 **Joint Summer School with the Lab of M. Seeger, E. Geertsma and D. J. Slotboom in Groningen, Netherlands**
Talk on '*Bacterial SKT member KtrB uncovered as the Na⁺-dependent subunit*'
- 12/2015 **GE Healthcare training course on ÄKTA™ system and UNICORN™ control software in Munich, Germany**
- 02/2015 **VAAM Conference in Marburg, Germany**
Poster on '*KtrB: A cation channel with low selectivity*'
- 02/2015 **Good Evening Symposium in Frankfurt, Germany**
Talk on '*Cation binding and translocation properties of the potassium ion transporter subunit KtrB*'
- 07/2014 **International Summer School 2014 in Hirschegg, Austria**
2nd place for best talk on '*KtrAB & KdpFABC chimeric proteins; Blurring the line between channels and transporters*'

Stipends and Memberships

- 12/2016 – present **Member of the Guest Speaker Committee of the Collaborative Research Center (CRC) 807 at Goethe University in Frankfurt**
- Selection, invitation and hosting of Guests
- 11/2014 – present **Member of the Integrated Research Training Group 'TRAM' of the Collaborative Research Center (CRC) 807 at Goethe University in Frankfurt**
- 11/2014 – 05/2015 **PhD Fellow of the Collaborative Research Center (CRC) 807 at Goethe University in Frankfurt**

Skills

- Techniques: Molecular biology, bacterial cell culture, membrane protein purification (detergent and SMALP) and lipid reconstitution, cell- and liposome-based transport assays, isothermal titration calorimetry (ITC), solid-supported membrane (SSM)-based electrophysiology, planer lipid bilayers
- Languages: German (native speaker), Croatian and Serbian (native speaker), English (good), Spanish (basic)